A foehn climatology of the McMurdo Dry Valleys of Antarctica using satellite remote sensing data.

By
Rajasweta Datta

A thesis submitted to the University of Canterbury in partial fulfilment of the requirements for the degree of

Doctor of Philosophy

University of Canterbury
Christchurch, New Zealand
2021

Acknowledgment

This thesis would not have been possible without the presence of some of the most amazing people in my life, who provided me with constant motivation, love, and emotional support through all the highs and lows. I want to thank my father (Nagadhiraj Datta) for supporting me in pursuing my dreams throughout my life. He has been my courage, my strength, and my patience throughout. Without his support, it would not have been possible for me to make a life for myself. I would like to thank my mother (Mahasweta Datta), who is not with us anymore but is always in my mind and heart, inspiring me to do something out of my life. I want to thank my husband (Deepak), who stood by me, especially during the days of failed attempts with my thesis analysis or pushing me when I was procrastinating with my work.

I want to thank my friends and colleagues who were there for me and always inspired me to go ahead despite all the hurdles. These issues were different from mine, but I still found strength in their spirit of handling family and career hand in hand (especially Huong and Ririn). Some friends made the gloomy days brighter (Rasool, Jiawei). To Suvojit, who has provided excellent bits of advice, edited my work, and supported me at any time of the day.

Lastly, I would like to thank my supervisor Peyman and Marwan. Marwan has been an amazing supervisor; he gave me time to sort things in my life when things were going low and helped me get back to my studies. He was always available for guidance and any help, be it research or looking out for me on field trips. Peyman has always inspired me to be calm and collected like him; his knowledge of things beyond his research area is motivating. He had been a constant support throughout my thesis and an amazing supervisor, where it be in providing critical inputs for my work or by arranging funds for my studies when my scholarship ran out.

I got the support of friends, family, and supervisors throughout my research, and everyone pulled me up when I was low and celebrated with me when there was a triumph. I am thankful to all the people in life, and I thank god for everything that he has blessed me with, including my two cats (Kimba and Leo), who are completely useless but have made me smile on days I frowned and let me cuddle them always.

Abstract

This thesis investigates the McMurdo Dry Valley (MDV) foehn meteorology and its impact on the region's hydrology utilizing satellite remote sensing data and *in-situ* meteorological observations. It aims to establish Satellite Remote Sensing as a tool for studying the spatiotemporal variabilities in surface temperatures across MDV. The thesis utilizes Land Surface Temperature (LST) data from the MODIS sensor mounted atop Aqua and Terra satellites, along with the meteorological and stream discharge data from Automatic Weather Stations (AWS)s and stream gauges installed by Long Term Ecological Research (LTER) program. The research assesses the long-term (18 years: 2000-2017) summer meteorology recorded by the AWSs and investigates their inter and intra-valley variabilities across MDV. The thesis identifies the control of summer foehn-induced warming and incoming shortwave radiation (radiative warming) in influencing the valley floor temperatures along with the trends in the occurrence of strong foehn events that occur mostly during clear sky days. As the thesis works into understanding wider spatial scale changes in temperatures using satellite LST data, it checks the data for inconsistencies and evaluates its accuracy and sensitivity to register the day-to-day temperature changes in the valley floor. It recognizes satellite-derived LST to be a reliable dataset for studying the meteorology-induced temperature variations across the valleys.

Over-dependence of foehn's study on *in-situ* measurement had been a major obstacle in comprehending the meteorological variations that are associated with foehn winds over a wider spatial scale. The study, therefore, developed a methodology that can not only detect foehn in MDV without AWS support but also identify the various degree of warming each region experienced during a foehn event. The methodology developed detected foehn events in MDV using long-term satellite LST data for summer and winter periods individually. Due to the independence of the methodology in using AWS data, this technique can be utilized in the areas where there are no AWSs installed.

The thesis overcame the constraints of investigating temperature fluctuations in the valley floor due to foehn winds, using *in-situ* measurements from a single location by investigating satellite-derived LSTs' spatiotemporal changes across MDV. It examines the influence of terrain properties on the LST values across the region and later investigates the spatio-temporal changes in surface temperatures that occur during a major foehn event over the 2015-16 summer. The thesis later differentiates the spatial temperature signatures that are associated with foehn-induced warming (adiabatic warming) from that of radiative warming. Foehn events in MDV trigger higher and more uniform warming of the valley floor compared to radiative warming, which affects the differential warming of each location based on albedo.

To identify the varying foehn-induced warming across the valleys, the study delineates the areas in the regions based on their warming. The warming across the valley floor during foehn is categorized into low, moderate, and high category groups, and potential hotspots associated with each group are identified that have temperatures that are higher than the rest of the valley. It was found that the lower elevation areas in the valley floor experienced a greater number of days with a higher degree of warming in the region.

The meteorology associated with foehn events during summer is often responsible for high glacial melt and flooding of the streams in the region, as a result, the summer meteorology controls the regions' hydrology and biodiversity. The thesis presents a broader study on the impact of valley floor temperature changes on the streams' hydrology using satellite LST datasets. It was able to identify the hotspots across the MDV floor that recorded a higher number of days with temperatures above melting point than the rest of the valley. The study recognizes the importance of incoming solar radiation in triggering high glacial melt over the summer. Austral summer ISWR can cause high glacial melt in large glacial sources like Brownworth despite fewer foehn hours. It was found that two seasons with high-frequency foehn events may have a different glacial melt due to differences in incoming solar radiation.

Lastly, the thesis is the first climatological study carried out on MDV using satellite remote sensing and delves into the wider spatial scale study of MDV foehn events and their effects on the region's temperature and hydrology.

Table of Contents

Introduction

Antarctica has experienced climate change; for example, western and northern parts of the Antarctic Peninsula have experienced the largest statistically significant trend of +0.54℃ per decade for the period 1951–2011(Turner et al., 2014), the winter temperature increased by +1.03℃ per decade from 1950 to 2006. Upper-ocean temperatures to the west of the Antarctic Peninsula have risen over 1℃ since 1955 (Turner et al., 2013). There has been a visible impact of climate change on Antarctica. A total of 28,000km^2 of the ice shelf is already lost from around the Antarctic Peninsula, with a volume equivalent to United Kingdom's domestic water requirement for more than 1,000 years. Antarctic Peninsula contributes around 0.16mm per year to global sea-level rise. (BAS, 2015). Antarctic Circumpolar Current is warming more rapidly than other ocean regions; in the current situation, ecosystems like MDV are quite vulnerable to changes. Studying the meteorology associated with these sites will help understand the impact of global climatic changes on the region's biodiversity and ecosystem.

Roughly 0.34% of Antarctica is free from snow and ice cover. These areas include exposed nunataks, mountain cliffs, and seasonal snow and ice-free areas (Convey, 2010) and are known as Antarctic oases. The McMurdo Dry Valleys (MDV) is the largest oasis in Antarctica (Gusain et al., 2014), located in Southern Victoria Land and it spans 4800km^2. MDV is one of the driest places on Earth and is a hyper-arid polar desert due to its exceptionally low annual precipitation of less than 100mm/yr. (Doran, McKay, et al., 2002). The valleys are located on the leeward side of the Transantarctic Mountains and are bounded by the McMurdo Sound/Ross Sea to the east and the East Antarctic Ice Sheet to the west (Figure 1.1) (Speirs et al., 2008).

MDV has been an area of interest for the past few decades because it has one of Earth's rarest ecosystems, where ice-free landforms are bounded by thick ice. Despite the extreme climatic conditions, a simple ecosystem, primarily of microbial nature, thrives when the climactic conditions allow. The extreme environment is also attractive for the other disciplinary sciences that focus on extra-terrestrial life forms on other planets such as Mars (Marchant & Head., 2005; Marchant & Head, 2007, Andersen et al., 1992).

Owing to the large fluctuations of seasonal solar radiation received on the surface (from sunless winters to night less summers), the seasonal meteorology in the valleys is very distinct; the summer temperatures between November and February have a typical range from -20℃ to 5℃, whereas in winter there is a dramatic cooling where temperatures typically range from -40℃ to -10℃. In summer, with a warmer temperature range and availability of liquid water – if above zero temperature is attained - a unique ecosystem can 'thrive' in at a micro climatological scale (Chapter 1). Despite low precipitation

and extreme temperatures, MDV hosts the largest river (Onyx) in Antarctica, and many other smaller streams may freely flow in the region. These streams are generated from glacial melt, and the moisture they provide can sustain microbial and other life forms. Therefore, the meteorological conditions in the MDV are a primary driver for biodiversity and hydrology.

Many multi-scale factors influence the variability in the meteorological conditions; the regional geography places the MDV between the relatively colder Transantarctic Mountains and warmer McMurdo Sound/Ross sea air masses, which influences the air temperatures and winds of the region (Steinhoff et al., 2013). The Transantarctic mountains act as a barrier in preventing the Ross sea region's moisture-bearing weather systems from moving inland (Speirs et al., 2008), causing MDV to have very low precipitation. Within the valleys, the interplay in a bimodal wind regime consisting of warm westerlies (originating from the Transantarctic Mountains) and colder easterlies (from the Ross Sea region) introduce pronounced temperature gradients (McKendry & Lewthwaite, 1992). Superimposed on the valley scale wind flow, in certain weather conditions (typically when radiative heating is significant), differences in land surface (with varying albedo values) influence the local temperature. The terrain warms up to varying degrees due to differential albedo, which leads to disparity in net radiation available for warming based on each land surface type. The terrain elevation plays a significant role in controlling the region's temperatures. Higher elevation ridges are colder than the valley floor; also, terrain shadow and cloud cover can cause differential warming of the area during summer (Katurji et al., 2013).

The variation in meteorological conditions across MDV and their influence on the region's biodiversity and hydrology have been previously studied using Automatic Weather Stations (AWS) and modeled meteorological data from Antarctic Mesoscale Prediction System. Previous research helped establish the ground knowledge of the meteorological conditions across the region and understand the effect of day-to-day summer weather on hydrology (Doran et al., 2008). In MDV, westerly winds play a significant role in increasing the valley floor's air temperature during summer and winter. The frequency of westerlies during summer controls the region's hydrology, such that the years with high-frequency westerly winds cause large-scale glacial melt in the valleys resulting in flooding of the MDV streams (Doran et al., 2008). These westerlies result from foehn events in the region due to cyclonic activities in the Ross and the Amundsen Sea region.

The cyclonic activities cause a high-pressure gradient between the Transantarctic Mountains and the Ross sea region; as the winds ascend, they encounter the mountain barrier, which causes them to converge and cool down; after crossing the mountains, the dry air diverges and flows down the leeward slopes towards MDV. As the winds descend into the valley floor, they dry and warm up adiabatically, causing an increase in the region's temperature (Sharples, 2018). These foehn winds last from few hours to days and they can increase the valley floor temperature by up to 30°C during winter and raise the

temperatures as high as 8°C during summers which can cause high glacial melt and eventual flooding of the MDV streams.

Even though all the valley systems within the MDV can simultaneously be under the influence of synoptic-scale flows, the valley winds can be markedly different. For example, when strong low-pressure systems force foehn in the MDV, each valley can exhibit different meteorological conditions, as the interaction between the foehn, the antecedent boundary layer condition, and the geometry of the landscape can influence the penetration of foehn into the valley system (Speirs et al., 2010; Doran et al., 2008). Therefore, there can be large spatial heterogeneity in foehn characteristics which the current AWS network will not resolve. This thesis aims to convey a more comprehensive understanding of foehn spatial heterogeneity and dynamics using Land Surface Temperature (LST; defined in Chapter 2) as a proxy for air temperature. A comprehensive study of foehn events and their effects across MDV is required over a broader area to identify the shifts in meteorology across each location. The present research studies the spatial-temporal variability in MDV floor temperatures during a foehn event over the summers. Some of the research questions identified by the current research related to large spatial scale study of foehn events across MDV are listed below.

Research Questions

- Question 1: How does summer incoming solar radiation along with the foehn winds control the valley floor air and surface temperatures across MDV?
- Question 2: What are the effects of foehn events across different parts of MDV?
- Question 3: Which regions in MDV are more susceptible to foehn events in summer?
- Question 4: What is the magnitude of influence from solar radiation and foehn events over the hydrological cycle (particularly melt) on the MDV?

Satellite remote sensing acts as a useful tool for broader spatial scale observations, which helps to study valley-wide events like foehn, even in areas with no AWSs installed. Satellite remote sensing data have been used across different fields previously, whether it be agriculture, urban planning, cryosphere study, forestry, climate studies, to name a few. The present research uses Land Surface Temperature (LST) data from MODIS sensors for studying foehn events and their effects on MDV surface temperatures over a large area (valley-wide). The present study aims to build on the past research on the meteorology of the region using observation data from satellite remote sensing while answering the research question mentioned above. Stated below are the research objectives for the current study:

Research Objectives

- Objective 1: To understand the trend in meteorological parameters across different time scales (inter-annually, seasonally, and diurnally). This is achieved by studying long-term meteorological data collected from the AWSs installed across MDV.
- Objective 2: To evaluate satellite LST datasets as a proxy for air temperature, check and correct the data for inconsistencies and errors. Also, assess the sensitivity of the datasets in registering daily temperature changes across the MDV floor.
- Objective 3: To develop a technique for detecting foehn events across MDV using satellite LST data for summer and winter that does not require meteorological data from AWSs.
- Objective 4: To study the changes in horizontal LST temperature gradient across different parts of MDV associated with radiative warming and/or to foehn-induced warming events.
- Objective 5: To identify the regions in MDV that are more susceptible to a higher degree of warming during a foehn event than the rest of the valley.
- Objective 6: To study the control of valley floor LST changes on stream discharge and identify the importance of radiative warming and foehn-induced warming events on glacial melt across the MDV.

Each chapter in the thesis addresses one or more of the research questions while performing the stated objectives. Every chapter in the thesis has its objectives and individual introduction, background, methodology, results, and discussions. The following section provides a summary of the work done in each chapter.

Chapter synopsis

Chapter 1 (Research question 1 and Objective 1)

The analysis focused on a long-term study over 18 years (2000-2017) of meteorological data collected from the 6 AWSs, to spatially investigate the current meteorological conditions (for the year 2017) and their trends over the 18 years, building on knowledge in Doran et al., (2002), Doran et al., (2008), Speirs et al., (2010) and Speirs et al., (2013). The chapter investigates the control of daily average incoming solar radiation and the total number of foehn hours during a day in influencing the daily average air temperature. It further explores the foehn events that occurred over 18-years of summer from the year 2000 till 2017 and the differences in meteorological conditions of a flood year and a non-flood year and their influence on the melt.

Chapter 2 (Objective 2)

Observation from a wider area is a requirement for studying the impact of foehn events across MDV. Satellite LST datasets provide observation over a large area across the MDV region. LST products from

MODIS sensors mounted atop Aqua and Terra satellite are used in the present study. Daily average LST data from the satellites at the location of the AWSs are compared with daily average air temperature collected from the AWSs for evaluating the accuracy and sensitivity of LST data in detecting day-to-day temperature changes in the valleys. Drawbacks and errors identified in the LST datasets are addressed and rectified for further use.

Chapter 3 (Objective 3)

Foehn detection technique previously developed is dependent on the use of meteorological data from the AWSs and provides a much-localized understanding of foehn events that might not be spatially representative. The study developed a technique that can detect foehn events in MDV using satellite LST datasets and is not dependent on meteorological datasets from the AWSs. The method developed detects foehn events in MDV over both summer and winter. The efficiency of the technique in detecting foehn events is evaluated using meteorological data from AWSs. The method developed can be used in the future over locations where there are no AWSs installed.

Chapter 4 (Research questions 2, 3, and objectives 4, 5)

The chapter initially investigates the surface temperature distribution at various MDV locations depending on their land surface, elevation, and location. Later, the chapter explores the changes in horizontal temperature gradient across MDV floor during a major foehn event to investigate the response of different locations in MDV to foehn events based on the event's time of onset and duration. It is hard to delineate the temperature rise due to foehn events from the temperature rise due to radiative warming during summer. The chapter identified specific meteorological conditions associated with foehn events over 13 years and characterizes which regions in MDV are more susceptible to temperature rise during foehn events than the rest of the valley. These helped identify the areas primarily affected by foehn events and show higher warming than the rest of the valley.

Chapter 5 (Research questions 4 and Objective 6)

This chapter investigates meteorological control over the region's hydrology by studying the influence of valley floor LST changes on the region's stream discharge. It identifies a threshold for daily average LST value that indicates conditions favourable for glacial melt and later recognizes the regions with temperatures above the threshold for most days, showing areas in MDV with conditions favorable for glacial melt. The chapter later investigates the LST changes, influenced by foehn's events, affecting the streams' discharge rates. The study delves into the importance of incoming solar radiation and foehn hours in controlling the glacial melts and eventual stream discharge by comparing the meteorology and streams discharge of two flood years experiencing different foehn hours.

Chapter 1: Climatology of the McMurdo Dry Valleys

1.1. Introduction

Long-term climate studies of the MDV show high variability in meteorological conditions within the valley system; for example, there is a gradient in temperature and precipitation from the maritime end of the valleys (near the Ross Sea Region) towards the Antarctic Plateau (which exhibits more continental conditions); this has been investigated for Taylor, Wright, and Victoria valleys (Doran et al., 2002). The contrast in meteorology within a valley can be such that Lake Bonney AWS, located in Taylor valley, can have a temperature difference of about 15°C from Lake Fryxell during summer and 30°C during winter (Figure 1.1). Due to the meteorological gradients, the spatial representativeness of data collected from each AWS can be an issue (Colacino & Stocchino, 1981). Many multi-scale factors are at play in producing meteorological variation, ranging from synoptic-scale circulation patterns that can influence wind velocity and temperature at a large scale and force airflow in the valleys, to the creation of microclimatic zones during certain weather conditions (typically low wind speed and significant radiative heating/cooling). During summers, solar (short-wave) radiative forcing (diurnal cycles in radiative heating) controls the hourly to seasonal changes in temperatures across the valley. Albedo (short-wave reflectivity) has a significant influence over the surface temperature, producing heterogeneities in the surface temperature depending on the spatial scale of the land-surface elements (Bliss et al., 2011). In addition, cloud cover, elevation, and aspect play a significant part in determining how much radiation is available for warming a location. An area's incoming solar radiation is often disrupted by terrain shadow and cloud cover (Katurji et al., 2013). Infrequent foehn events associated with strong synoptic-scale climatic conditions over the Ross Sea region add to the meteorological variability across the MDV surface. They cause the valley floor's rapid warming and change the meteorological conditions, which may last between few hours to days.

To better understand the variability of the meteorological parameters and their current trends, a long-term study of the meteorological conditions is necessary over different time scales (inter-annual, seasonal, and diurnal). This chapter is a synthesis of knowledge gained from a literature search augmented by new data analysis of the LTER dataset performed for the research project.

Objectives of this chapter

i) To present long-term trends in surface meteorological parameters at diurnal, seasonal, and inter-annual scales across the MDV (over 18 years across 2000 to 2017) across different locations in MDV and study the response of one meteorological variables to the changes in the other.

ii) To understand the degree to which the radiative heating (incoming solar radiation; ISWR) and foehn-induced warming control the valley's near-surface temperatures and drive the melting rates and stream flows. In particular, to compare and contrast the meteorological dynamics and their influence on hydrology for a non-flood and a flood season.

Figure 1.1 shows the Landsat True Colour Composite (TCC) of the MDV (derived from LIMA) region along with the location of the AWSs used in the thesis. The conglomerate structure of the various land surface types can be identified from the image. The major land surface types include ice-free barren lands, exposed rocks, major lakes, glaciers, and snow cover regions in the MDV (Marchant & Head, 2007). The visual interpretation of the satellite image shows a rugged terrain with uneven surfaces of varied elevations. Terrain shadow can be observed as dark patches on the surface due to lack of illumination from incoming solar radiation as they get disrupted by the rugged terrain.

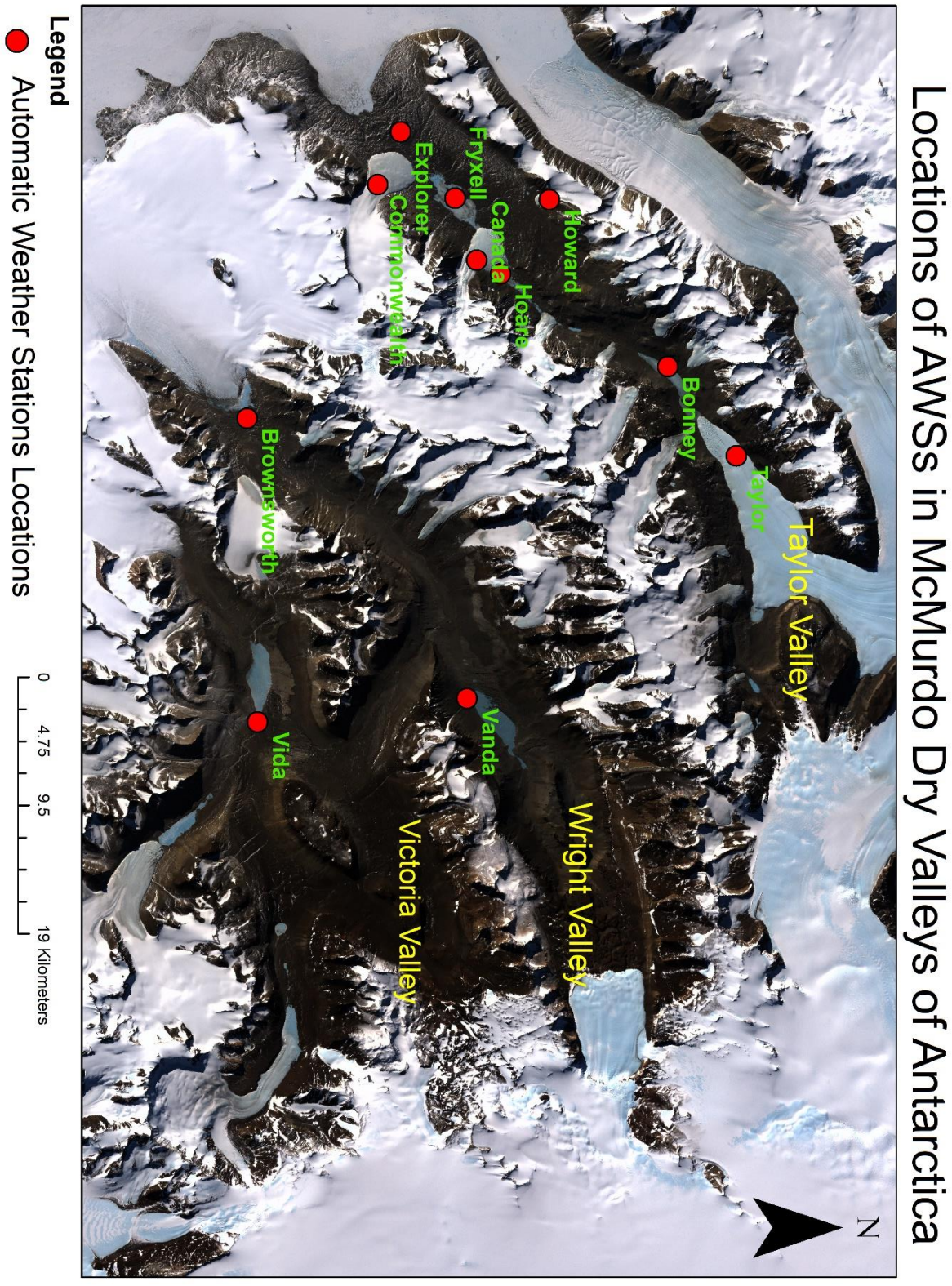

Figure 1.1 Location of the AWSs across MDV.

1.3 Context

The Transantarctic Mountains typically block the precipitation-bearing cyclonic (low pressure) storms that migrate south over the Ross Sea region and rarely reach the MDV. The valleys are characterized as polar deserts with annual total precipitation of less than 100 mm per year (Doran, McKay, et al., 2002). Despite low precipitation, seasonal streams that support the microbial ecology are generated due to glacial melt over the summer. The streams feed the lakes in the valleys and are the region's biodiversity hotspots. The life forms that have found a niche in the harsh conditions of the MDV include cyanobacteria, diatoms, heterotrophic bacteria, and mosses in the streams and phytoplankton in the lakes. Valley floor soil can support heterotrophic bacteria, nematodes, tardigrades, and rotifers (Fountain et al., 1999; Takacs-Vesbach et al., 2010; Zeglin et al., 2009). These lifeforms can only flourish in the presence of liquid water from the glacial melt (or other sources) and warmer temperatures during the summer.

The glacial mass balance is controlled by residual energy of the Surface Energy Balance (SEB), which causes sublimation and glacial melt during summers (A G Fountain et al., 2006) (Section 1.3.2, equation (ii)). Liquid water available in the valley's soil from snowmelt varies between sites and ranges from 1.7 – 3.4 cm per year (Hunt et al., 2010). The water retained by the soil during the summer is lost due to evaporation and sublimation depending on the depth of water infiltrated (Hunt et al., 2010). The maximum streamflow in MDV occurs over 6 to 12 weeks of the summer (Cozzetto et al., 2006), and the discharge rates of the streams depend on the changes in meteorological conditions in the valley during summer (Conovitzl et al., 1998). Thus, the meteorology in MDV directly controls the hydrology and biodiversity of the region.

While there is an increase in air temperature of the Earth's surface by 0.06 ℃ per decade during the 20th century (IPCC, 2001), the MDV has shown a negative trend. Contrary to popular belief and model predictions showing polar warming, MDV has cooled by 0.7 ℃ per decade between 1986 and 2000 (Doran, Priscu, et al., 2002). The MDV surface's cooling trends make it intriguing to study the region's meteorology and further explore these decadal meteorological changes with more research. Past research on the regions' meteorology was mostly based on the data collected from AWSs and modelled data from Polar WRF. Some of the previous findings are discussed below.

1.3.1 Air temperature

Air temperature (Ta) across MDV varies between the three major valleys (inter) and within a valley (intra). Out of the three major valleys, Taylor valley is the warmest, followed by Wright and Victoria (Doran, McKay, et al., 2002). The seasonal trend in Ta is controlled by yearly solar forcing, with maximum air temperatures observed over summer, while the diurnal and daily trends are influenced by

incoming solar radiation (in summer) and bi-modal wind regime of westerly winds from the direction of Transantarctic mountains and easterly winds from the Ross sea's direction region.

During the winters, Ta's fluctuations are influenced by MDV's wind regime in the absence of radiative warming. A sharp increase in Ta occurs during intense westerly wind events that last between few hours to days. During these events, the local Ta across MDV can increase by 30°C during winters (Land et al., 2004) and can reach up to 8°C during summers. The strong westerly flows are due to foehn events which were previously thought to be katabatic winds. These winds extensively influence Ta across MDV; for example, Ta at Lake Bonney can be 15°C warmer during summer and 30°C during winter compared to Lake Fryxell, located in the same valley roughly 16 km apart (Doran et al., 2002). The temperature difference results from differential interaction of the terrain with warm foehn wind descending from the Transantarctic mountains. Similar conditions are observed when there is a high-temperature difference between two ends of Wright valley, with Vanda showing 25°C warmer temperatures than Brownworth and Brownworth, sometimes being 32°C warmer than Vanda (Doran, McKay, et al., 2002). Cold pools formed at the bottom of the valleys cause the warm westerly wind to override them without affecting the cold valley floor temperatures. Occasionally strong westerly flow breaks into the cold pools introducing warmer air from the upper atmosphere (McKendry & Lewthwaite, 1992) to the valley.

Incoming solar radiation during summer influences the Ta and wind conditions across MDV (Colacino & Stocchino, 1981). Incoming solar radiation causes radiative heating of the valley floor. Changes in zenith and elevation angles of the sun influence the diurnal changes in the temperature during the day; also, topographic shading due to low solar elevation can significantly decrease a shaded region's temperature (Katurji et al., 2013). During summer, overcast periods disrupt the incoming solar radiation from reaching the valley floor while decreasing radiative warming and associated air temperatures.

1.3.2 Surface Radiation Balance (SRB)

Incoming radiation is the amount of energy received by Earth's surface in the form of short-wave radiation from the sun and longwave radiation from the atmosphere. Outgoing radiation is the amount of energy reflected and (re)radiated by Earth's surface in the form of reflected short-wave radiation and emitted longwave radiation. Net radiation is the difference between incoming and outgoing radiation that results in the heating of Earth's surface and the atmosphere. The net radiation, Q*, is given by the radiation balance equation.

$$Q^* = K\downarrow - K\uparrow + L\downarrow - L\uparrow \ (W/m^2) \qquad (i)$$

Where K and L represent short and longwave radiation respectively. Net radiation available at a site depends on the balance of the net short and longwave radiation components. The total amount of short-

wave radiation reflected from a surface is directly proportional to the surface's albedo. MDV floor is a patchwork of the glaciers, ice, perennially ice-covered lakes, large panels of bedrock, and sandy, gravelly soils. Depending on the land surface type, each location's surface albedo is different, affecting the net radiation budget at each site and causing differential warming of each area. Net radiation is responsible for heating the valley floor, especially the barren landscape (Lacelle et al., 2016). In MDV, most of the AWSs are not equipped to measure net radiation at a location. Thus, to understand the influence of radiative warming on temperatures across MDV, incoming short-wave radiation is the only measurement available that gives an insight into how much radiation is received by the surface.

The amount of direct radiation received by the MDV glaciers influences their melt and eventual stream discharge (Conovitz et al., 1998). The stream gauges' data show that the stream flows are strongly related to incoming short-wave radiation; the highest stream discharge during a day occurs around the same time as maximum incoming short-wave radiation. The difference in incoming solar radiation between locations can cause variations in glacial melt across the regions. The vertical terminal cliffs of the glaciers can have higher or lower melt rates than the horizontal surfaces due to differences in incoming solar radiation (Hoffman et al., 2016). Incoming solar radiation is responsible for diurnal and seasonal variability in air temperatures and wind regimes (easterlies), thus indirectly affecting MDV turbulence (Colacino & Stocchino, 1981). The incoming radiation at a location is affected by frequent cloud cover (Doran, McKay, et al., 2002) and topographic shading (Katurji et al., 2013). Topographic shading controls the region's surface heating and provides a good laboratory for studying the thermally forced circulations during the summers (Lewthwaite et al., 1990). Cloud cover disrupts incoming radiation and influences the temperatures across MDV, and they are known for delaying the response of surface temperatures to solar control (Katurji et al., 2013).

There has been a trend of increasing incoming solar radiation, which is related to cooler and less cloudy conditions in MDV over a period of 15 years from 1986 to 2000 (Doran et al., 2002), with mean annual incoming short-wave radiation ranging between 73 to 117 W/m^2, and the daily mean incoming short-wave radiation in the summer tends to be around 300 W/m^2 (Bliss et al., 2011). The outgoing short-wave radiation depends on the surface's albedo, which varies with Snowfall, cloud cover, solar zenith angle, and the ice surface's nature (Bliss et al., 2011).

The energy fluxes responsible for warming the Earth's surface and atmosphere and changing the state of water are given by the Surface Energy Balance (SEB). The term surface energy balance is specifically used to describe the balance between all surface energy inputs and outputs over a given interval of time. The surface energy balance is the sum of all energy fluxes at a surface and is represented by :

$$Q^* = GHF + SHF + LHF \ (W/m^2) \quad \text{(ii)}$$

Where GHF is ground heat flux, SHF is sensible heat flux, and LHF is latent heat flux. During summers, as the ice temperatures get closer to the air temperatures, the sensible heat flux responsible for convective heat transfer from the surface to the atmosphere reduces in magnitude but stays positive (transfer of heat from atmosphere to surface) over the ice surface. The land surface and air temperature differences are higher over the ice-free valley floor (barren surface), which causes an increase in sensible heat flux over the land (Bliss et al., 2011). The latent heat flux, responsible for the change of state of water, almost always stays negative (transfer of heat from surface to atmosphere) and increases during the summer (Bliss et al., 2011). Ground heat flux is absorbed into the subsurface during summer and radiated out during the winter. The maximum magnitude of ground flux is usually smaller than the latent and sensible heat flux components (Bliss et al., 2011).

Apart from influencing other meteorological parameters (wind velocity, air temperature), the radiative fluxes also have other physical influence over the MDV surface. Radiative fluxes affect the lakes' limnology in MDV by controlling the temperature, ice thickness, and the lake level rise and fall (Dowling et al., 2014). The energy balance components (latent heat and net radiation) contribute to the temperature difference between the lakes located in the same valley and the water column rise and fall due to inflow (Ragotzkie & Likens, 1964).

1.3.3 Wind speed and Direction

MDV has a bi-modal wind pattern of westerlies (wind from the direction of Transantarctic Mountains) and easterlies (winds from the Ross Sea region direction). The westerly and easterly winds show a diurnal arrangement in time of occurrence. Easterlies occur less during the morning hours and higher during midday and evening, whereas calm events and westerlies are more frequent during the early morning hours (Doran et al., 2002). Studies indicate a spatial variability in the occurrence of easterly and westerly winds within a valley, with easterly winds being more frequent on the eastern end of the valley, while westerly winds predominate the western end (Lewthwaite et al., 1990). Apart from diurnal and spatial patterns, there is a seasonal trend in the wind regime; the easterlies (sea or ice breeze) are more frequent during summers, while the westerlies are more frequent and stronger during the winters. During the summertime, the wind flows are dominated by thermal forcing, which generates easterlies. The cold and moist easterlies run across the valley floor and their flow is disrupted and pushed down by strong warm westerlies developed in the polar plateaus. The boundary between westerly and easterly flow drifts up and down the length of the valley, and with its passage at any single location, there occurs a complete reversal in wind direction and a marked change in temperature and humidity (Lewthwaite et al., 1990).

At times, westerlies can be observed at the downslope stations and not at the upslope stations (especially in the Wright valley). This happens when the westerly winds over-ride the cool easterlies which occupy

the valley floor at lower altitudes (Doran, McKay, et al., 2002; Lewthwaite et al., 1990), while only the strongest of the westerly flows penetrate through the easterlies and reach the eastern end of the valley (McKendry & Lewthwaite, 1992). Interactions of the westerly and easterly winds are often associated with the formation of vertical structures of wind and temperature (they influence the static stability), easterlies form the bottom of the inversion, and moderately strong westerlies override the easterlies (Lewthwaite et al., 1990). It was previously thought that the vertical wind profiles during westerlies are similar to those associated with shallow foehn, katabatic surges, bora, and boulder windstorms (Lewthwaite et al., 1990), but the wind regime's spatial and temporal patterns supported the idea that the westerlies may not be katabatic surges but aerodynamically deflected upper-level winds that produce foehn effects (McKendry & Lewthwaite, 1992). Past research suggested that the foehn mechanism is responsible for the strong westerly wind events in MDVs and that the influence of katabatic surges from the polar plateau is minimal (Speirs et al., 2010; McKendry & Lewthwaite, 1992).

Taylor valley and Wright valley have similar bi-modal wind regimes of westerlies and easterlies. Meteorological data showed that the upper valley region of Taylor valley near Lake Bonney is warmer and windier (Doran, McKay, et al., 2002) than the lower end region around Lake Fryxell. The interaction of westerlies and easterlies in Nussbaum Riegel's presence, which diagonally bisects the valley at approximately 20 km inland, enhances the meteorological differences between the two parts of the valleys by largely confining the effects of the westerly wind to the western part of the valley and coastal winds (easterlies) to the eastern parts of the valley (Fountain, et al, 1999). Victoria is the coldest of the three major valleys. It only experiences the severest of the westerly wind flows. It allows the formation of cold pools and strong, stable boundary layers across the valley floor, which are resistant to all westerly flows except the strongest ones. During the summer months at Lake Vida, winds are predominantly from the coast, and during the winters, there is almost a complete absence of an easterly wind, and average wind speeds are lower from all directions in all seasons (Doran, McKay, et al., 2002).

The westerlies occur infrequently compared to easterlies during summer, and they cause an increase in air temperature and the number of degree-days above freezing point across MDV. The warming effects lead to the rise in the glacial melt which increases the streamflow in MDV. The year 2001-2002 summer had high-frequency westerly winds, which led to high glacial melt and eventual flooding of the streams (Doran et al., 2008) (figure 1.9). Westerly winds transport snow from the valley walls, glaciers, and occasionally from the Antarctic Plateau and accumulate it in the valley floor. There is a positive correlation between the snows accumulated in a region with the frequency of westerly wind experienced by that region (Fountain et al., 2009). Westerlies are suspected of having significant effects on the landscape forming process of MDV (Doran et al., 2008), which include rock weathering, Aeolian processes (Bourke et al., 2009), and biological productivity (Doran et al., 2006 ; Katurji et al., 2019).

1.3.4 Foehn events

The driving mechanism behind the foehn winds in MDV is the strong synoptic pressure gradient across the Transantarctic mountain region generated because of cyclonic activities in the Ross sea region that causes topographically modified south-westerly winds across MDV (Speirs et al., 2010; Speirs et al., 2013b). Foehn winds are associated with strong pressure gradients generated over the Transantarctic mountain ranges. Foehn events are common in MDV as the Amundsen/Ross Sea region is climatologically favoured for cyclonic activities, with a consistent high frequency of cyclogenesis and cyclolysis (Carrasco et al., 2003; Speirs et al., 2013a). Due to the strong influence of foehn events over the MDV's meteorological conditions, the intensity and track of cyclonic activities in Ross and the Amundsen Sea act as major contributors to climate variability in MDV (Speirs et al., 2013a). Foehn winds, previously thought to be katabatic winds, are more frequent in winter (5–55% per month) than summer (1–11%) (Turner, 2004). There is a spatial pattern in the westerly events' occurrences; a 14% increase in the frequency of westerly winds can be observed for every 10 km up the valley toward the Transantarctic Mountains (Land et al., 2004). Foehn events experienced by each location in MDV is different from the other. It is due to the topographic effect, the angle at which the wind enters the valley, local convective turbulence, and the presence of a cold pool, such that sometimes the down valley stations experience foehn before the upper valley stations (Speirs et al., 2010; Doran et al., 2008).

Foehn winds are warm, dry, and strong winds that form over the leeward side of mountains or a major hill. Foehn winds can be observed globally. The term "foehn" (or "föhn") is derived from the winds over the lee of the European Alps, but numerous other names have been given to similar winds around the globe (Sharples, 2018). In the Rockies, the foehn winds are generated because of a steep pressure gradient; as the air encounters the mountain barrier, it converges and is forced to ascend and cool. If the dew point of the air is reached, condensation occurs, resulting in precipitation primarily on the windward flank. After crossing the mountains, the dry air diverges and flows down the leeward slopes, warming adiabatically and drying as it descends. These dry, warm winds blow out across the prairies and obtain very high speeds when the regional pressure gradient is large (*foehn - an Overview | ScienceDirect Topics*, n.d.).

A generalized mechanism of foehn events across MDV was explained previously (Steinhoff et al., 2013), which states foehn as a sequence of mesoscale processes. A gap flow forces the air into the MDV and is accelerated by mountain waves to flow at low levels; the pressure-driven channelling brings the warm, dry air down the valleys. Easterly winds during foehn events are independent of their diurnal cycles and are primarily caused by flow deflection around Ross Island, as localized pressure gradients counter pressure-driven channelled westerly flow over the MDVs (Steinhoff et al., 2013). Foehn winds can be slowed or forced from the ground by phenomena that are similar to hydraulic jumps (Steinhoff et al., 2013).

Foehn events over MDV have a specific climatic signature. The foehn onset is identified by an increase of wind speed above 5 m/s from a south-westerly direction, a rise in air temperature by at least 1°C/ hr, and a decrease in the value of relative humidity by at least 5% /hr (Speirs et al., 2010). A foehn day is a day that experienced at least six or more hours of foehn conditions (Speirs et al., 2010). Taylor and Wright valley are more susceptible to foehn events, and even the weakest events can be detected by the AWSs located in these valleys, while Victoria valley only experiences the stronger foehn events which last for days (Doran, McKay, et al., 2002).

1.4 Data

The data collected for the study is between the years 2000 till 2017 from the 6 Automatic Weather Stations (AWSs) installed across MDV as a part of McMurdo Dry Valley Long Term Ecological Research (LTER) Network (Doran, McKay, et al., 2002). The LTER project is an interdisciplinary study of the aquatic and terrestrial ecosystems across the MDV. In 1992, MDV was selected as a study site within the National Science Foundation's LTER Program (*McMurdo Dry Valleys LTER*, n.d.). The meteorological data used in the study includes 15 min interval data, which are calculated by averaging the samples taken over the 15 min interval for each meteorological parameter (*MCM LTER Data File Format Protocols for Database Submission | McMurdo Dry Valleys LTER*, n.d.). The data used for the study are listed below.

- Incoming Shortwave Radiation (ISWR)
- Air Temperature (Ta)
- Relative Humidity (RH)
- Wind Speed (WS)
- Wind Direction (WD)
- Soil Temperature (Ts)
- Precipitation (PPT)

Valley	Inner valley AWS	Centre valley AWS	Outer valley AWS
Taylor Valley	Bonney (elevation: 64.3m)	Fryxell (elevation: 19m)	Explorer (elevation: 25.7m)
Wright Valley		Vanda (elevation: 296.1m)	Brownworth (elevation: 279m)
Victoria Valley		Vida (elevation: 351.90m)	

Table 1.1 AWS selected from each valley for the study.

Table 1.1 shows the AWSs selected from each valley for the study, along with their elevation (Figure 1.1). Taylor has the highest number of AWSs installed among all the three valleys, and each station is installed at a distinct location representing a specific meteorology. AWSs selected are located over the barren surface type or on the side of a lake and not on an ice surface as they may introduce glacial wind to the observation (Speirs et al., 2010). Five of the AWS (Bonney, Brownworth, Vida, Vanda, and Fryxell) are located near major water bodies, whereas Explorer is situated over the dry, barren surfaces. Not all the installed AWSs across MDV provide long-term data; some operate only for a short duration. AWS that provided long-term data were selected for ease of analysis, as they have shorter period of missing data, which helps in the long-term study of meteorology. The AWSs chosen covered a more expansive study area; the stations selected are located at the two ends of the valley, one towards the Transantarctic Mountains and the other towards the Ross Sea, to understand the variability of meteorology across the length of the valleys. Also, the stations chosen are mostly located on even (similar surface type) land surface, which would further help analyze the region's temperatures using satellite data.

Stream discharge data from 10 stream gauges (Chapter 5, Figure 5.2) are used to study the flow rates. The stream gauges used for the study are listed below.

- Aiken
- Andersen
- Canada
- Commonwealth
- Crescent
- Delta
- Green
- Harnish
- Vguerard
- Onyx_vanda

1.5 Methodology and Results

There can be large inter-annual variability in the summer climatology due to influences from ENSO (Speirs et al., 2013). Every summer season (between 1st of November till 28th of February) has its unique meteorological conditions across MDV, and multiple factors work together to influence the meteorological variability and glacial melts across the valleys. It is essential to briefly overview the meteorological conditions prevailing across MDV and understand their past and present trends while forming a base knowledge for the current research's objectives.

1.5.1 Meteorology across MDV

Data collected from six AWSs across MDV is used to study the temporal (interannual, seasonal, and diurnal) and spatial variability of the meteorological parameters across different MDV locations between the year 2000 till 2017. For some of the AWSs, meteorological datasets were unavailable for either the whole summer or for a short duration. Data unavailability while calculating seasonal averages for any of the meteorological parameters cause unwanted biases in the values. The summer seasons with more than one week of missing meteorological data were not used to calculate seasonal averages. Appendix Table: 1 shows the number of days of missing meteorological data for each season from the six AWSs. Recent available meteorological datasets are from the year 2017-2018 summer; the data from the season is used to study the recent trend in meteorological parameters across MDV.

1.5.1.1 Incoming Shortwave Radiation (ISWR)

Incoming short-wave radiation (ISWR) is the direct and diffuse solar radiation flux that reaches the Earth's surface; it is measured in Watts per meter squared, W/m^2 (Waters et al., 2002). ISWR includes ultraviolet, visible, and a limited portion of infrared energy (T.R.OKE, n.d.). It is responsible for the radiative heating of the Earth's surface and atmosphere. Clouds reflect part of ISWR, some parts are absorbed by the atmosphere, and some pass through the Earth's atmosphere and reach the surface. The part of ISWR reaching the Earth's surface is either reflected or absorbed by the surface. The amount of radiation absorbed and reflected by the surface depends on the surface's albedo, which varies depending on the land surface type. MDV valley floor is a conglomerate structure of various land surface types. Each land surface type has its albedo value, so the absorption and reflection of ISWR can vary across the region and cause differences in surface heating. Apart from albedo, the region's elevation and aspect also play a role in determining the ISWR it receives due to terrain shadow effects during low solar elevation periods.

Figure: 1.2 (a) shows inter-annual (seasonal average) changes in ISWR across 18-years of summer from 1st of November till 28th of February of each season for the 6 AWSs. The ISWR for Vida shows a sudden dip in the values for the season 2011-12 and 2012-13; it could be a result of persistent cloud cover over the region during the summer or due to malfunction of the ISWR sensor during this period as none of other AWSs show similar trend. For Taylor valley, Bonney AWS, located on the inner end of the valley towards the Transantarctic Mountains, persistently received lower ISWR than Fryxell and Explorer located at the valley's outer end towards the Ross Sea. For Wright Valley, Brownworth AWSs located at the outer end of the valley received the highest ISWR for most of the years than any other AWSs. Vanda, located in the same valley towards the valley's inner end, persistently received the lowest ISWR among all the stations. Table 1.2 shows the 18-year average ISWR from all the AWSs across the summer. The ISWR values are significantly different considering the values are average of 18-years of

summer. Explorer and Brownworth receive the highest ISWR among all the stations, while Bonney and Vanda are among the lowest. Yearly changes in ISWR and the 18-year average of ISWR show valley end stations close to the Ross Sea region (Brownworth and Explorer) receive higher ISWR for most years in comparison to inner valley stations. AWSs at the inner end of the valley toward the Transantarctic Mountains (Bonney, Vanda, and Vida) receive low ISWR; it could be due to more cloud cover over the inner end of the valley towards the Transantarctic Mountains than the region at the outer end of the valley towards the Ross sea region.

Stations	**Bonney**	**Brownworth**	**Explorer**	**Fryxell**	**Vanda**	**Vida**
18-year average incoming short-wave radiation in W/m^2	255.01	270.55	271.06	264.79	243.05	259.51

Table 1.2 18-year average incoming short-wave radiation for 6 AWSs

Apart from yearly changes, the ISWR varies seasonally; during winter MDV is devoid of ISWR, but during summer, the intensity of the ISWR increases. The tilt in the Earth's rotating axis does not change while it revolves around the sun, which causes seasons and parts of Earth's Polar Regions to get exposed to sunlight during a particular time of the year (MSFC, 2015). Figure 1.2 (b) shows the seasonal changes (daily average values) in ISWR over the summer of 2017-18 from the six AWSs. Explorer received the highest ISWR among all the stations during the period. The intensity of ISWR gradually increases at the beginning of summer and is highest roughly between the start of the second week of December till the mid of January (peak summer period). During the peak summer, there are stretches when the ISWR values are low, and this is due to the long duration overcast period over the region. The clouds disrupt the ISWR from reaching the MDV surface.

There is spatial and diurnal variability in ISWR received by each location in MDV. MDV is always lit (no nights) during summer; only the radiation's intensity changes throughout the day due to varying solar positions. The 24-hour composite average of ISWR (Figure 1.2 (c)) shows the diurnal changes in ISWR across all the 6 AWSs. ISWR gradually starts to increase roughly around 0500 Hrs (NZST) in the morning and reaches intensity greater than $400Wm^{-2}$, between 1300 Hrs to 1500 Hrs of the day, and gradually decreases in intensity. The lowest value of the ISWR is between 0100 Hrs and 0300 Hrs during the day's early morning hours. There is a variation in the time of maximum ISWR during a day among the AWSs; some of the AWSs (Vanda) attain peak ISWR earlier than the other due to the location of the AWSs. AWSs located in a more exposed area receives direct sunlight, while the ISWR received by some of AWSs near a mountain or a cliff is hinder by terrain shadow.

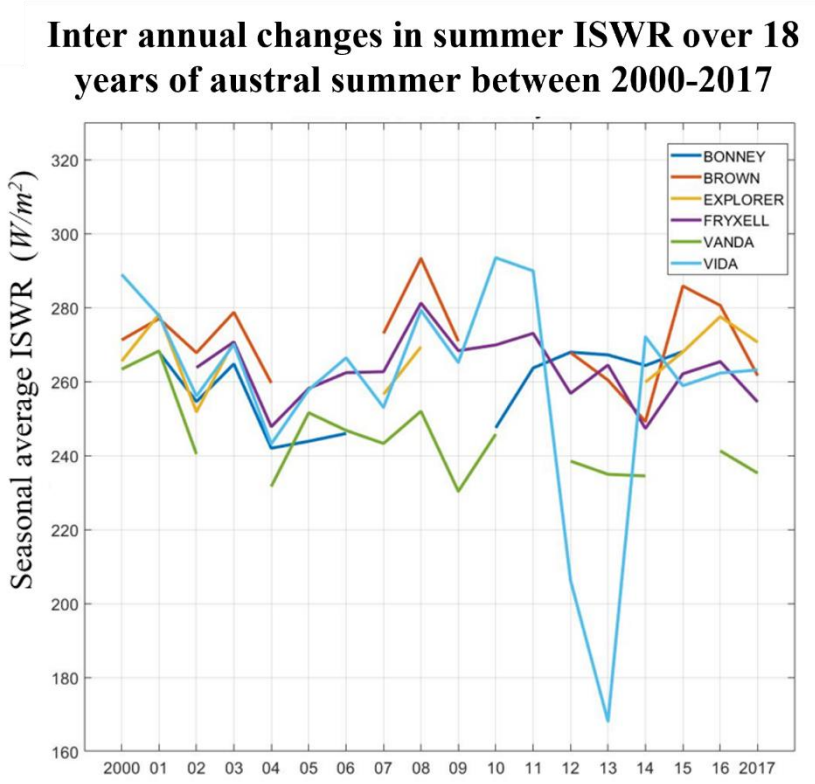

(a) Years: 2000- 2017

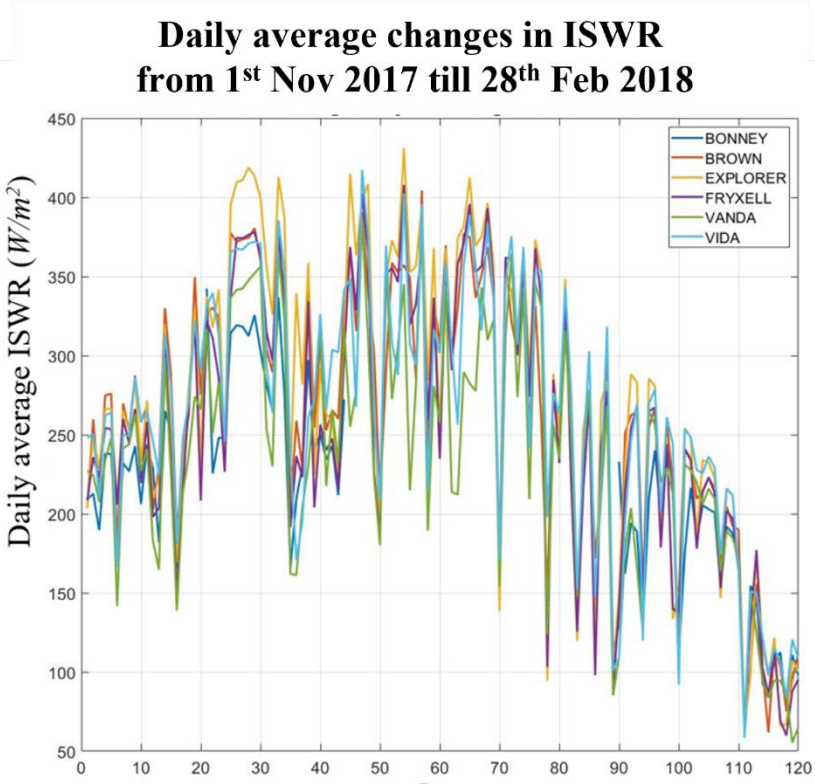

(b) Days: 1 Nov 2017 – 28th Feb 2018

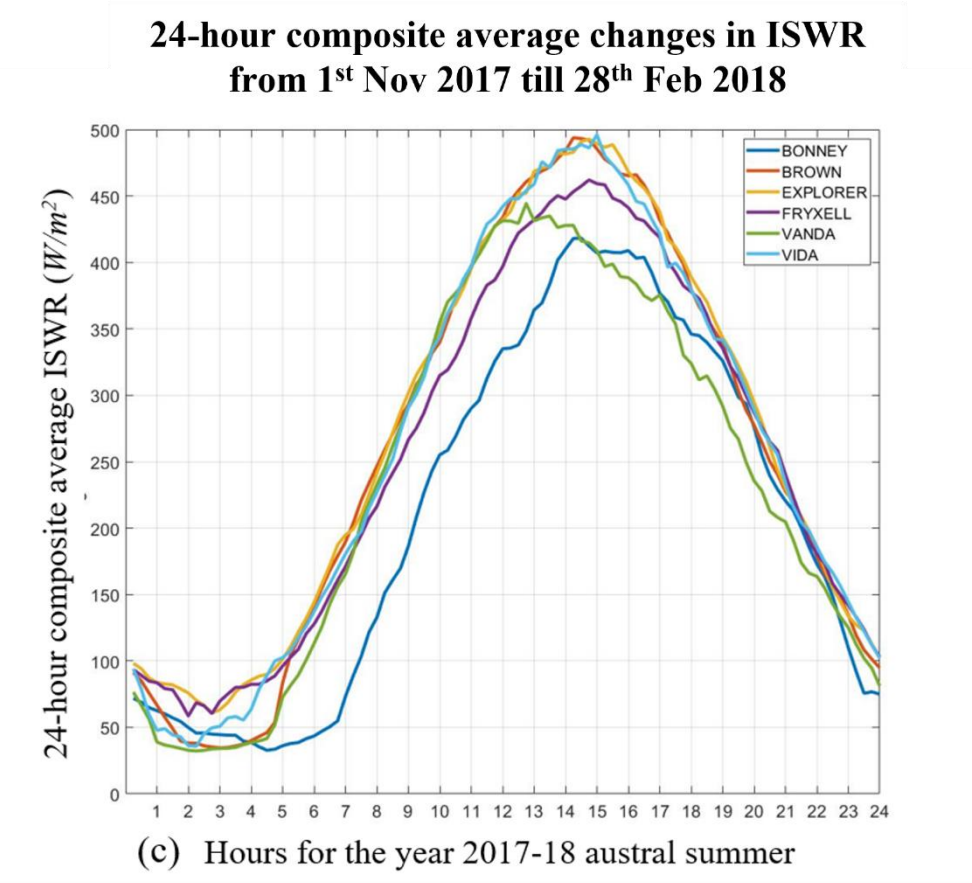

Figure 1.2 Incoming short-wave radiation across MDV at different time scales, inter-annual (a), seasonal (b), and diurnal (c).

1.5.1.2 Air Temperature

Factors that influence the Air Temperature (Ta) at a place are its location on the Earth's surface (latitude), Surface type (land surface type and smoothness), distance from the sea (coastal or inland), elevation, and radiative heating from solar radiation. Ta in MDV is also affected by the intensity and duration of the foehn events occurring in the valleys.

Figure: 1.3 (a) shows inter-annual (seasonal averages) Ta changes across 18-years of summer from 1st of November till 28th of February of each season for the six AWSs. In Taylor Valley, Bonney AWS, located at the inner end of the valley towards the Transantarctic Mountains, has persistently higher Ta throughout all the seasons than Fryxell and Explorer AWSs at the outer end of the valley near the Ross sea region. Though Fryxell and Explorer are neighbouring AWSs, Fryxell is farther from the Ross Sea region and has a higher seasonal average Ta than Explorer for most of the years. For Wright valley, there is a stark difference in the average yearly Ta of the two AWSs. Vanda, located on the inner end, records the highest temperatures among all the AWSs throughout all the years, except for the 2007-08 summer, while Brownworth, located at the outer end, has one of the lowest averages Ta among all the

AWSs. Vida in Victoria valley has a similar Ta range to those of the AWS s located on the outer end of the valley. Table 1.3 shows the 18-year average Ta for all the AWSs. Bonney and Vanda recorded higher Ta values among all stations. Both the AWSs are located at the inner end of their respective valleys towards the Transantarctic Mountains. In contrast, the stations located at higher proximity to Ross Sea regions like Explorer and Brownworth have comparatively lower average Ta throughout the 18 years. The regional differences in Ta among the AWSs can be due to their exposure to foehn winds; the inner valley stations experience higher foehn winds than those located on the valley's outer end. Other factors include elevation, land surface type of the region surrounding the stations of the station, and the ISWR they receive during the summer.

Stations	**Bonney**	**Brownworth**	**Explorer**	**Fryxell**	**Vanda**	**Vida**
18-year average air temperature in °C	0.3144	0.0576	0.0842	0.1210	0.5255	0.1698

Table 1.3 18-year average air temperature for 6 AWSs

Apart from the yearly changes, Ta also varies across the summer. Figure 1.3 (b) shows the changes (daily average values) in Ta across the summer for all the 6 AWSs over the summer of 2017-18 (1st Nov 2017- 28th Feb 2018). There is a significant increase in the daily average Ta for all the AWSs after the 2nd week of November. Vanda recorded the highest Ta throughout the season, whereas Brownworth and Explorer show the lowest Ta values during the peak summer (beginning of 2nd week of December till the end of 2nd week of January) when the ISWR is the highest. The Ta gradually increases at the beginning of the summer when incoming solar radiation causes radiative warming of the MDV surface. Ta is highest (near or above 0°C) roughly between the start of the 2nd week of December till the end of the 2nd week of January. The magnitude of Ta gradually decreases from the 3rd week of January following the decrease in ISWR

There is spatial variability in Ta across the valley floor due to the land surface, elevation, and ISWR received by a location in the valleys. The diurnal changes in Ta for each of AWSs show temporal and spatial variability across MDV. Figure 1.3 (c) shows the 24-hour composite average Ta from all the AWSs for the summer of 2017-18. Vanda experienced the warmest temperatures among all the AWSs at any time of the day. The diurnal changes in Ta follow the diurnal changes in ISWR and solar elevation at different times of the day. The lowest air temperatures are roughly between 0400 and 0700 Hrs (NZST), and the highest temperatures were roughly between 1300 Hrs and 1500 Hrs. Some of the stations (Explorer, Fryxell) show late response in reaching maximum temperature during the day, and some show earlier response (Brownworth) than the usual trend of the AWSs. The difference in time occurs due to variability in different stations' elevations; the higher elevation AWSs have more exposed surroundings (plain surface with no nearby terrain for shadowing) and receive more

ISWR than stations with lower elevation, which results in delay or rapid warming of an MDV location, causing different locations to have different time of peak Ta. The difference between the maximum and minimum air temperature between AWSs show stations located in the inner end of the valley (Bonney and Vanda) have higher temperatures (both max and min) than the stations with high proximity to the Ross sea region. This trend is opposite to ISWR received by the stations, which indicate higher ISWR received by station near the Ross Sea than those located near the Transantarctic Mountains.

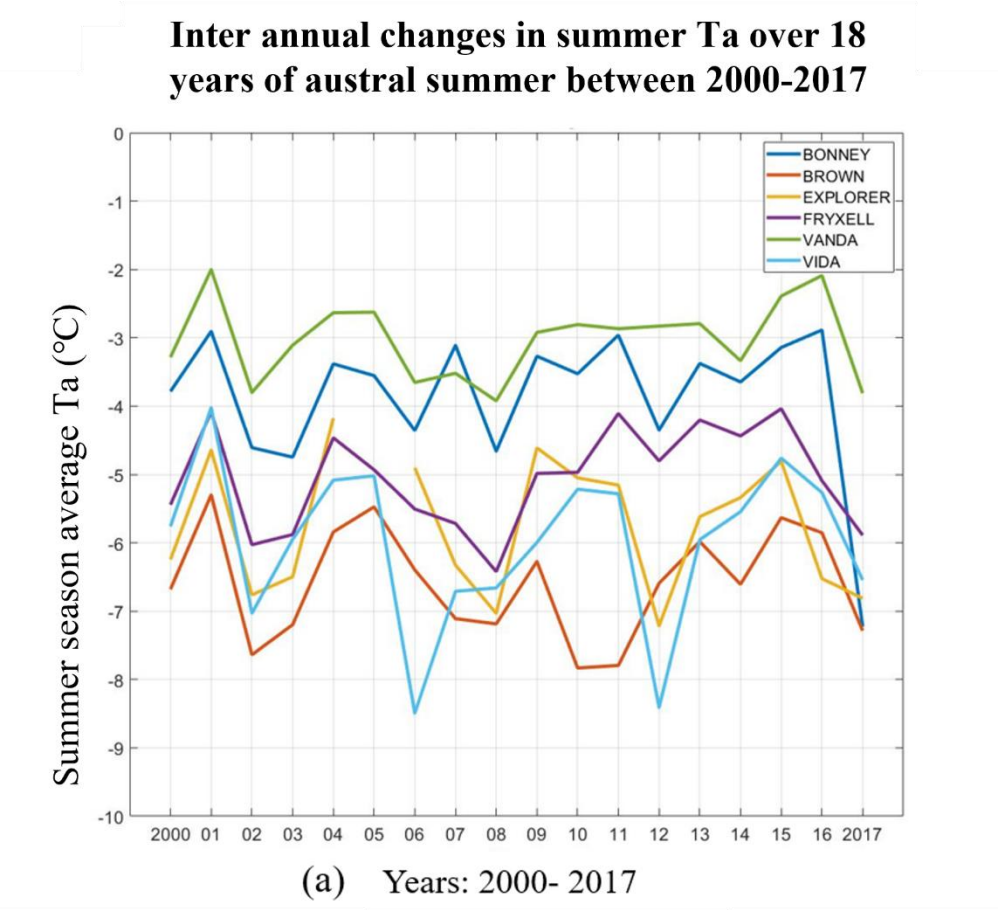

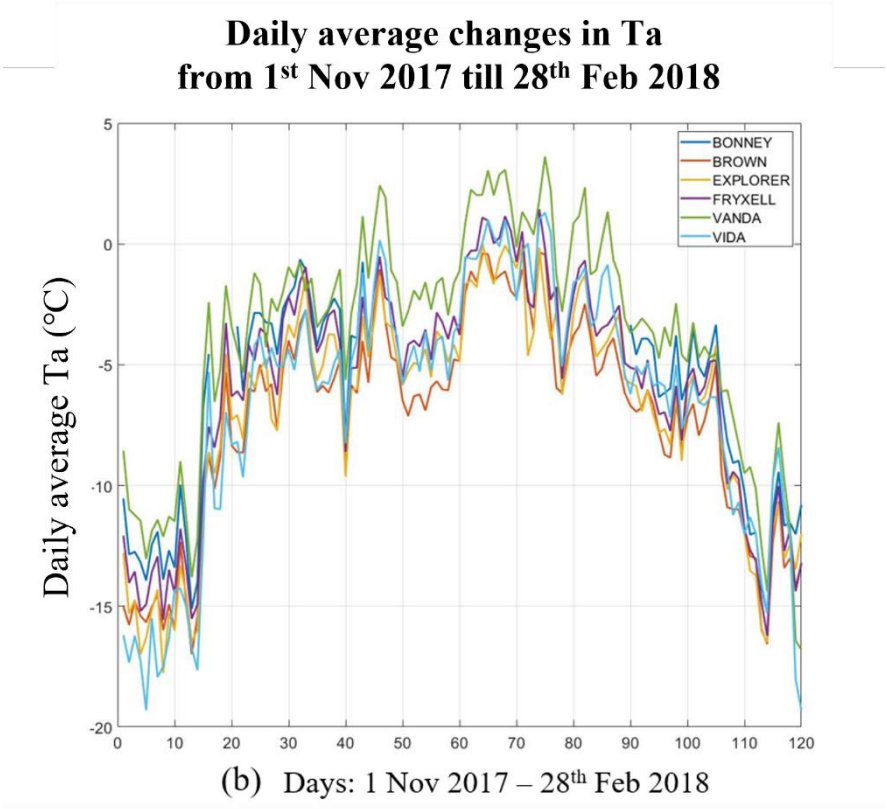

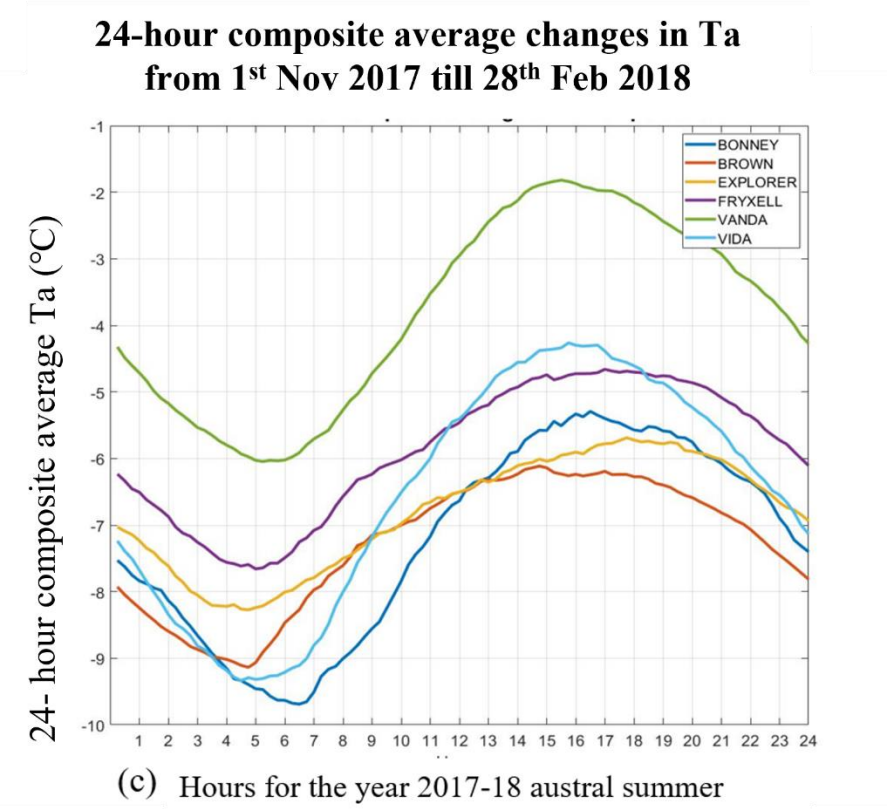

Figure 1.3 Air temperature across MDV at different time scales, inter-annual (a), seasonal (b), and diurnal (c)

1.5.1.3 Relative Humidity

Relative humidity (RH) is the ratio of the partial pressure of water vapour to the equilibrium vapour pressure of water at a given temperature. Relative humidity depends on the temperature and pressure of the system of interest. The same amount of water vapour results in higher relative humidity in cool air than warm air. The relative humidity is mostly low in MDV, but changes in RH values are an essential characteristic of foehn events occurring in the region. Low humidity values are often associated with foehn winds in the MDV.

Figure 1.4 (a) shows inter-annual (seasonal average) RH changes across 18-years of summer from 1st of November till 28th of February of each season for the 6 AWSs. Vanda distinctly shows the lowest RH value across all the years among all the stations, with values ranging between 40 -50 % RH, whereas Fryxell, Brownworth, and Explorer are among the stations with higher values of RH ranging between 55 to 75% across all the years. Vida and Bonney have RH values ranging between 45-65% RH. Years like 2001-02, summer shows a dip in the RH value for all the stations; these years experienced a high frequency of foehn events over the summer (Doran et al., 2008). Foehn events are associated with lower RH values, and thus, the seasonal average RH values for all the stations are low during the 2001-02 summer. Table 1.4 shows the 18-year average RH over the summers for all the AWSs. Vanda being the warmest station among all the AWSs, also happen to have the lowest RH. The AWSs located on the valley's outer end towards the Ross sea region show higher RH values than the AWSs located at the valley's inner end. The inner valley AWSs experience more westerly wind with low RH compared to the outer valley stations.

Stations	Bonney	Brownworth	Explorer	Fryxell	Vanda	Vida
18-year average relative humidity in %	54.62	63.85	66.95	67.14	43.82	55.57

Table 1.4 18-year average relative humidity for all AWSs

Figure 1.4 (b) shows the average summer season changes (daily average values) in RH for 2017-18 across the 6 AWSs. Explorer recorded persistently high RH followed by Fryxell, and Vanda had lower RH values throughout 2017-18. Apart from changes in RH values across summer, the RH does not show any significant trend in 2017-18.

Figure 1.4 (c) shows a 24-hour composite average RH of all the 6 AWSs for the 2017-18 summer. Explorer experienced higher RH values among all the AWSs at any time of the day. The diurnal changes in RH follow the clockwise changes in solar elevation throughout the day. RH values throughout a day are lowest during the peak hours of the day when ISWR (1300 to 1500 hrs) is maximum, and the RH values are highest over the period when ISWR is low.

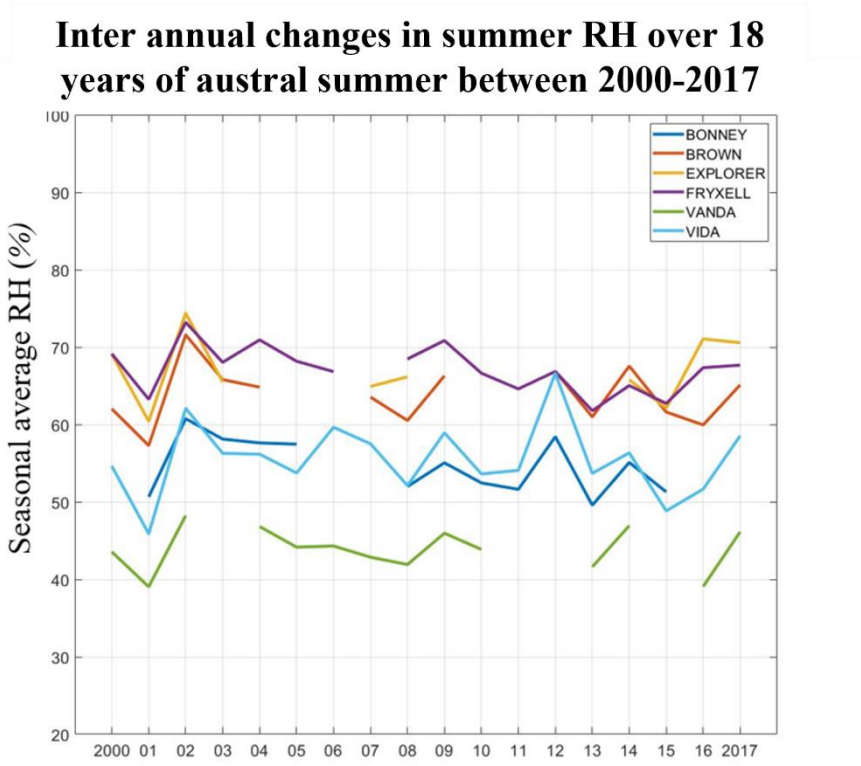

(a) Years: 2000- 2017

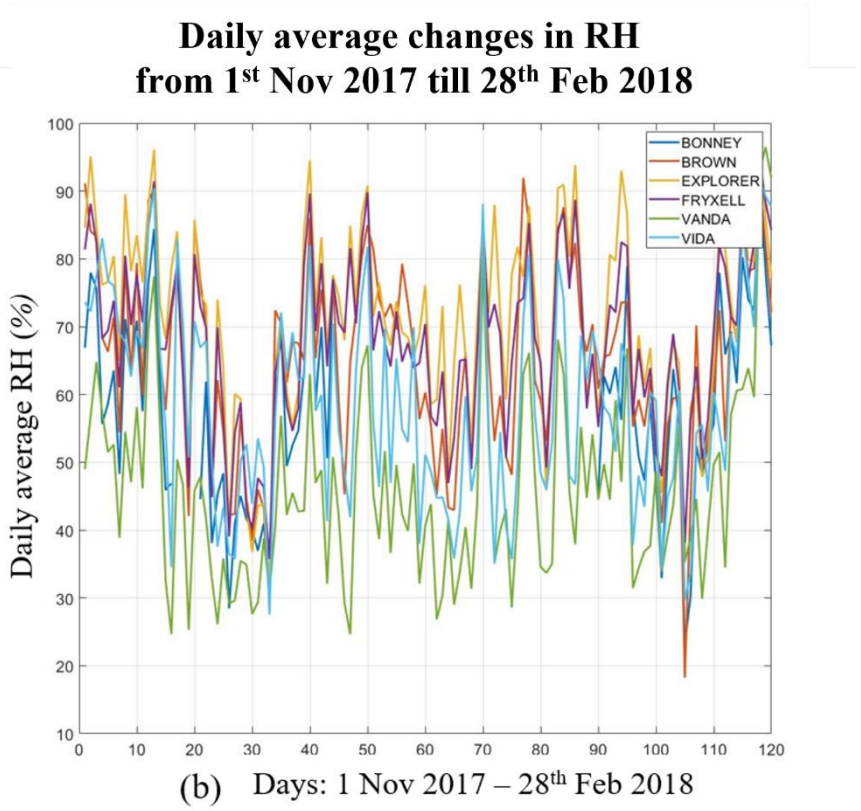

(b) Days: 1 Nov 2017 – 28th Feb 2018

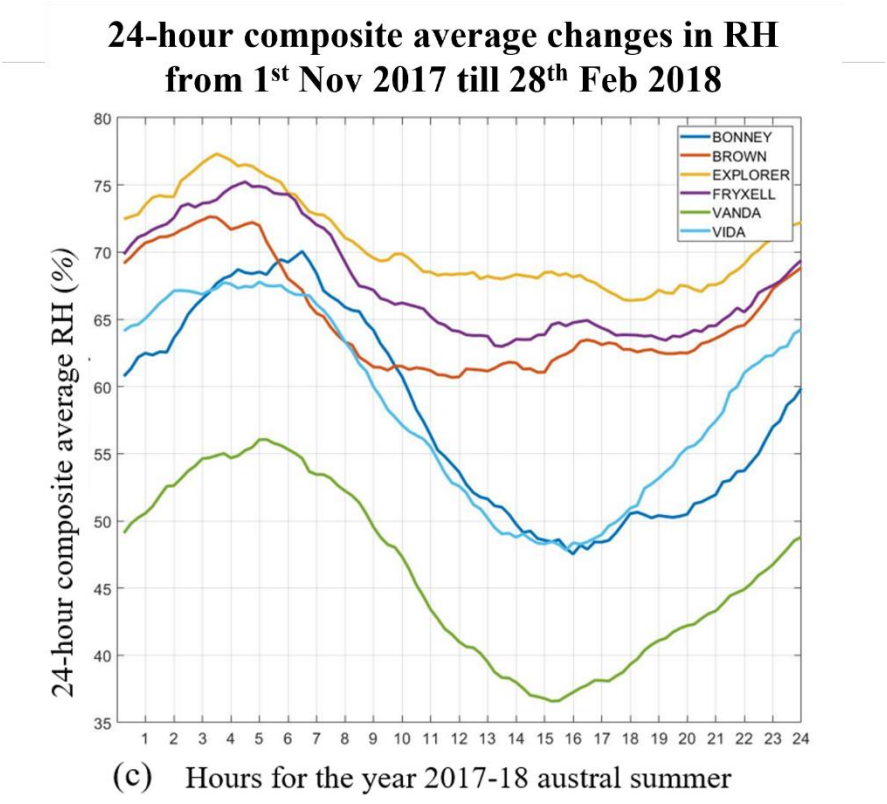

Figure 1.4 Relative humidity across MDV at different time scales inter-annual (a), seasonal (b), and diurnal (c)

1.5.1.4 Wind Speed and Direction

The bimodal wind regime of westerly and easterly winds over MDV influences the variabilities in air and surface temperatures across the valleys. The warm westerly wind from the Transantarctic Mountains and cold easterlies from the Ross sea regions interact with each other while influencing the valley floor temperatures. The long-term study of wind speed previously done identified a diurnal and seasonal pattern in the wind speed across MDV and their influence in modulating the meteorology of the region (Doran et al., 2002).

Figure 1.5 (a) shows inter-annual (seasonal average) Wind Speed (WS) changes across 18-years of summer from 1st of November till 28th of February of each season for the 6 AWSs. Vanda, Vida, and Bonney are some of the windiest stations in the valley and experienced higher wind (>4m/s) speeds in comparison to the others. Table 1.5 shows the 18-year average of wind speed values over the summer. Vanda being the warmest station among all the AWSs, also experience the highest wind speeds throughout the 18 years. Brownworth, Fryxell, and Explorer located at the outer end of the valleys towards the Ross sea region experienced lower wind speeds in comparison to the AWSs located in the inner end of the valleys towards the Transantarctic Mountains. The 18-year average wind speed values

across the 6 AWSs show significant differences in wind speeds over different locations across MDV surface.

Stations	Bonney	Brownworth	Explorer	Fryxell	Vanda	Vida
18-year average wind speed in m/s	4.45	3.90	3.52	3.81	5.50	4.83

Table 1.5 18-year average wind speed for all 6 AWSs

Figure 1.5 (b) shows the seasonal changes (daily average) in wind speeds. The wind speed shows seasonal changes with a gradual increase from the beginning of summer and being at the highest over the mid of summer and then gradually decreasing. There are sudden surges in wind speed when the values shoot up above 10m/s; these are often associated with foehn events in the valleys.

The 24-hour composite of wind speed (Figure 1.5 (c)) shows diurnal changes in the parameters, the wind speed increases around 0700 hrs (NZST) in the morning and reach a maximum (>4m/s) between 1500hrs and 2000 Hrs following the clockwise changes in the solar elevation throughout the day. The differential warming of the valley floor and the Ross Sea causes an easterly wind flow from the direction of the Ross Sea during the latter part of the day.

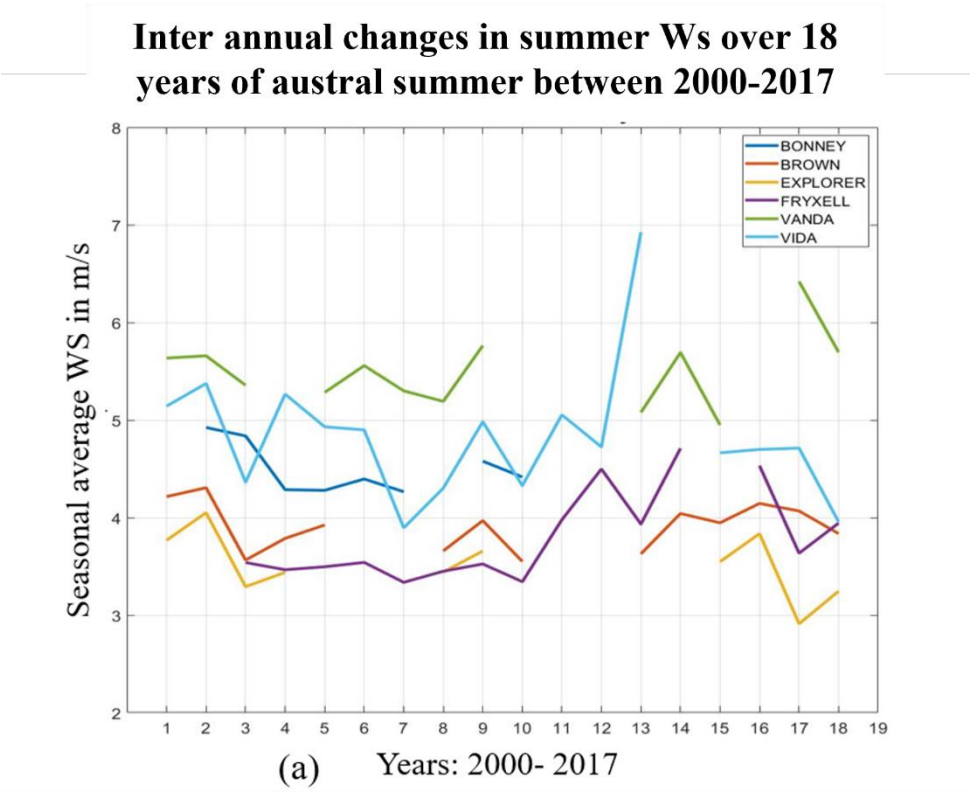

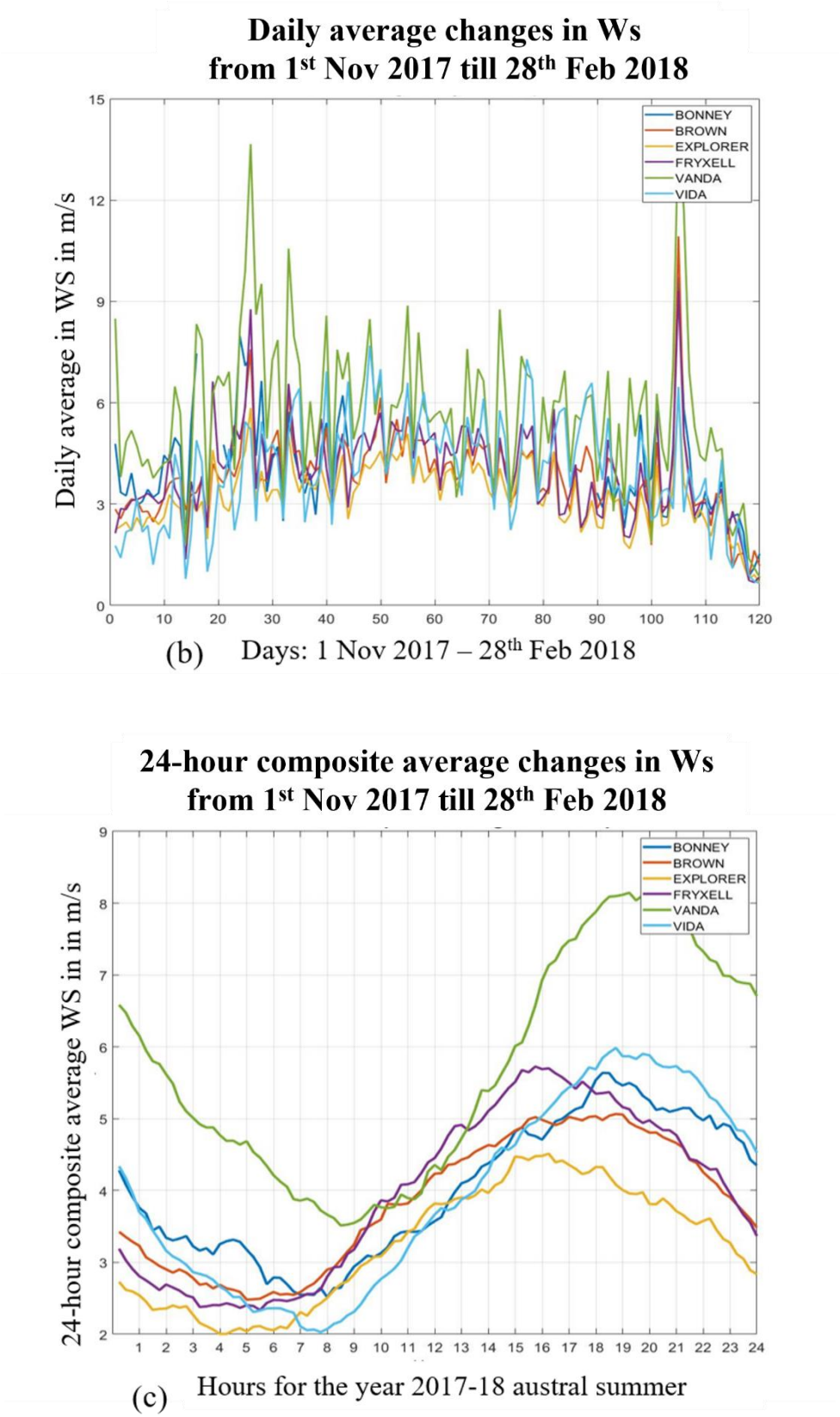

Figure 1.5 Wind speed across MDV at different time scales inter-annual (a), seasonal (b), and diurnal (c)

To better understand the direction of the wind during the period, a scatter plot between wind speed and direction is generated using 15 min interval data over the summer period. Bonney AWS has wind direction data missing during the peak summer period. Figure 1.6 shows Vanda is the windiest station among all the AWSs, with wind speed reaching up to 20m/s during a day. For most of the station the wind speed below 10m/s are from the north-easterly direction, whereas wind reaching over 10m/s are from the south-westerly direction. The high wind speeds from the south-westerly direction are mostly associated with foehn wind whereas a lower wind speed, north-easterly winds are the winds coming from the Ross Sea region.

The differences in wind speed and direction at different locations in MDV are due to the interaction of easterly and westerly wind with the valley floor. The station located towards the Transantarctic Mountains experiences a higher number of wind events (westerly/foehn winds) that are from the direction of the mountains, these events have high wind speeds and temperatures. On the other hand, the stations located near the Ross sea region mostly experience wind events (easterly) from the direction of the Ross Sea that is weaker and colder.

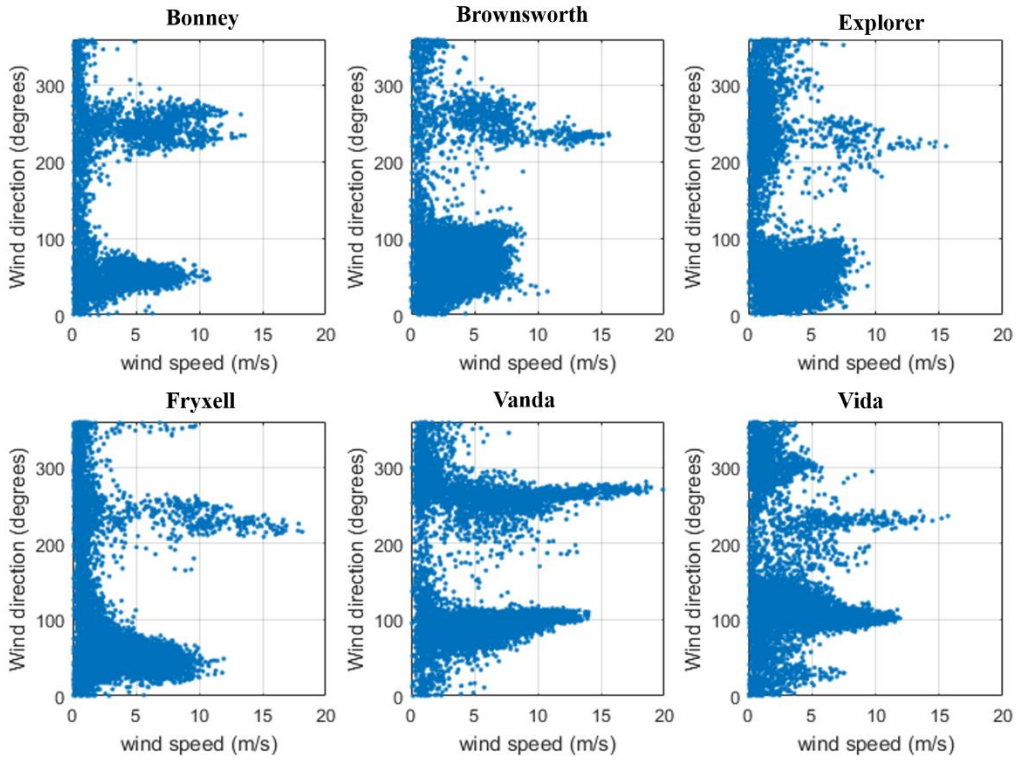

Figure 1.6 Scatter plot between wind speed and direction over 2017-18 summer from 15 min interval meteorological data.

1.5.1.5 Surface Soil Temperature

Soil temperature (Ts) at a location influences the physical, chemical, and microbiological processes in the soil. These processes may control the fate and transport of contaminants in the subsurface environment. In MDV, Ts influences the population of the polar (micro) organisms (Knox et al., 2017); thus, it plays a significant role in controlling the region's ecology. As our study is not on subsurface microbial life form and is mostly on the near-surface meteorology, the Ts at 0 cm depth is used for the study, which is more prone to meteorological changes in the valley floor. Ts at a depth of 0 cm can be assumed to be the surface temperature at the location of the AWSs.

Figure 1.7 (a) shows inter-annual (seasonal average) Ts changes across 18-years of summer from 1st of November till 28th of February of each season for the 6 AWSs. Bonney persistently had the highest soil temperatures and Vida the lowest among all the 6 AWSs. Table 1.6 shows the 18-year average Ts values over the summers. Bonney experienced exceptionally higher average soil temperatures (positive summer soil temperature) than all the other AWSs. Vida had recorded the lowest Ts values throughout the 18-years of summers. Victoria Valley is known to have longer durations of cold pool formation on its valley floor surface, which are not interrupted unless strong warm westerly winds reach the region and disrupt them; this causes the colder temperatures to persist longer over Victoria valleys' Vida AWS. On the other hand, Bonney is continuously susceptible to the westerly wind because of its proximity to the Transantarctic Mountains, increasing the region's temperature. The 18-year average Ts values over summers show a significant difference in the surface temperature values at different MDV locations.

Stations	Bonney	Brownworth	Explorer	Fryxell	Vanda	Vida
18-year average Soil temperature in ℃	2.07	-2.10	-0.7	-0.33	-0.77	-4.44

Table 1.6 18-year average soil temperature for all AWSs

Figure 1.7 (b) shows the seasonal (daily average) changes in soil temperatures over the summer of 2017-18 for all the 6 AWSs. Soil temperatures show seasonal variability; the magnitude increases across MDV at the beginning of the summer and gradually decreasing after reaching the maximum value over the peak summer. Temperatures from the 6 AWSs have high discrepancies in their values at the beginning of the summer; as the temperatures start to rise over the summer, the stations' temperature differences reduce, and all the 6 AWSs show a similar range of soil temperatures.

Apart from the seasonal changes, the diurnal pattern in the soil temperature can be observed from a 24-hour composite average of the season's soil temperatures. Figure 1.7 (c) shows a 24-hour composite average soil temperature for all the 6 AWSs for the 2017-18 summer. The soil temperatures of the

AWSs are controlled by ISWR throughout the day. The time of occurrence of maximum soil temperatures is during the peak hours of the day (between 1300 Hrs to 1500 Hrs) when ISWR is maximum.

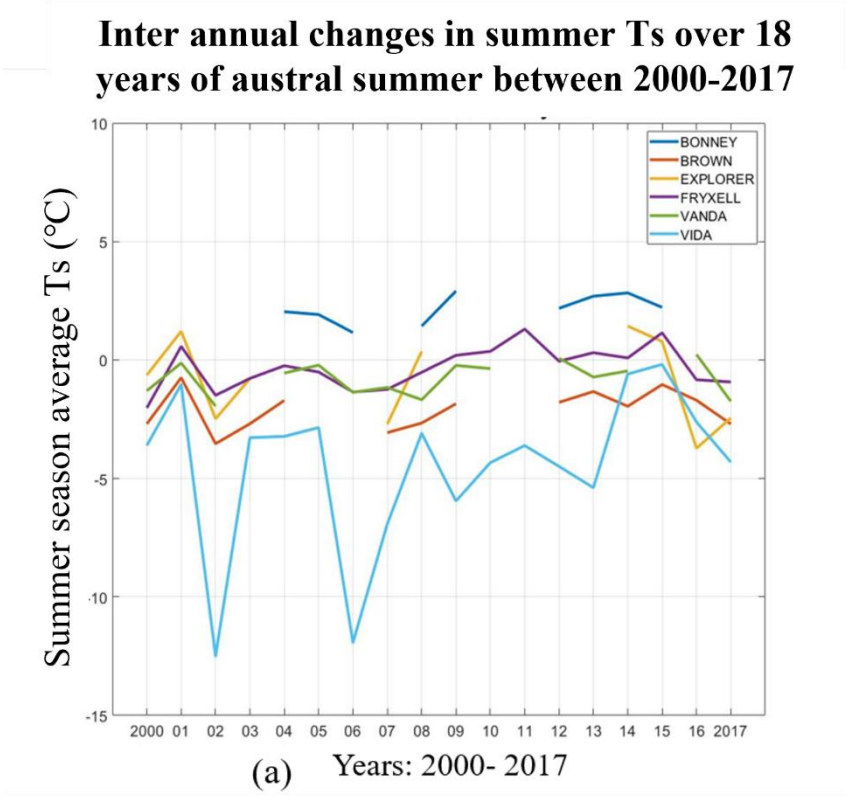

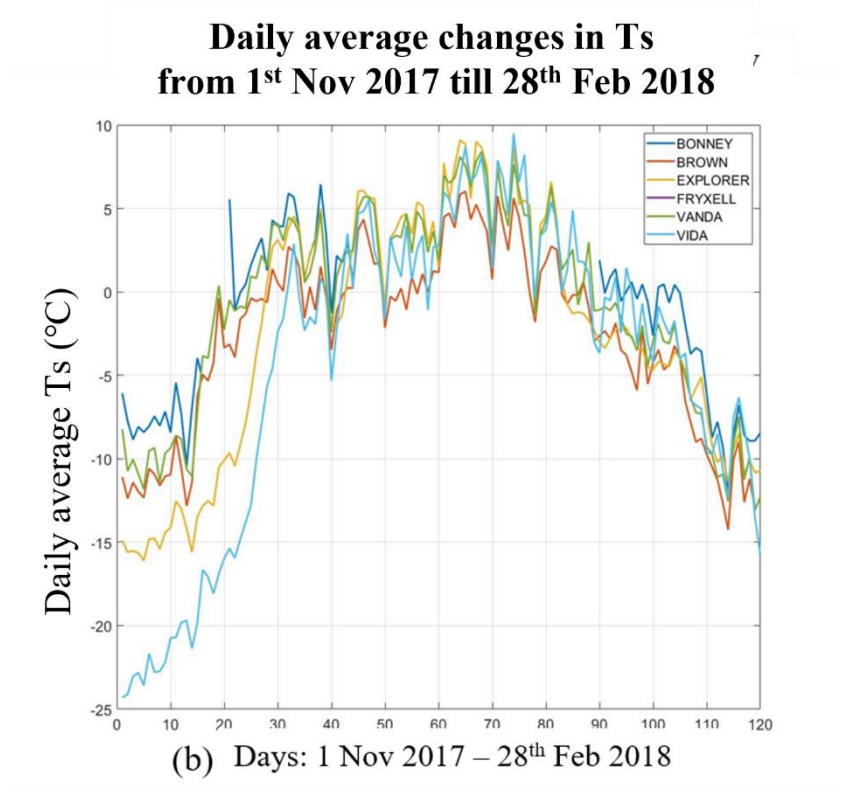

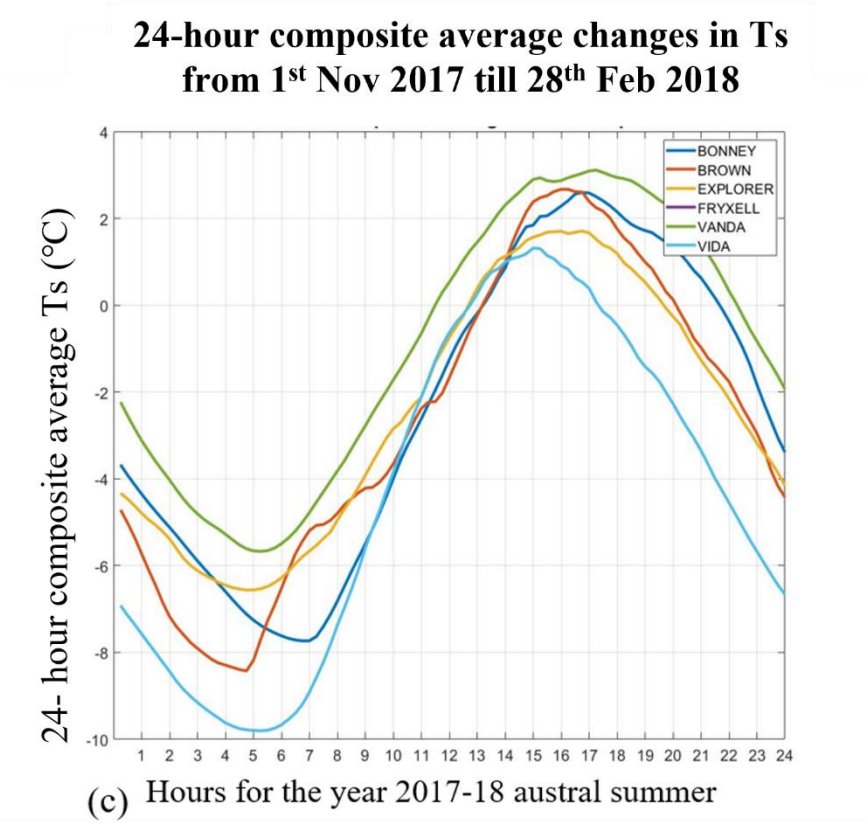

Figure 1.7 Soil temperature across MDV at different time scales yearly (a), seasonal (b), and diurnal (c), x-axis represents the different scales in time while the y axis represents the soil temperature in ℃.

1.5.1.6 Precipitation

Precipitation in MDV is extremely low, for which it is one of the driest places on Earth. Annual snowfall ranges between 3 - 50 mm of water equivalents, and the highest precipitation occurs near the coast with a gradual decrease in magnitude on moving inland (Fountain et al., 2009). Precipitation measurements in MDV are highly inaccurate because of the following reasons:

- Redistribution of snow across the valley due to strong winds causes wrong measurements of snowfall at a location (Knuth et al., 2010)
- AWSs installed cannot take accurate precipitation measurements, as a low-power automated measurement system that can accurately measure falling snow is yet to be developed (Knuth et al., 2010).

Despite not being highly accurate, precipitation data from the AWSs help study the yearly average precipitation at an MDV location and understand the valley-wide pattern. Figure 1.8 shows the total accumulated precipitation in mm/year over the 18 years (2000-2017) of summers (Nov - Feb) from Explorer and Bonney AWSs. During the 18 years, total precipitation was below 400mm/year for all the years except for the year 2006-07, which registered high precipitation above 1000mm for both Bonney

and Explorer AWSs. Though there was higher precipitation compared to the rest of the years, there were no significant changes in the hydrology of the region because of the higher precipitation. Most of the precipitation in MDV is sublimated or absorbed by the soil during summer. Precipitation in Taylor valley is controlled by the Nusbaum Riegel which causes the wind to have a higher accumulation of snow on the lower end of the valley (Fountain et al., 2006). Snow is a major contributor to glacial mass balance and a strong spatial trend of smaller mass-balance values with distance inland (R square = 0.80) can be observed, which reflects a climatic gradient to warmer air temperatures, faster wind speeds, and less precipitation (Fountain et al., 2006).

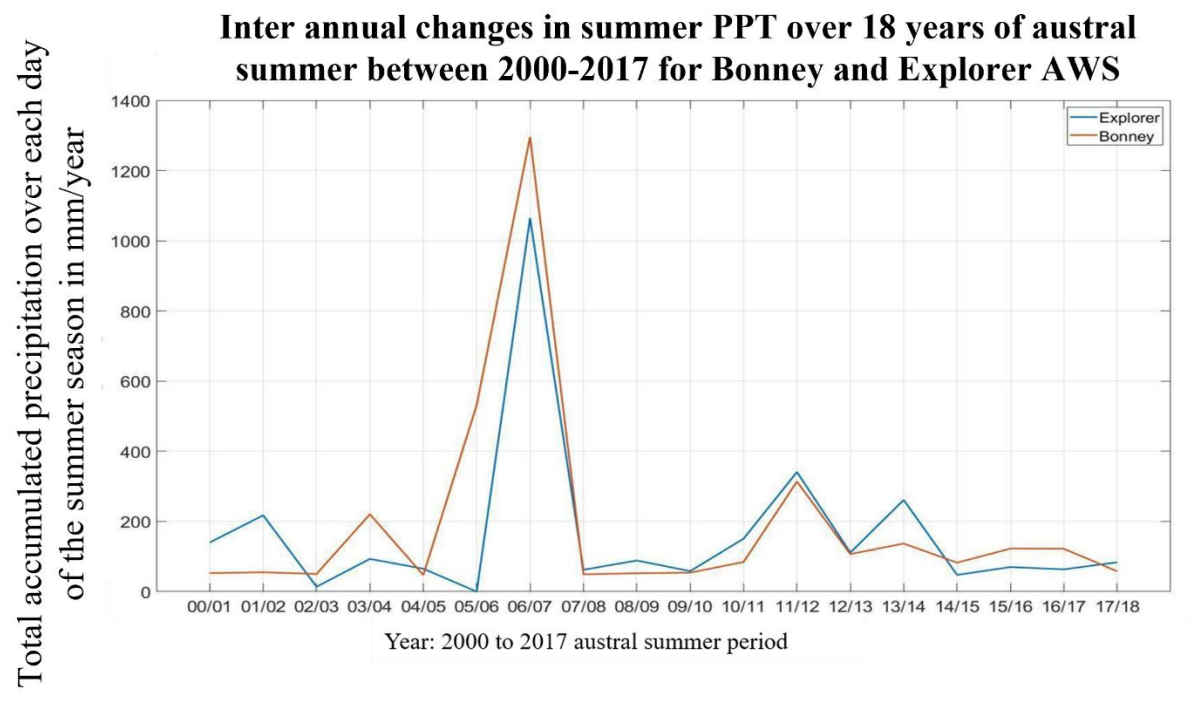

Figure 1.8 Total snow water equivalent from precipitation from 2000 till 2017

Bonney and Explorer, located in Taylor valley, show spatial differences in precipitation values at the two ends of the valley. Out of 18 years, for 10 years, Explorer received more precipitation than Bonney, and the difference in precipitation values between the two AWSs was not high. The low precipitation measured from the stations is not enough to cause significant flooding in MDV during the summers, and thus the primary source of liquid water during the summers is from glacial melt.

1.5.2 Foehn in summer

Foehn winds formed due to a robust synoptic-scale pressure gradient over the Transantarctic Mountains because of cyclonic activities in the Ross sea region. Within the Dry Valleys, the foehn onset is identified by an increase in wind speed above 5 ms^{-1} from a south-westerly direction (down-valley winds from Transantarctic mountains), a rise in air temperature by at least 1°C hr^{-1}, and a decrease in

the value of relative humidity by at least 5% hr^{-1} (Speirs et al., 2010). Due to this specific signature of foehn events, a foehn identification scheme was previously developed, based on which foehn events were identified from the meteorological data collected by the AWSs. The study's foehn event identification scheme is based on previous work done by Speirs et al., (2010) and Steinhoff et al., (2014). The study used 15 min interval meteorological data from the 6 AWSs, and the following criteria were applied to them to identify the foehn events and their durations.

- Temperature: increase of 1°C over a 1 h period OR any reading above 0°C.
- Relative humidity (RH): decrease of 5% over a 1 h period OR any reading below 30%.
- Wind speed: greater than 5 m/s
- Wind direction: between 180° and 315°, for all the AWSs except Vida, 360°.

Foehn events cause an increase in the valley floor temperatures. A higher frequency of foehn events previously thought to be katabatic winds induces extreme glacial melt (Doran, McKay, et al., 2002). During summer, radiative warming from incoming solar radiation is also responsible for causing an increase in valley floor temperatures. Though summer incoming solar radiation is enough to cause high glacial melt, the foehn events over the summer cause a rapid increase in the temperatures of MDV and resulting in an unusual increase in glacial melt and eventual flooding of the streams.

Figure: 1.9 shows the seasonal average discharge rates of all the monitored streams in MDV across 18 years (2000-2017) of summer. During some of the years, the discharge rates are significantly higher than the 18-average discharge rates of 140 litres/ sec (red line). The year 2001-02 show extremely high discharge rates and is considered a flood season (Doran, McKay, et al., 2002). As for 2001-02, the summer of 2008-09, 2010-11, 2013-14, 2015-16, and 2016-17 flow average shows discharge rates that are higher than the average and can be considered flood seasons.

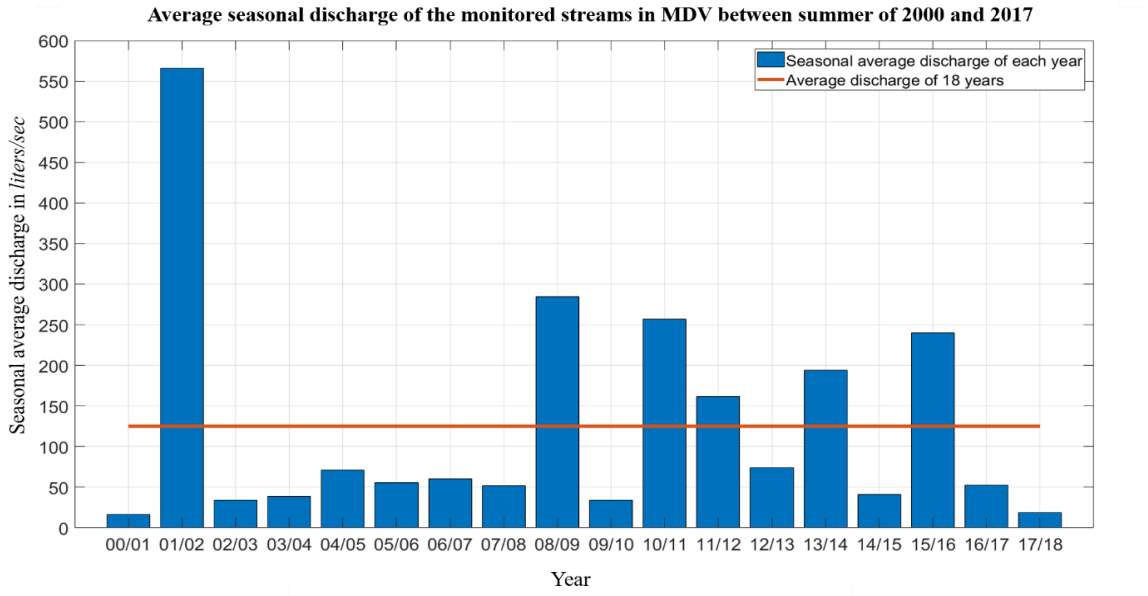

Figure 1.9 Average discharge rate of all the monitored streams across the 18 years; the x-axis represents the summer season while the y axis represents the average seasonal discharge.

Figures 1.10 shows the foehn events experienced by the 6 AWSs across MDV from 2000 till 2017 summers. Some of the stations had missing data for certain periods; thus, if any of the meteorological data (wind speed, wind direction, air temperature & relative humidity) were not registered by the AWSs for a particular year, the foehn events were not detected for that period. It can be observed that the flood seasons with high discharge rates have a higher number of foehn events as compared to the non-flood seasons. 2001-02 has the highest average seasonal discharge rate and shows a higher number of long durations foehn events detected by all the 6 AWSs in comparison to other years. These events occurred over the peak summer season between the 6^{th} and 10^{th} week when radiative warming of the valley floor is maximum, causing a significant increase in valley floor temperature leading to rapid glacial melt and eventual flooding of the streams.

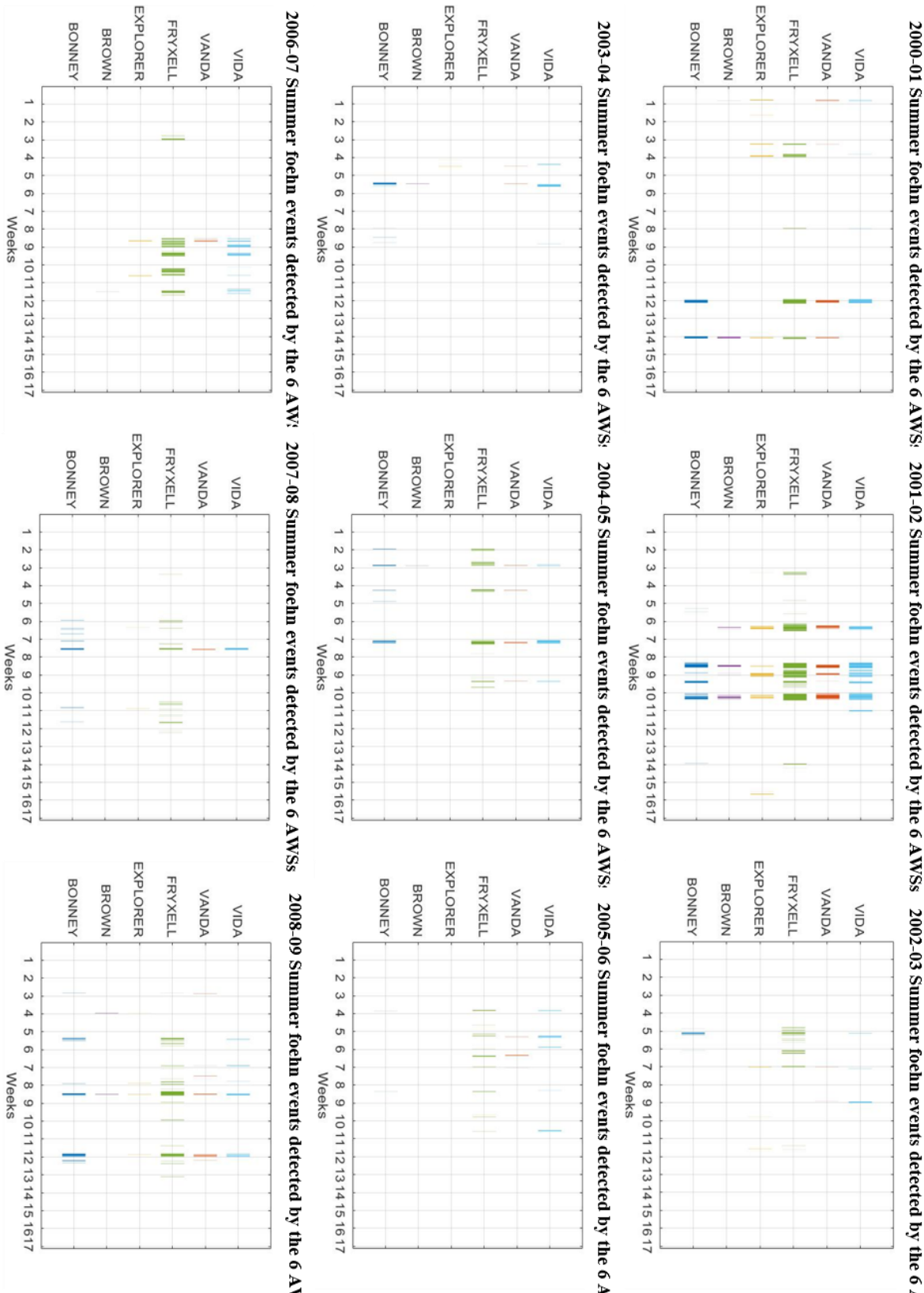
2000-01 Summer foehn events detected by the 6 AWSs
2001-02 Summer foehn events detected by the 6 AWSs
2002-03 Summer foehn events detected by the 6 AWSs
2003-04 Summer foehn events detected by the 6 AWSs
2004-05 Summer foehn events detected by the 6 AWSs
2005-06 Summer foehn events detected by the 6 AWSs
2006-07 Summer foehn events detected by the 6 AWSs
2007-08 Summer foehn events detected by the 6 AWSs
2008-09 Summer foehn events detected by the 6 AWSs
VIDA
VANDA
FRYXELL
EXPLORER
BROWN
BONNEY
Weeks

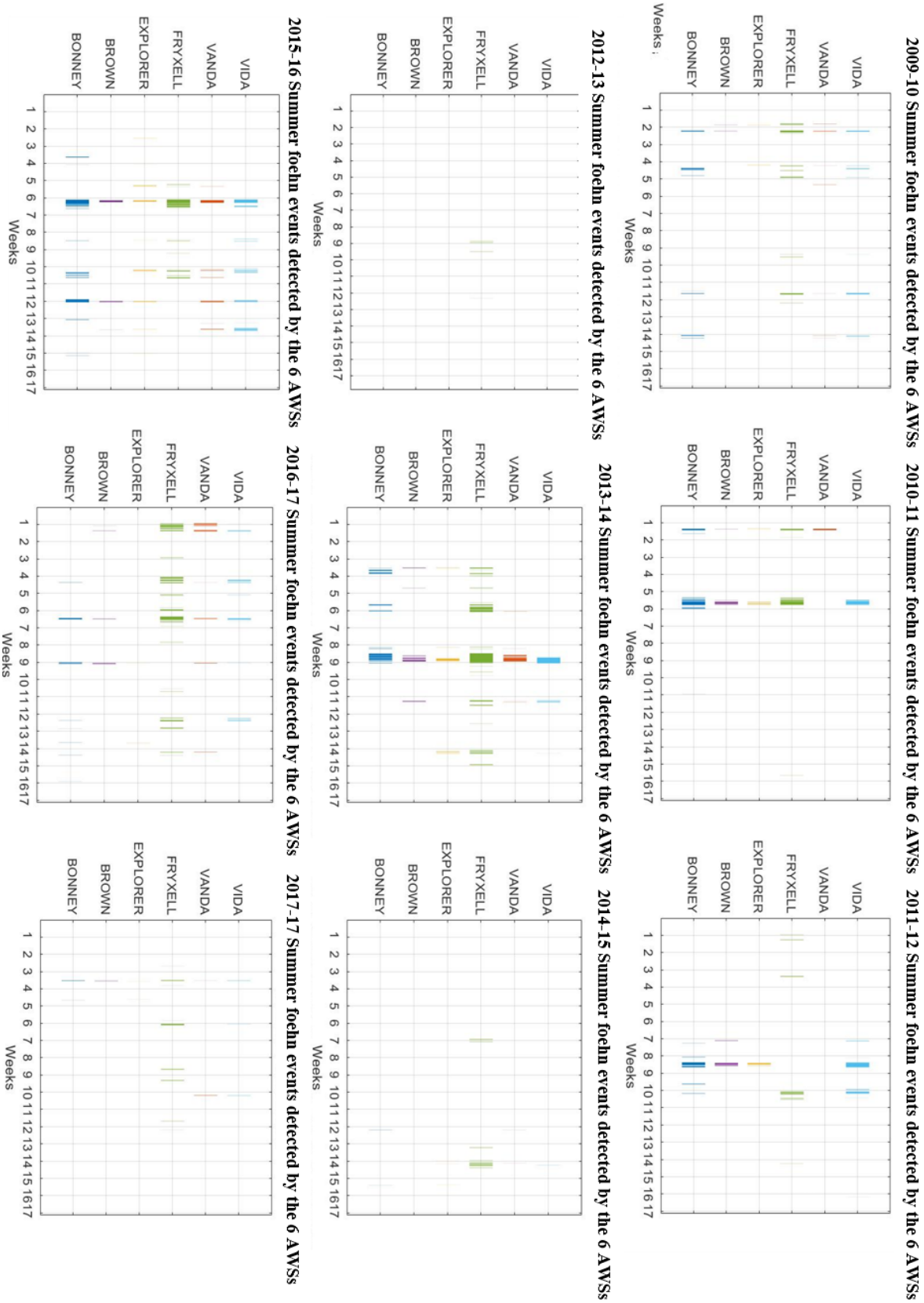

Figure 1.10 Foehn events registered by 6 AWSs for 18 years of summer 2000-2017, the x-axis represents the week in the summer from 1st Nov till 28th Feb of the season, while the y-axis represents foehn events detected by all the AWS across MDV.

The number of foehn events experienced by a region varies across MDV. Some of the foehn events are detected by all the AWSs, though their duration might vary between stations, while the others are detected by a few stations which include mostly the short duration (lasting for few hours) events. In MDV, stronger foehn events are detected by most AWSs, and they last for few days. Figure 1.11 shows the total foehn hours experienced by the 3 AWSs located in Taylor valley (Bonney, Fryxell, and Explorer) over the 18 years from 2000 till 2017 summer, from 1st Nov till 28th Feb of the season.

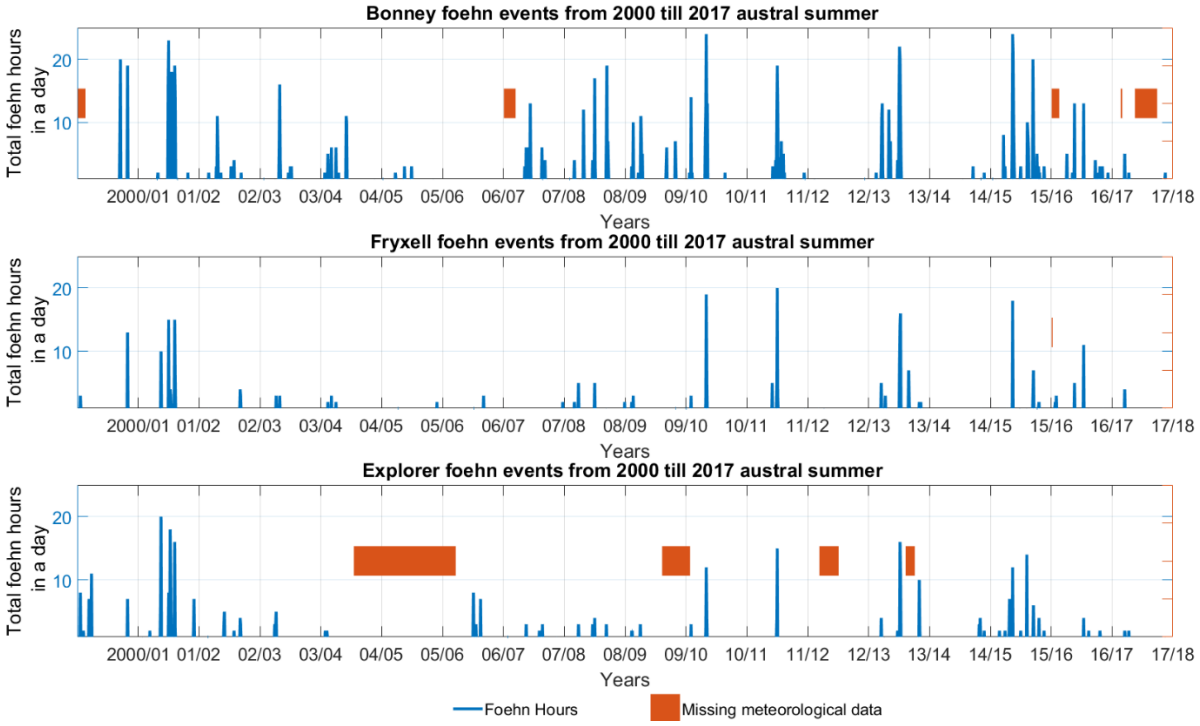

Figure 1.11 Taylor valley foehn events over 17 years of summers; the x-axis represents the yearly summer seasons, and the y-axis represents the total number of hours occurring during each day of the season.

Bonney AWS, located at the inner end of Taylor valley towards the Transantarctic Mountains, experienced a higher frequency of foehn events than Fryxell and Explorer, located at the valley's outer end towards the Ross sea region. The duration of the foehn events varies between the stations, with Bonney experiencing higher frequency, longer duration foehn events in comparison to Fryxell and Explorer, indicating higher frequency foehn events at the upper end of the valley than at the lower end towards the Ross sea region (Land et al., 2004).

1.5.3 Influence of solar radiation and foehn warming on air temperature.

Foehn winds and solar radiation control the Ta across MDV. Both cause an increase in air and surface temperature values of the region. Solar radiation causes seasonal and diurnal changes in the Ta, whereas foehn events are infrequent and cause abrupt changes in the valley floor temperatures, lasting between

few hours to days. It is essential to understand the influence of these two factors on the region's Ta, as higher Ta values induce glacial melt. Figure 1.12 is a scatter plot showing total foehn hours experienced by each of the 6 AWSs and the daily average incoming solar radiation during a day over 18 years (2000-2017) of summer. The scatter plot points are colored with the daily average Ta. This specific plot was created to understand the influence of the foehn event and solar radiation on the Ta at different MDV locations over the summers. The data is clustered into four groups, the groups are divided based on ISWR intensity and the number of hours of foehn winds experienced by each station during a day. The maximum daily average ISWR over a day is around 450 W/m^2. The value 250 W/m^2 was considered as a mid-point to divide the high and low-intensity ISWR category. The foehn intensity is divided based on the duration of foehn events; a day with foehn events lasting for more than 6 hours is referred to as a foehn day (Speirs et al., 2010); any events lasting more than or equal to 6 hours are considered high-intensity foehn events and any events lasting less than 6 hours are considered low-intensity events.

Group 1 includes the days when the foehn events lasted for less than 6 hours during low ISWR periods. These days can occur during the early summer period when the ISWR is low or during an overcast period. This group's events show temperatures mostly below 0°C, indicating short duration foehn events during low ISWR mostly cannot raise the air temperatures above 0°C, though there are very few exceptions to this trend.

Group 2 includes the days when the foehn events lasted for less than 6 hours during high ISWR periods. Most of the events with a duration of over 3 hrs show a rise in temperatures above 0°C. Some of the foehn events with a duration of less than 3 hr show a rise in temperatures above 0°C; this can be due to high ISWR, which heats the valley radiatively rather than foehn events. It can be inferred that the short duration foehn events can raise the temperature above 0°C when associated with high ISWR.

Group 3 includes the days when the foehn events lasted for more than 6 hours during high ISWR periods. This group includes all the favourable meteorological conditions for extreme temperatures across the MDV floor. Events in the group indicate that most of the long-duration foehn events occur during high ISWR periods over the summer and result in exceptionally high daily average Ta, some nearing 6°C.

The combined effect of radiative warming due to high ISWR and conductive warming due to long-duration foehn winds can increase the daily average temperature to extreme highs, which are favourable for triggering glacial melts across MDV. These are the cases when foehn events mostly occur during peak summers (between 6th week and 10th week) when incoming ISWR is highest.

Group 4 includes the days when the foehn events lasted for more than 6 hours during low ISWR periods. These events are significantly less in number in comparison to any other group, indicating long-

duration foehn events mostly happen during high ISWR periods. The temperatures during these events are relatively high and are mostly above 0°C, indicating long-duration foehn winds even in absence of high radiative warming can cause higher temperatures across MDV which can trigger glacial melts during summer, but the events in this group mostly result in temperatures lower than group3.

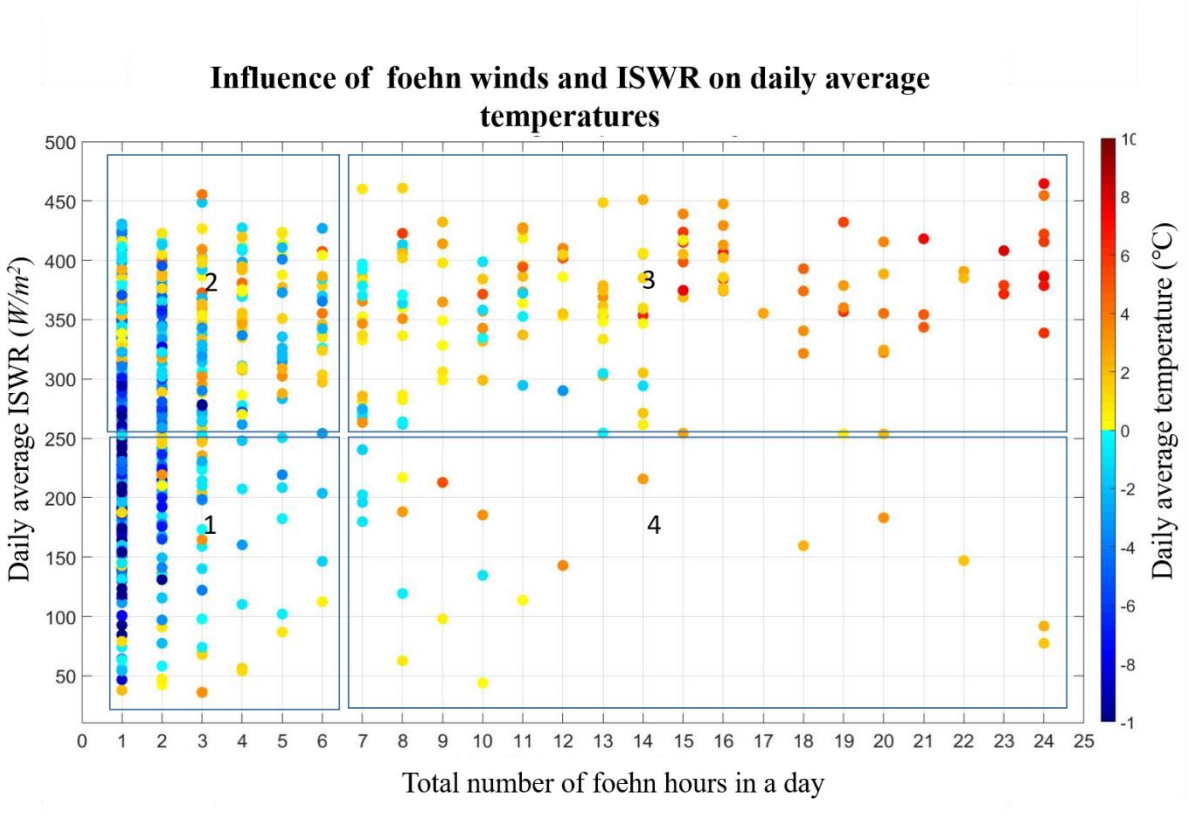

Figure 1.12 Scatter plot between daily average ISWR from 6 AWSs and total number of hours of foehn winds experienced by them in a day, the points are coloured using daily average Ta.

The time of occurrence foehn events, its duration, as well as the intensity of ISWR, play a significant role in modulating the Ta across MDV. Long duration foehn events over peak summer (during higher ISWR days) are responsible for extremely high temperatures (above 0°C), which can last for days triggering flooding of the MDV streams. The year 2001-02 had several long-duration foehn events detected by all the 6 AWSs occurring between the 6th and 11th week of summer, which caused a rapid increase in Ta and eventual flooding of the MDV streams during that period.

1.5.4 Climatology of flooding

As stated earlier, the flood and non-flood seasons have drastic contrast in their stream discharge rates. To understand the cause of these drastic contrasts in yearly flow rates, it is necessary to study the difference in the meteorological conditions between the two seasons. On studying the stream gauge data over the 18 years of summer (Figure 1.9), the year 2015-16 is identified as a recent flood season and 2014-15 as a non-flood season. Previously, a comparative study of 2001-02 (flood year) and 2000-01

(non-flood year) was done by Doran et al., (2008), which showed the importance of summer westerly winds in causing extreme glacial melt across MDV. The study intends to do a similar analysis for the recent flood and non-flood seasons. Figure 1.13 shows the hydrograph of the different streams including Onyx in MDV. Figure 1.13 (a) & (b) shows the stream discharge data from the 9 stream gauges over a non-flood season (2014-15) and a flood season (2015-16), respectively. The discharge rates from the year 2014-15 show one peak period in discharge rates over the summer during the 8th and 11th week of the season, whereas the hydrograph for the flood season shows two peak discharge periods, one from 4th till 7th week and the other from 10th till 12th week of the summer. Figure 1.13 (c) shows the contrast in the onyx rivers' discharge for the two seasons, the Onyx_Vanda stream gauge's data show the drastic difference in the discharge between the flood and non-flood season, where the flood season discharge reaches up to 10 times the non-flood season discharge.

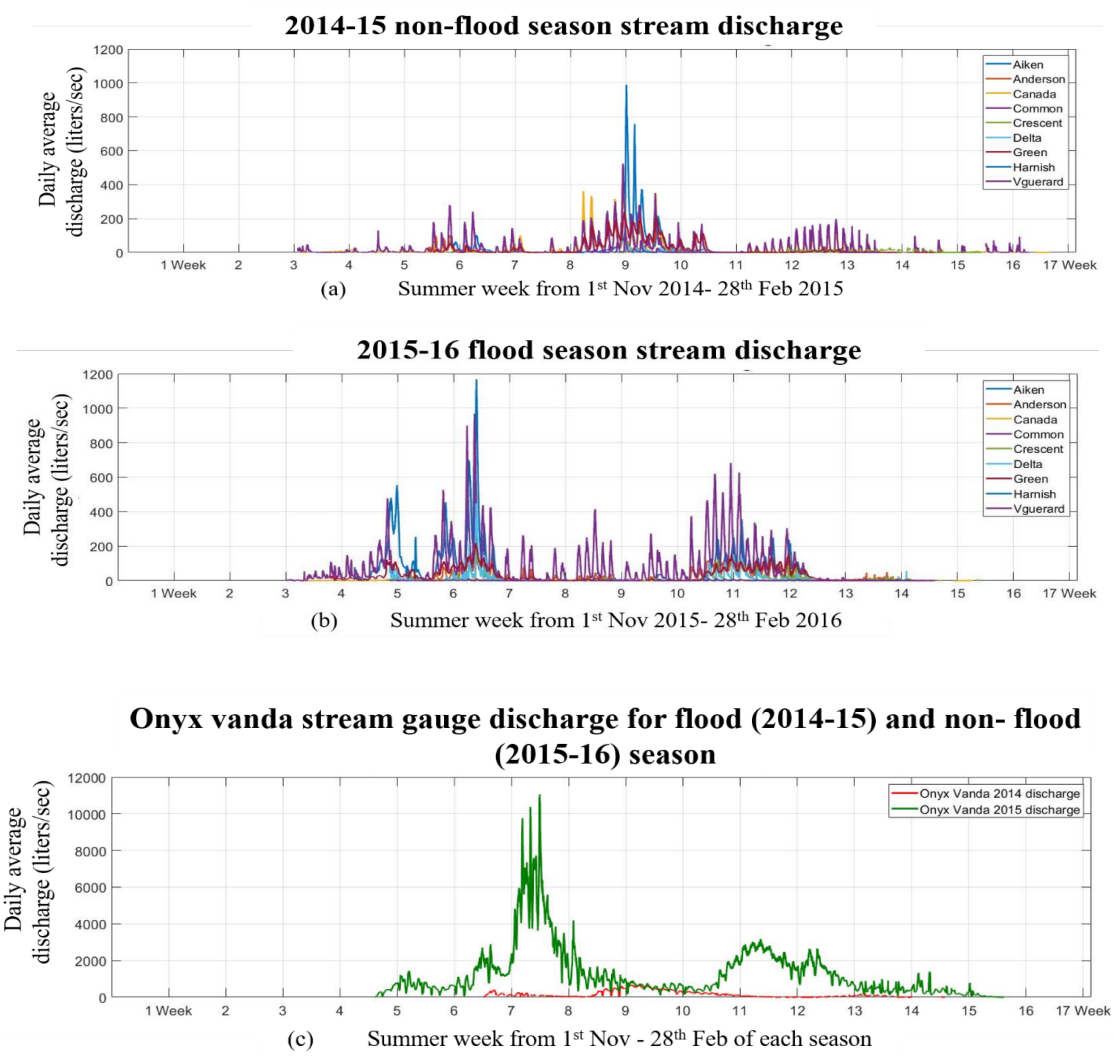

Figure 1.13 Hydrograph showing the discharge rates monitored by the stream gauges installed over the streams in MDV for flood and non-flood season, the x-axis represents the week in the summer from 1st Nov till 28th Feb of the season, while the y-axis represents the daily average discharge.

Few of the streams attain their peak discharge early, around 1400Hrs (NZST), whereas some of them have delayed response in attaining the peak discharge. The maximum discharges occur when the incoming shortwave radiation is highest, which is around 1400Hrs (Conovitz et al., 1998). The variation in the peaks of discharge rate of the streams in MDV can be accounted by the distance of the stream gauges from the source, the presence of hyporheic zones along the streams, solar position, and terrain structure causes variations in the melt rates and delay the meltwater to reach the measuring stream gauge (Conovitz et al., 1998).

Table 1.7 shows the contrast in meteorological conditions between the flood and non-flood seasons. The seasonal mean Ta and maximum Ta do not differ significantly between the two seasons, with 2015-16 being slightly warmer than 2014-15. The maximum Ta difference between the two seasons is 4°C recorded over Brownworth and Explorer. The year 2015-16 received slightly higher ISWR than 2014-15 for most stations except Vida. 2015-16 was a windier year than 2014-15, with both average and maximum wind speed higher than 2014-15 for most stations.

	Degree Day above freezing	**Mean air temperature in °C**	**Max Air temperature in °C**	**Relative Humidity in %**	**Mean solar Flux in Watts/ m^2**	**Max solar Flux in Watts/m^2**	**Mean wind speed in m/s**	**Max wind speed in m/s**
2015-16								
Bonney	67	-3.14	7.47	51.30	268.07	1026.0	4.65	16.87
Brownworth	31	-5.63	8.30	61.61	285.79	1041.0	4.14	13.93
Explorer	43	-4.81	9.33	62.12	267.98	845.00	3.84	15.17
Fryxell	57	-4.04	7.54	62.72	262.06	892.00	4.53	18.00
Vida	48	-4.76	7.65	48.85	258.84	851.00	4.70	13.15
Vanda	42	-2.39	6.99	46.11	236.82	897.00	5.38	16.32
2014-15								
Bonney	52	-3.65	6.84	55.10	264.31	1053.0	4.37	12.70
Brownworth	11	-6.61	3.39	67.55	249.20	862.00	3.95	12.27
Explorer	29	-5.34	4.74	65.78	259.80	919.00	3.55	11.45
Fryxell	38	-4.44	6.69	65.03	247.26	904.00	4.31	15.68
Vida	29	-5.55	4.65	56.35	272.08	930.00	4.66	12.00
Vanda	55	-3.34	7.27	46.94	234.45	813.00	4.95	14.74
Difference								
Bonney	15	0.50	0.63	-3.80	3.75	-27.00	0.28	4.17
Brownworth	20	0.97	4.91	-5.94	36.59	179.00	0.20	1.66
Explorer	14	0.53	4.59	-3.67	8.18	-74.00	0.29	3.72
Fryxell	19	0.40	0.85	-2.31	14.80	-12.00	0.23	2.32
Vida	19	0.78	3.00	-7.50	-13.24	-79.00	0.03	1.15
Vanda	-13	0.95	-0.28	-0.82	2.37	84.00	0.43	1.58

Table 1.7 Contrast in meteorology between flood and non-flood season

Though most of the meteorological parameters that aid in glacial melt like max Ta, ISWR, and the number of days above freezing temperature are higher in magnitude for the year 2015-16 in comparison to 2014-15, a striking difference in the meteorology of the two years cannot be observed that can explain the contrast in flowrates between the two seasons. The meteorological parameters' seasonal average does not provide much information about the day-to-day difference in the two seasons' meteorology. Thus, a thorough analysis of the meteorological conditions during the two years is required.

1.5.4.1 Incoming shortwave radiation (ISWR):

Mean ISWR for most of the stations is higher for the year 2015-16 in comparison to 2014-15, showing the flood year was a sunnier year. A higher ISWR over a season can result in higher temperatures, as the valley floor surface is more radiatively heated. Figure 1.14 shows the histogram plot of daily average ISWR for the two seasons (2014-15, blue and 2015-16 yellow) from the 5 AWSs (Bonney, Brownworth, Explorer, Fryxell, Vida). The histogram helps understand the differences in the number of occurrences of days with high ISWR between the two seasons.

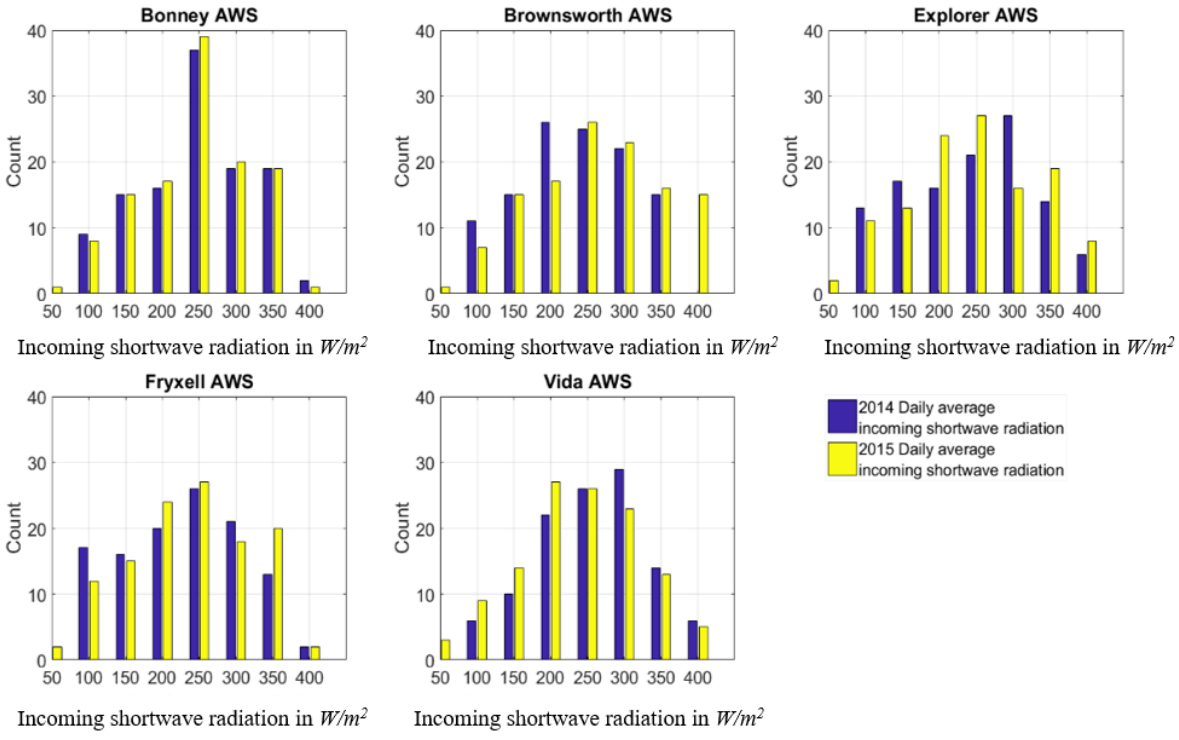

Figure 1.14 Histogram of daily average ISWR for non-flood (2014-15: blue) and flood (2015-16: yellow) season.

Bonney, Brownworth, Explorer, and Fryxell show more days with a high ISWR above 250W/m^2 for 2015-16 (flood year) than 2014-15 (non-flood year). The year 2015-16 was a sunnier year for most

parts of the valley, and there were fewer overcast periods than the non-flood season, which caused higher radiative warming of the valley floor during flood season than the non-flood.

24-hour average composite of ISWR and the standard deviation are produced for the 120 days of both seasons. The plots help identify the diurnal changes in the ISWR values for both seasons. Figure 1.15 shows the 15-min composite average of incoming solar radiation for both flood (black lines) and non-flood (red lines) seasons. The graph shows the diurnal variability in incoming shortwave radiation over the summer (red solid -2014-15, black solid -2015-16) from all the AWSs, along with the standard deviation of ISWR data over the 24 hours of the 2 seasons (red broken 2014-15, black broken 2015-16) indicating the fluctuations in ISWR.

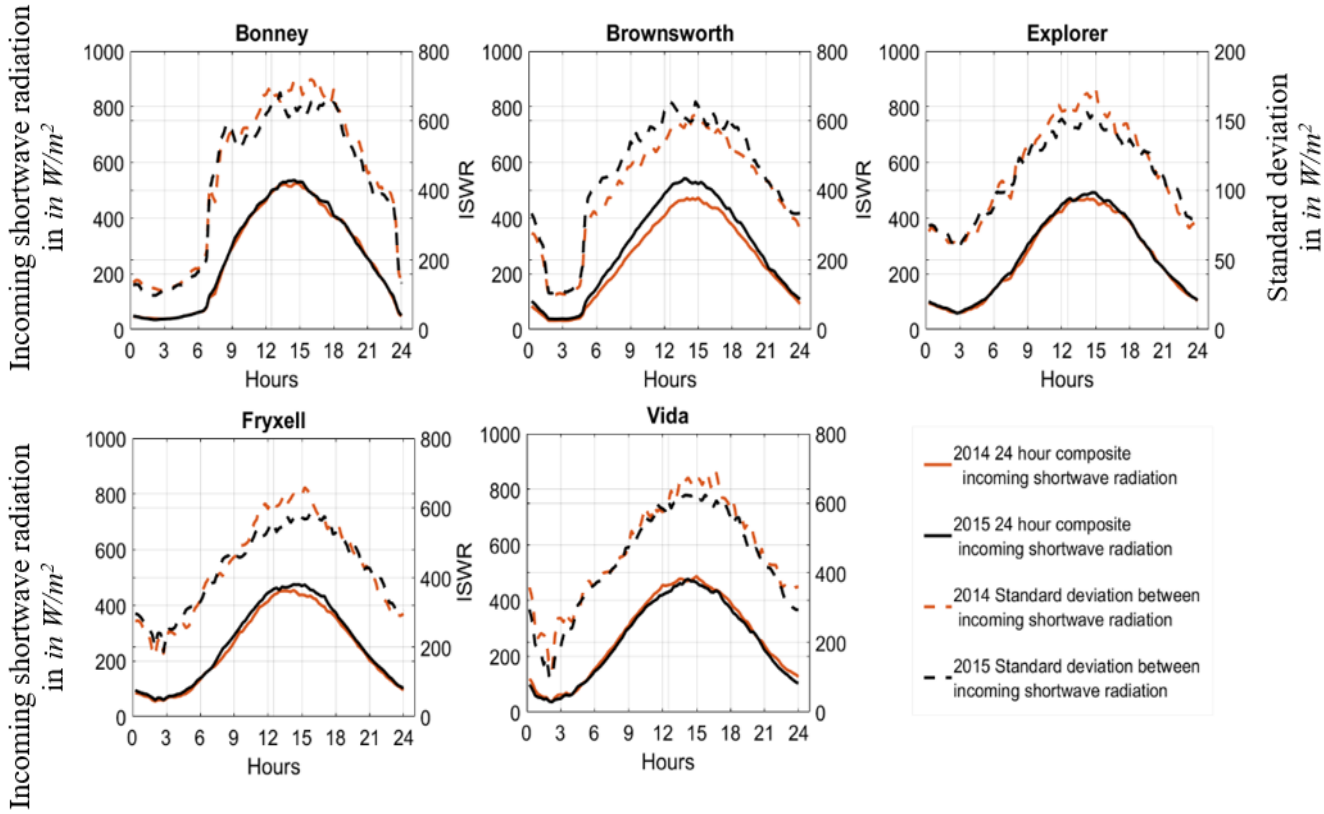

Figure 1.15 24 hours composite average of ISWR and the variance over the summer of 2014-15 and 2015-16, the x-axis represents the hours during a day while the y axis to the right represents the daily average ISWR) and the y- axis to the left represents the standard deviation.

The diurnal changes of ISWR show similar patterns across the valley throughout the flood and non-flood seasons. Brownworth distinctly received higher ISWR throughout the day for the flood season in comparison to non-flood season. The highest magnitude of ISWR is between 1400Hrs to 1600Hrs for all the stations. Standard deviation plots (broken lines) for the two seasons show the inconsistencies in incoming solar radiation's value throughout the summer season.

1.5.4.2 Air temperature

The yearly average Air Temperature (Ta) values for the two seasons are comparable. The differences between the values are too small to indicate a significant difference between the two seasons' temperature, which would have justified the difference in glacial meltwater availability for two seasons. As it is not the case, an in-depth analysis of the two seasons' day-to-day temperatures is required to shed light on the influence of the daily variation in Ta. Figure 1.16 shows the histogram plot of daily average Ta for the two seasons (2014-15, blue and 2015-16, yellow) for the 6 AWS (Bonney, Brownworth, Explorer, Fryxell, Vanda, Vida). The histogram plot of the two seasons shows distinct differences in the two seasons' meteorology; there is a higher number of days with warmer temperatures above 0 °C during flood season than the non-flood season. Similarly, the non-flood season graphs show a higher number of days with lower temperature ranges than flood season. High air temperatures are often caused by infrequent westerly winds (Doran et al., 2008), which were later identified as foehn events (Speirs et al., 2010).

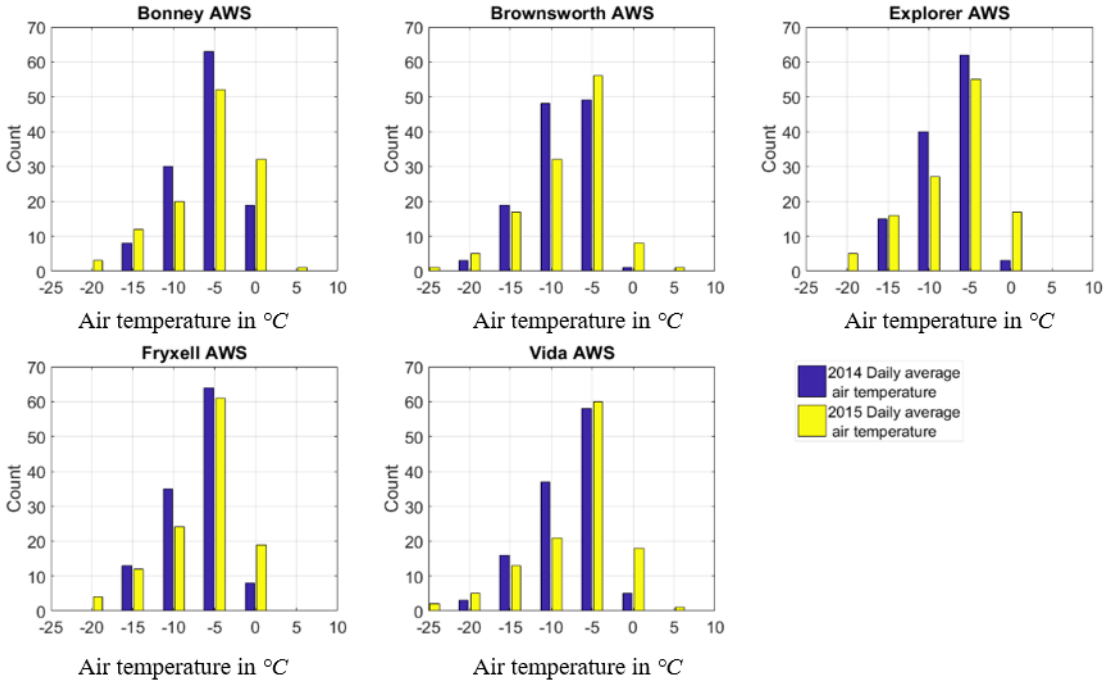

Figure 1.16 Histogram of daily average Ta for non-flood (2014-15: blue) and flood (2015-16: yellow) season

Figure 1.17 shows the 15-min composite average of air temperature for both flood (black lines) and non-flood (blue lines) seasons. The graph shows the diurnal variability in Ta over the summer (blue solid -2014-15, black solid -2015-16) from all the AWSs, along with the standard deviation of Ta data over the 24 hours of the 2 seasons (blue broken 2014-15, black broken 2015-16) indicating the fluctuations in Ta.

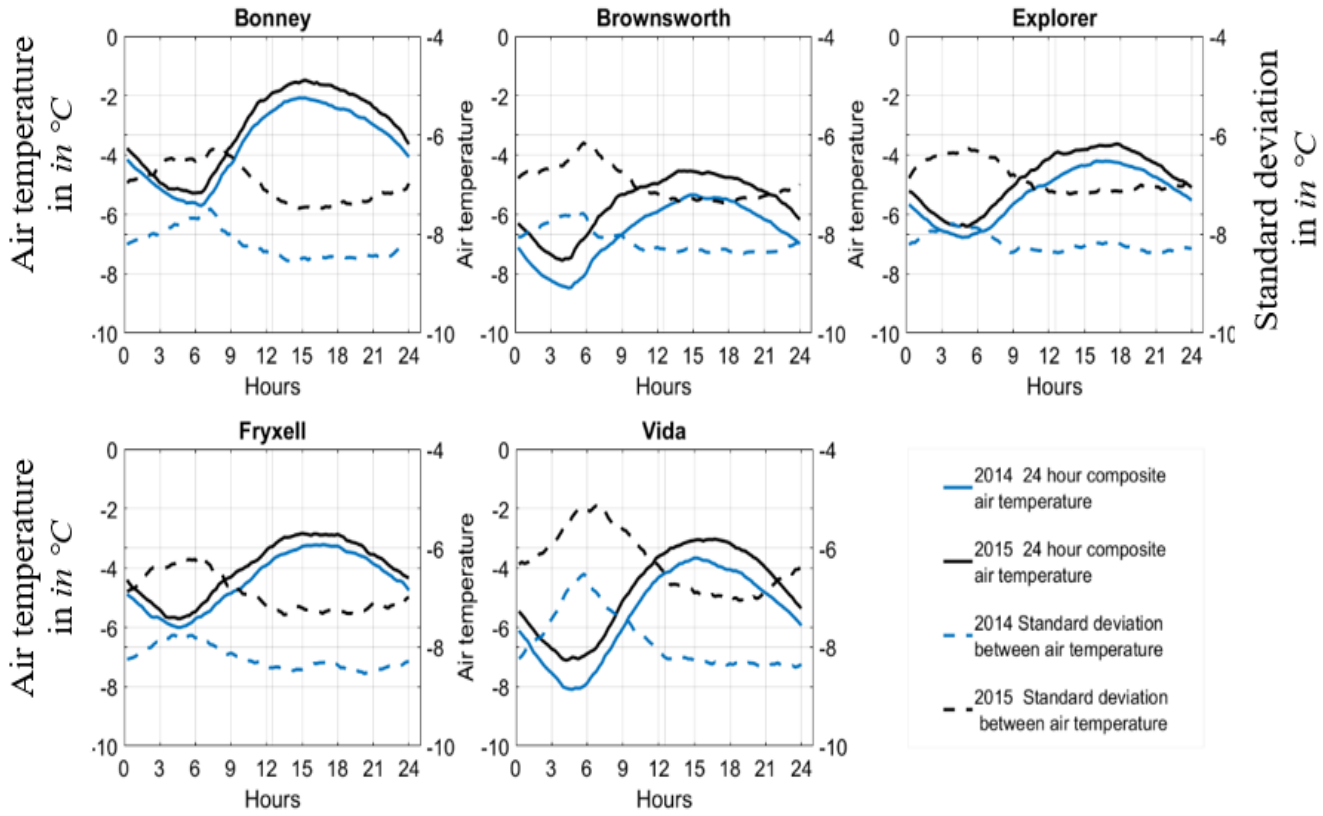

Figure1.17 24 hours composite average of Ta and the standard deviation over the summer of 2014-15 and 2015-16, the x-axis represents the hours during a day while the y axis to the right represents the daily average Ta (°C) and the y- axis to the left represent the standard deviation.

The plots show all the AWSs recorded higher daily average Ta throughout the days during the flood season than the non-flood season. There is variability in the Ta experienced by each of the AWSs. Few stations like Bonney are persistently warmer than their nearby stations; due to Bonney's proximity to the Transantarctic Mountains, it is more exposed to foehn winds which raise the Ta. Few stations show lower temperature fluctuation throughout the day (Explorer, Fryxell) compared to stations that show higher fluctuations throughout the day (Bonney and Vida). The fluctuation in temperature is mostly during the early hours of the day. In previous research, it was identified that the warm westerly winds occur mostly during the early morning hours, which answers the high variability in temperatures during that time of the day.

1.5.4.3 Wind speed and direction

Wind speed and wind direction play a significant role in introducing warmer westerly and cooler easterly flow to the valley floor. The bimodal wind flow pattern across MDV plays a significant role in controlling the temperature variability across MDV. Inter-annual patterns of winds across the summers can be different. Figure 1.18 shows the scatter plot between 15 min wind speed and direction measurements taken by the AWSs across the summer of 2014-15, coloured by the period's air temperature values. Figure 1.19 shows similar scatter plots for the year 2015-16.

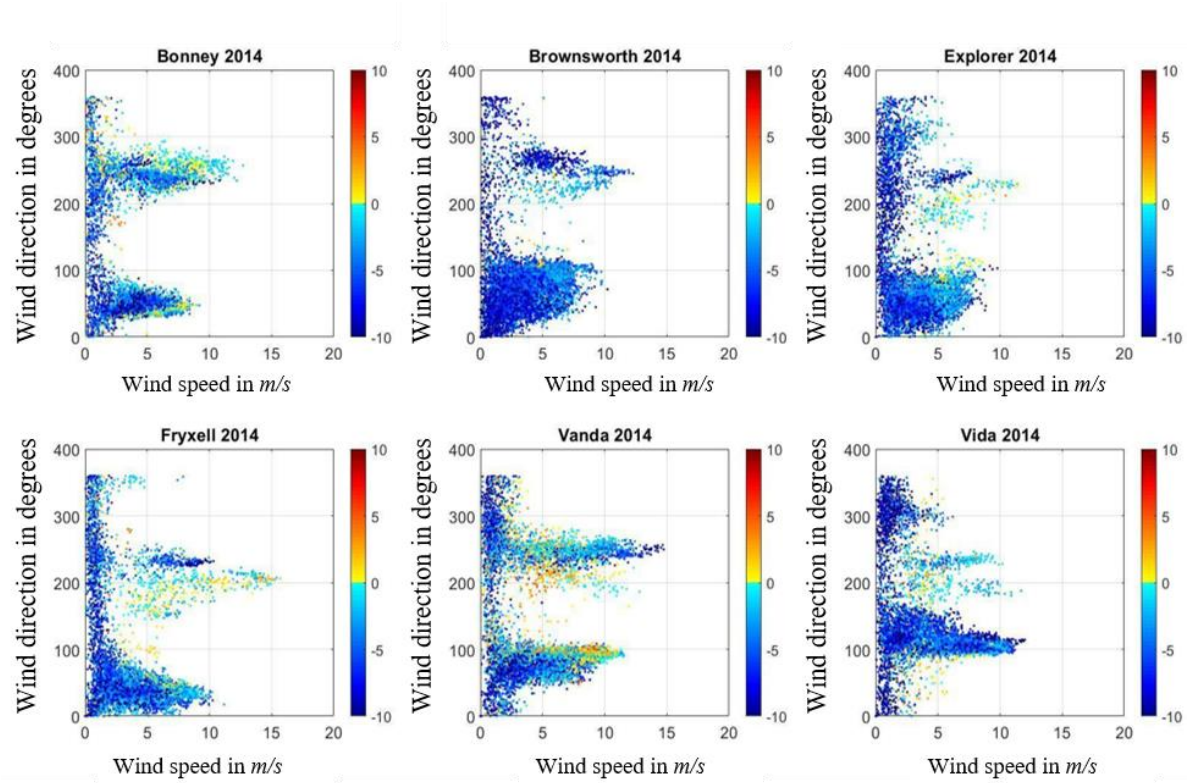

Figure 1.18 Scatter plot between wind speed and direction across 6 stations in MDV over the 2014-15 season, the points are coloured with the daily average temperature (°C).

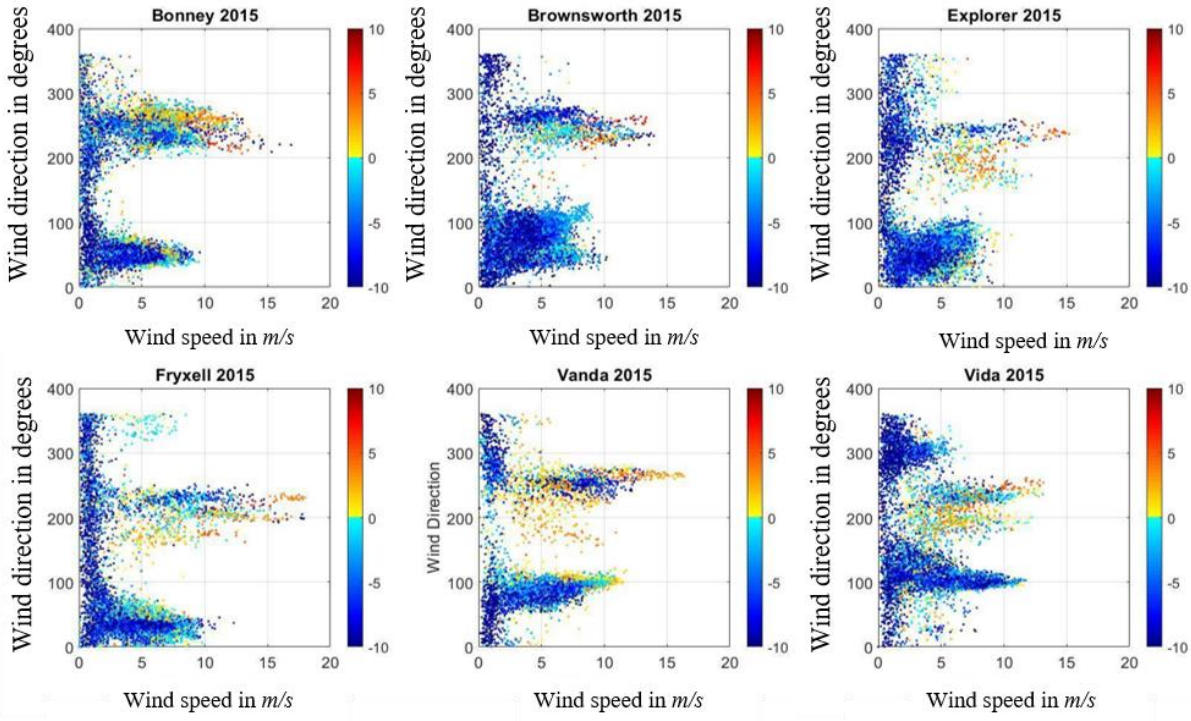

Figure 1.19 Scatter plot between wind speed and direction across 6 stations in MDV over the 2015-16 season the points are coloured with the daily average temperature (°C).

It can be observed that during 2015-16, all the AWS s experienced higher wind speeds which are greater than 5m/s from the south-westerly directions. The winds were associated with higher temperatures greater than 0℃ as compared to the year 2014-15. Comparing the scatter plot of the summer of 2014-15 and 2015-16, it can be identified that 2015-16 experienced windier and warmer days in comparison to 2014-15, which can be indicative of higher frequency foehn events during the summer of 2015-16. The strong winds with air temperatures greater than 0℃ can cause a rapid increase in temperature of the valley floor and trigger glacial melt.

1.5.4.4 Foehn event occurrence and duration

Foehn events were identified from meteorological data collected from the 6 AWSs (Chapter 1 Section 1.4.2). Figure 1.20 shows the foehn events identified from the 6 AWS across MDV.

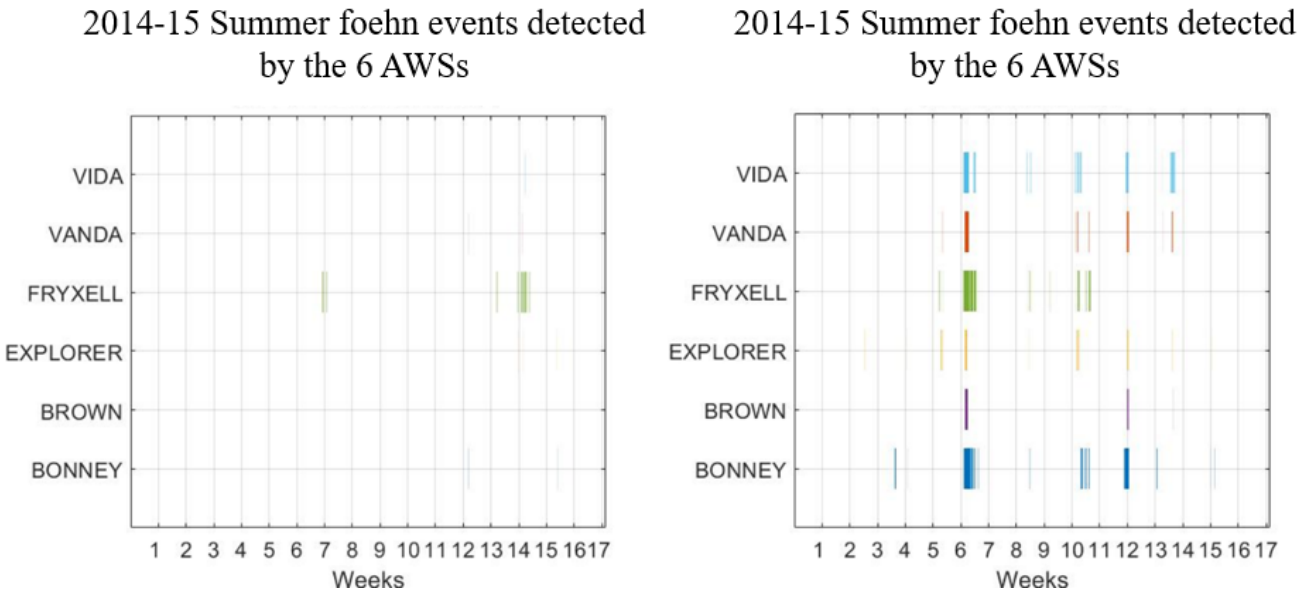

Figure 1.20 Foehn events from 6 AWSs across MDV for the summer of 2014-15 and 2015-16, the x-axis represents the week in the summer from 1st Nov till 28th Feb of the season, while y represents foehn events detected by all the 6 AWSs.

The foehn events during 2015-16 were higher in number and lasted for a longer duration. Foehn events for the year 2014-15 were very scarce, and any major foehn event cannot be identified that lasted for a long duration. Foehn events over the flood season were more persistent and more substantial in terms of both spatial coverage and duration, affecting most of the MDV floor. The flooding of 2015-16 is the result of radiative warming due to ISWR and radiative warming due to strong foehn events that lasted for days. The foehn events and high ISWR raised the valleys' temperature resulting in the rapid melting of the MDV glacier and streams flooding.

1.6 Discussion and Conclusions

The chapter aimed to study climatology, as well as seasonal and diurnal meteorology across MDV to understand different temporal trends in meteorology across MDV. The study highlights that the meteorological conditions in mountainous systems can be spatially heterogeneous depending on the synoptic conditions, therefore the density of the AWS networks is unlikely to be adequate to capture the variation in temperature across the whole valley. Different meteorological conditions in the MDV floor can lead to multiple zones with unique meteorology or microclimates. The meteorology differs between locations in the same valley and among the three significant valleys of MDV. The stations' meteorology located towards the Ross sea region differs from those located towards the Transantarctic Mountains.

Westerly and easterly wind of MDV plays a significant role in influencing the meteorology of the upper and lower MDV regions. Inter-annual variability in summer meteorology shows the striking difference in the meteorological conditions between years, and these differences are significantly influenced by the occurrence of foehn events in the valley. The 18-year trends along with the seasonal and diurnal trends in meteorology are similar to observations by Doran et al.,(2002) between 1986-2000.

New findings from this chapter show stronger foehn events mostly occur during high ISWR periods (clear sky days) and raise the Ta above 0°C, which contributes to high glacial melt in the peak summers and aid in flooding the MDV streams. Warming due to weaker foehn events occurring during high ISWR are aided by radiative warming from ISWR can mostly cause high temperatures, on the other hand, weaker foehn events occurring during, low ISWR are mostly not capable of raising temperatures above 0°C and cause conditions favorable for glacial melt. The meteorology of a flood and a non-flood season may not be strikingly different, but the occurrence of foehn during the summer can alter the meteorology for a short duration (few hours to days) and raise the temperature to cause high glacial melt.

Foehn events have a valley-wide impact on meteorology and hydrology of the region; a broader spatial scale observation is needed for studying these events across MDV and observations from the AWSs are not sufficient for this purpose. Satellite remote sensing acts as a useful tool in studying phenomena like foehn over a large spatial area. The following chapters utilize satellite data for studying the foehn events and their effects on the MDV floor. Chapter 2 explores the sensitivity and accuracy of satellite remote sensing data in capturing the changes in meteorology across MDV to be used further in the research.

Chapter 2: Evaluation of accuracy and correction of MODIS LST products over McMurdo Dry Valleys

2.1 Introduction:

The study of the local meteorology associated with the interaction of weather systems with mountainous terrain in Antarctica is often restricted to data from Automatic Weather Stations (AWS) – which only sample the surface layer. Valley-wide phenomena like foehn which are responsible for extreme temperature fluctuations across the MDV have been studied using *in-situ* (AWS) and modelled meteorological datasets (such as Antarctic Mesoscale Prediction System – AMPS) (*Antarctic WRF Mesoscale Prediction System*, n.d.). In such studies, the AWS data is used to verify the model-generated data, and in return, the model data augments the AWS by providing a spatially comprehensive wind field. This analysis mode is useful as AWS data are typically restricted in their spatial representation of the wind field, particularly in mountainous landscapes. (Colacino & Stocchino, 1981; Doran, McKay, et al., 2002).

The intrusion and detection (and subsequent cessation) of foehn in the valleys is sudden and spatially nonsynchronous (Speirs et al., 2007). Some regions may not even experience any foehn. This may be related to either topographic blocking or the existence of a strong inversion layer. The foehn induced warming (adiabatic) of the MDV boundary layer atmosphere (which is more pronounced in winter) and differential radiative heating (radiative) of the surface during summer cause spatially complex temperature patterns. The AWS network is not suitable to capture this complexity and a more spatially comprehensive dataset is needed to capture the spatio-temporal variability of temperatures across MDV.

MODIS Land Surface Temperature (LST) datasets can be used to study the interaction of the surface with the boundary layer for investigating local phenomena such as the urban heat island effects (Jia & Zhao, 2020), impact of snow-cover on regional climate (Baral et al., 2020), global dessert temperatures (Zhou & Wang, 2016). They proved to be a reliable observational tool over various land surface types. Over Antarctica, MODIS datasets were previously used by several investigators, which include large scale monitoring of the region (Lubin et al., 2009); study of spatial-temporal patterns of the LSTs across Antarctica and their variance based on the distance from coastline, and latitude and longitude in Antarctica during summer (Miliaresis, 2014); estimation of daily air temperature from LST using machine learning (Meyer et al., 2016); and for studying polynya movements across Terra Nova Bay of Antarctica (Ciappa et al., 2012). For the MDV, few researchers focused on using satellite data, and a broad spatial scale study of the meteorological conditions across MDV has not been done previously.

The data from the Moderate Resolution Imaging Spectroradiometer (MODIS) sensor mounted atop Aqua and Terra satellites provide low spatial (1km) and high temporal (hourly, daily) resolution data that can help in studying the diurnal, daily, and monthly changes in surface temperatures over the larger spatial scale.

The objectives of this chapter are to:

- To evaluate the sensitivity and accuracy of MODIS Land Surface Temperature (LST) data in detecting the temporal (daily) and spatial (1km) changes in surface temperature across the MDV (to confirm its utility as a proxy for air temperature).
- To determine the suitability of LST data for studying the temperature changes across MDV while presenting results from cursory statistical analysis (and data wrangling) of the MODIS datasets.

2.2 Context

Any substance that has a temperature above absolute zero (-273.15 K) radiates electromagnetic energy, W, depending on temperature T, according to the Stefan-Boltzmann law,

$$W = \varepsilon \sigma T^4 \quad (W/m^2) \text{ (i)}$$

Where emissivity ε is equal to 1 for black bodies and less than 1 for grey bodies, σ being the Stefan Boltzmann constant (5.67x10-8 $Wm^{-2}K^{-4}$). LST is a measure of the amount of electromagnetic radiation that is emitted by the surface (of the land) in response to thermal exchanges with the air, and radiative heating; a simplified definition would be how hot the "surface" of the Earth would feel to the touch at a location. From a satellite's point of view, the "surface" is whatever that is under the Field of View (FOV) of the satellite when it looks through the atmosphere onto the ground. LST is the earth's surface temperature as detected by satellite sensors; it can be snow and ice, canopy, barren land, water bodies, or concrete structures (*Land Surface Temperature - Applications - Sentinel-3 SLSTR - Sentinel Online*, n.d.). There are two LST images acquired from Terra and Aqua satellites each; the image acquisition occurs over both day and night periods. This assists in studying the diurnal and daily changes in surface temperatures across the MDV. Though MODIS LST products have a high temporal (4 times a day) and low spatial resolution (1km), which is suitable for the present study there are some limitations to MODIS LST products that are listed below:

- Cloud cover hinders the acquisition of clear LST images of the earth's surface (Kang et al., 2018). LST datasets are passive remote sensing products, where the satellite sensor measures the energy emitted from the earth's surface (thermal infrared) (*Passive vs. Active Sensing |*

Natural Resources Canada, n.d.). Therefore, during overcast periods, the radiation from the earth's surface does not reach the satellite sensor, resulting in loss of data.

- The MODIS product's retrieval algorithm cannot distinguish low-level cirrus clouds from snow and ice-covered areas, causing an error in LST values in the form of a sudden spike/drop in LST values, which do not match the usual trend. LST images acquired over MDV regions are affected by these errors along with the datasets acquired over the rest of Antarctica (Meyer et al., 2016).

Due to the above-mentioned error, MODIS datasets require accurate assessment and correction before use. MODIS LST datasets can be very accurate, with a deviation usually below 1K in the range between -10°C and 58◦C (Wan, 2014). For colder environments, MODIS LST was validated for Svalbard in Norway, and a bias of 3K was identified (Westermann et al., 2012). No decrease in performance was observed with low temperatures up to - 40°C. The present study aims to evaluate MODIS LST's performance in picking up the temperature changes because of day-to-day warming and cooling of the valley floors during summers.

2.3. Data

2.3.1 Meteorological data:

The study utilizes meteorological data from an existing network of AWSs installed and maintained by LTER (*McMurdo Dry Valleys LTER*, n.d.). Air temperature data collected at 3m above the ground at 15 min intervals for 2008-09 summer (1 Nov 2008 - 28 Feb 2009) is used to evaluate LST products from MODIS. The period was chosen because it's one of the flood seasons. The period had a higher number of foehn events resulting in stream discharge that was greater than the 18-year average. Table 2.1 provides more details on the AWSs chosen for this study. The stations were chosen based on the land surface types they were installed over, elevation, and valley's location, which us helped evaluate and understand the variability in temperatures across different locations in the valleys.

Station	**Bonney**	**Common wealth**	**Explorer**	**Fryxell**	**Hoare**	**Taylor**	**Browns worth**	**Vanda**	**Vida**
Elevation	64.43m	290.24m	25.74m	19m	77.10m	334.13m	279.05m	296.10m	351.03m
Location	Taylor Valley	Taylor Valley	Taylor Valley	Taylor Valley	Taylor Valley	Taylor Valley	Wright Valley	Wright Valley	Victoria Valley

Table 2.1: MDV AWS stations with their located valley and elevations.

2.3.2 MODIS data:

The MODIS LST products for the 2008-09 summer with 1km spatial resolution (1 Nov 2008- 28 Feb 2009) are used for this study. Aqua and Terra satellites mounted with MODIS sensors orbit the earth from north to south, covering the earth's surface 4 times a day. The satellites have a typical overpass time over a location on earth at 1030 Hrs for Terra and 1330 Hrs for Aqua. LST is the product of passive remote sensing, and it does not require the terrain to be lit for reflectance from solar radiation. The LST products from both satellites are acquired during the day and night times.

2.4 Methodology and Results

MDV has multiple overpasses by MODIS during a day due to its location on the poles, enabling us to acquire the best images from both satellites over the same area at different times of a day with minimal cloud cover. For this study, the MODIS LST data for the period was pre-processed by LANDCARE, New Zealand (Meyer et al., 2016). The data is a mosaic of the best LST (less data gap) images with minimal cloud cover, acquired during multiple overpasses by each satellite during the day.

2.4.1 Comparison between MODIS LST and air temperature from AWS station across MDV (2008-09):

LST datasets were previously used to estimate the near-surface air temperature (Ta) over larger areas in different parts of the world (Colombi et al., 2007; Vancutsem et al., 2010; Zhu et al., 2013), along with Antarctica (Meyer et al., 2016). A comparative study between LST and AWS in Antarctica showed MODIS LST has a strong correlation with the Ta between 1 m to 2 m AGL, and both have registered similar seasonal variation patterns over the Lambert Glacier basin of Antarctica; the correlation between the two sets of temperature measurements also varies between the locations of the AWS (Wang et al., 2013). Though the datasets are different, their response to meteorological changes in the MDV can be considered similar as many studies utilize simple linear regression for estimating near-surface Ta from LST (Benali et al., 2012; Hereher., 2019). Thus, Ta can be used as a reference for assessing the response of LST to temperature changes in the valley floor.

The present study focuses on the daily changes in temperatures over the summer and not on the diurnal changes. A daily average LST image was generated from four instantaneous LST images acquired during the day and night period. The images corresponding to the daily average LST for 120 days are stacked to form a time series dataset from 1 Nov 2008 to 28 Feb 2009. Daily average LST values are extracted from the satellite images at the location of the nine AWSs, which provided a 120-day time-series LST data from the location of the 9 AWSs. Ta from AWSs is collected at 15 min intervals. Daily average Ta is calculated by averaging 96 Ta observations throughout a day, and their values were

converted to Kelvin from Celsius for comparing with satellite derived LST values. The nine AWSs with different elevations, land surface types assist in examining the response of LST to meteorological changes at different locations in the valley. Figure 2.1 shows the graph comparing daily average LST from satellites (Red solid line) and daily average Ta (Blue solid line) from the 9 AWSs.

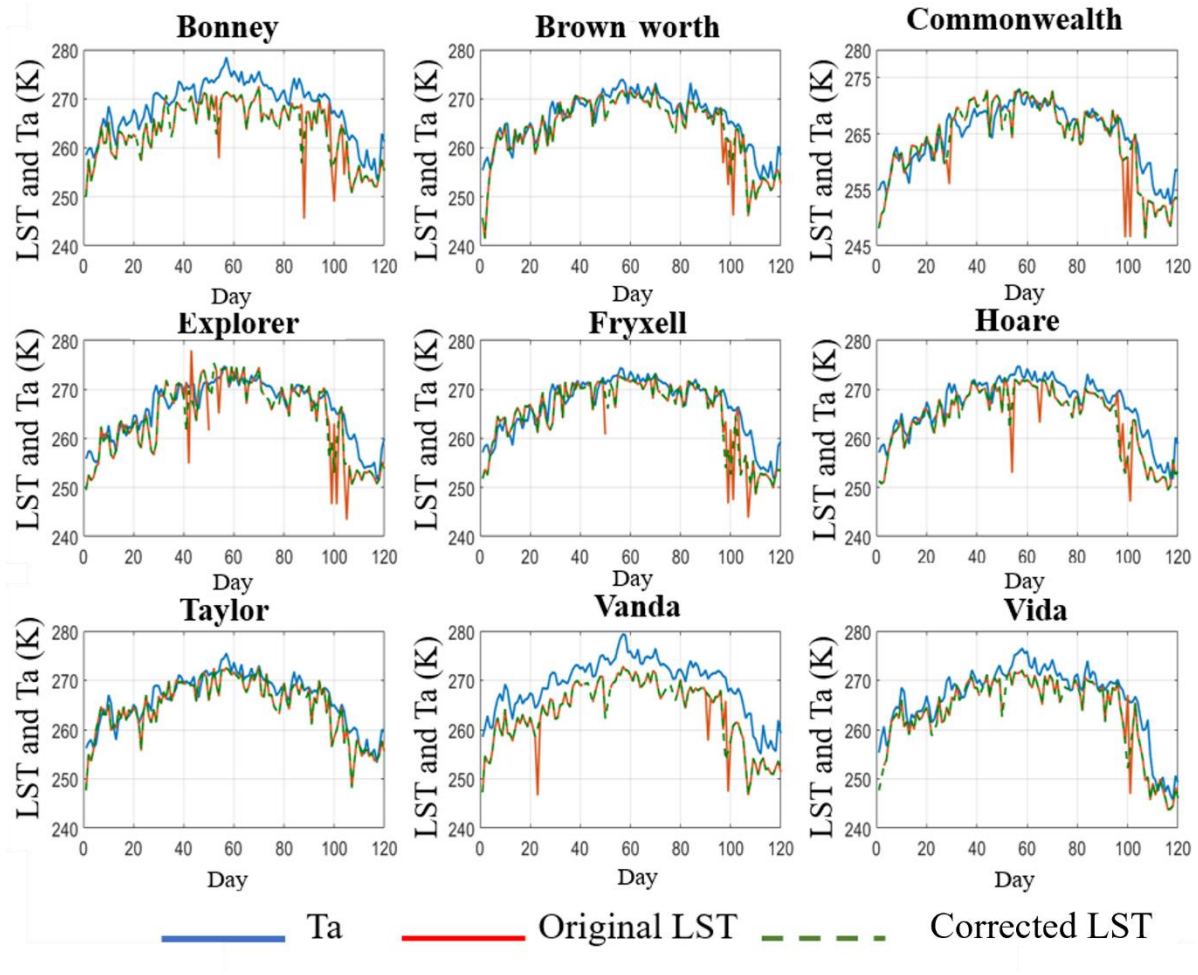

Figure 2.1 Comparison between daily average LST, corrected daily average LST, and daily average air temperature for all the 9 AWS, the x-axis represents the day of the seasons between 1 Nov 2008 till 28th Feb 2009, while the y axis represents the daily average temperature (LST and Ta).

Daily average LST and daily average Ta show a similar trend across the season, with a gradual increase in temperatures at the beginning of the summer and then a gradual decline after mid-January (around Day 80). The temperature difference between the LST and Ta is low for few of the stations (Fryxell, Taylor), while some of them have a higher temperature difference (Vanda, Bonney). Apart from the difference between LST and Ta values, there are also sudden outliers present in LST values. The outliers are in the form of abrupt drops in values of LST by up to 15K between two consecutive days, whereas the daily average Ta does not register these anomalies. The LST data outliers can occur due to the appearance of cloud covers, which were not removed by the LST product algorithm. Though the MODIS LST products are cloud masked, cirrus clouds cannot be removed reliably from the data. The

other reason identified for the occurrence of outliers is the averaging of the two day and night-time LST images. Though the region is sunlit throughout the season, the solar oscillation causes a fluctuation in the temperature throughout the day. The occurrence of cloud cover during either day or night can cause a bias in the daily average LST. Cloud cover causes the data's unavailability during a specific period, either day or night; the daily average calculated from the data is biased towards the available data's values. The daily average LST calculated with the values from night-time LST have a lower average LST than the average calculated from both daytime and night-time LSTs and vice versa.

Overcast conditions during a day or more causes the absence of LST values in all 4 images acquired during that period. If neither day nor night-time LSTs are available, daily averages cannot be calculated. These data gaps are observed as breaks in the solid line of daily average LST graphs. These two significant inconsistencies in the data in the form of outliers and missing data associated MODIS LST are required to be removed, to form a continuous time-series dataset. Correction techniques are applied for removing the outliers and gap-filling the data so that the daily average LST at a location is more in sync with the daily average Ta. The two correction techniques for removing missing data and outliers are discussed below.

2.4.2 Removing missing data

Missing data are mostly removed while calculating the daily average LST from the four instantaneous LST images acquired at different times of the day. Long-term overcast conditions result in missing data from all 4 images, leading to missing LST values. This study did not use any data-wrangling methods for removing the missing data. MODIS datasets are low-resolution datasets where surface temperatures are highly variable. A pixel value representing the LST of one region cannot be used to gap-fill neighbouring pixels due to the high variability in the land surface type and elevation across the valleys. Additionally, cloud cover causes missing data over a larger area, and thus spatial averaging of the pixel values was not a viable solution for filling up the data gaps. The research used temporal averaging instead of spatial average for removing the missing LST. To gap-fill, each pixel with the missing data is replaced with the average of the preceding day and following day LST value of the same pixel. Figure 2.2 shows a schematic diagram of how pixels with missing data are replaced in the time series datasets by averaging the LST values of the same pixel from the preceding and the following day. NA represents missing values.

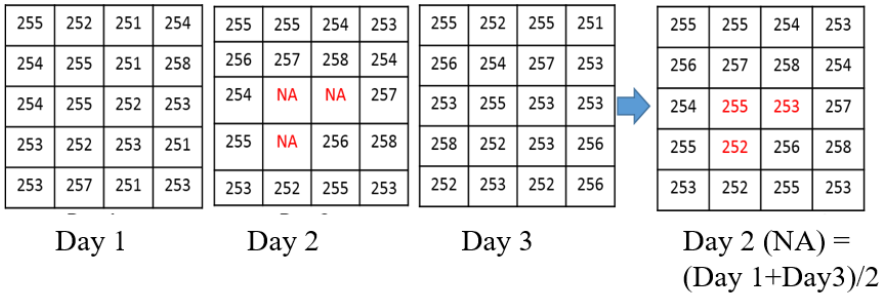

Figure 2.2 Schematic diagram showing the process of removing missing data from average daily LST.

Overcast periods of more than three days cannot be removed using this method. Long-term overcast conditons causes change in the temperatures by decreasing the air and surface temperatures due to the lack of radiative warming from solar radiation. Replacing long term unregistered colder temperatures with warmer known LST values is not a feasible option as the study looks explicitly into temperature fluctuations.

2.4.3 Removing outliers in the data

The time series LST value for any pixel throughout the summer season may show sudden drops/spikes in the LST values. As discussed above, the anomalies in LSTs are due to undetected lower-level Cirrus clouds or due to averaging of the 4 LST imagery either with an only day or night-time LST values. For removing the outliers, daily average Ta data was taken as a reference. Daily average Ta difference between two consecutive days for all the 120 days from the 9 AWSs was calculated. The maximum Ta difference between 2 consecutive days is considered a threshold for removing the outliers. Table 2.2 shows the maximum value of the daily average Ta difference between two consecutive days for all the nine AWSs. The maximum temperature difference between two consecutive days is 8.29°C for Hoare AWS. A threshold 'T' of twice the maximum value, i.e., 16.58°C, was considered as a threshold for the 2008-09 summer. Every year a different threshold needs to be chosen depending on the air temperature profile for that year.

Stations	Browns worth	Common Wealth	Explorer	Fryxell	Hoare	Howard	Taylor	Vanda	Vida
Temp diff	6.12	6.57	6.81	6.27	8.29	6.25	4.91	6.29	7.16

Table 2.2: Maximum daily average Ta difference between two consecutive days for the 9 AWS over 2008-09 summer.

A 3D matrix of all the LST imagery of 120 days is generated, where each element of the matrix represents a pixel with an LST value of a specific day at a specific location in the MDV. A moving window was run through three elements at a time for a specific location: P_{XYDn-1}, P_{XYDn}, and P_{XYDn+1}.

The three-elements represent the daily average LST of three consecutive days at a specific location in the MDV. X, Y represents the pixel location, whereas D_n represents the day of the data acquisition. The temperature difference between two consecutive days was calculated, P_{XYDn} day pixel value was subtracted from preceding day pixel values P_{XYDn-1} and succeeding day pixel value P_{XYDn+1} individually, resulting in values D1 and D2. The sum of the modulus of the two differences D_1 and D_2 was calculated to get the value D. For detecting an outlier D is compared with the threshold, and if D is greater than the threshold T, then the P_{XYDn} pixel value was replaced with the average of P_{XYDn-1} and P_{XYDn+1} pixel values. This condition was chosen as the sum of temperature differences between two consecutive days in a 3-day window cannot be higher than twice the maximum daily average Ta difference of the season. The moving window ran through all the elements of the 3D matrix except for the Day1 and Day 120 image elements. Figure 2.3 shows a schematic diagram for removing outliers from the LST datasets by replacing the outlier value with an average of the preceding and following day LST at the same location based on a threshold.

$$D_1 = P_{XYDn} - P_{XYDn-1}$$

$$D_2 = P_{XYDn+1} - P_{XYDn}$$

$$D = |D_1| + |D_2|$$

If D>T

Then

$$(P_{XYDn} = (P_{XYDn+1} + P_{XYDn-1}) / 2)$$

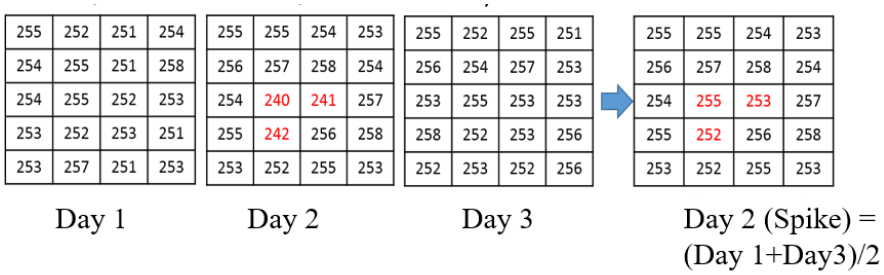

Figure 2.3 Schematic diagram showing the process of removing outliers in daily average LST data.

In Figure 2.1, the edited LST (broken green line) is overlaid over the actual LST (solid red line) from the satellite data for all 120 days. It can be observed that the outliers were removed from the signal successfully. The time series of daily average LST extracted from Taylor did not have any significant outliers; thus, the signal was intact, which shows that the algorithm does not distort the signal unnecessarily.

2.4.4 Correlation between corrected MODIS LST and air temperature from AWSs across the MDV (2008-09)

To check if the daily average LST values follow similar trends and temperature fluctuations as daily average Ta, the daily average LST collected from the 9 AWSs are compared to the daily average Ta value from the AWSs. Figure 2.4 shows the scatter plot between the daily average LST from MODIS with the corresponding daily average Ta from the 9 AWSs. There is a high correlation between LST and Ta values, with some of the stations showing nearly identical LST and Ta values. Apart from few points in the scatter plot showing anomalies caused due to higher or lower LSTs values compared to Ta, all points are along the trend line. The removal of the outliers and filling up the data gap provided a better correlation between daily average Ta and LST.

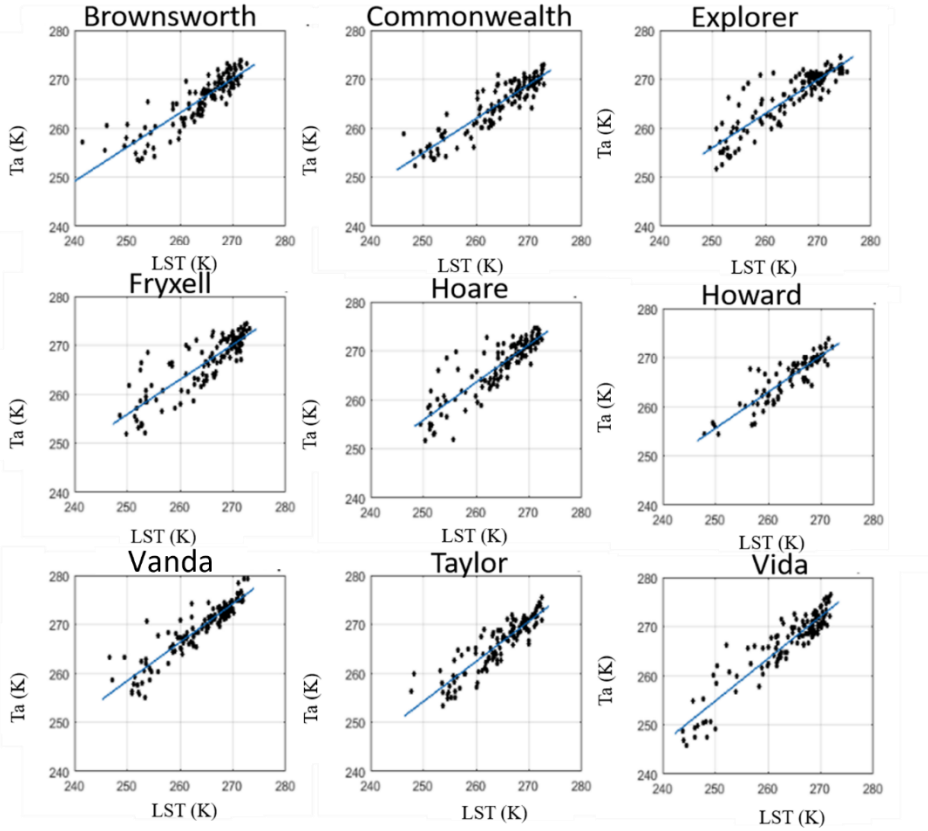

Figure 2.4 Scatter plot between average daily LST and air temperature (Kelvin) for all AWSs

Table 2.3 shows the R square and RMSE values between daily average LST and daily average Ta for all the 9 AWSs. The stations register good R Square values between LST and Ta, with R square values above 0.7, showing a high correlation. Also, the deviation of the two values from each other, defined by RMSE, is low and within 2-3°C range. The deviation is quite acceptable because the surface and air temperature always have temperature differences between them, and the difference identified are small.

Stations	Browns worth	Common wealth	Explorer	Fryxell	Hoare	Howard	Taylor	Vanda	Vida
R Square	0.78	0.81	0.78	0.73	0.77	0.77	0.80	0.84	0.86
RMSE	2.46	2.26	2.73	2.97	2.75	2.25	2.33	2.23	2.66

Table 2.3 RMSE and R Square values between the daily average LST and air temperature

The Index of Agreement (d) developed by Willmott in 1981 is a standardized measure of the degree of model prediction error and varies between 0 and 1. A value of 1 indicates a perfect match, and 0 indicates no agreement at all (Willmott, 1981). To check if the LST values follow a similar daily fluctuations pattern as Ta, an index of agreement between them was calculated. Table 2.4 shows the index of agreement between LST and Ta for all the AWSs, before and after removing outliers and data gaps. The index of agreement improved after the LST data was cleared of outliers and data gaps. All stations except Vanda and Bonney show a high agreement of 0.7 or above, indicating that both signals follow similar fluctuation patterns. Bonney and Vanda are located at the upper valley region of the Taylor and Wright valleys, respectively, and represent mixed pixels due to their proximity to Lake Vanda and Lake Bonney. Fryxell and Brownworth are in the outer end of the valley towards the Ross Sea; though they are lake edge pixel, they show a better index of agreement than those at the inner end of the valley. The lake edge pixels (mixed pixels) have a lower agreement than pixels from homogenous terrain like snow and land surface (pure pixel).

AWS	Index of Agreement (d) before data cleaning	Index of Agreement (d) after data cleaning	Pixel land surface type	Elevation	location
Bonney	0.4898	0.4824	Lake edge pixel	81.30m	Upper Valley
Brownworth	0.7055	0.7628	Lake edge	276.1	Lower Valley
Commonwealth	0.7256	0.7958	Glacier	288.41	Lower Valley
Explorer	0.6907	0.7188	Land	69.66	Lower Valley
Fryxell	0.7316	0.7764	Lake	51	Valley floor
Hoare	0.6926	0.7324	Lake edge	51.58 m	Valley floor
Howard	0.6574	0.8514	Glacier	472.49343	upper valley
Taylor	0.756	0.7703	Glacier	335.17 m	Upper Valley
Vanda	0.4015	0.4951	Lake edge	160.09 m	Upper Valley
Vida	0.7315	0.7496	Lake edge	348.97 m	Lower Valley

Table 2.4 Index of the agreement before and after the correction of the data

2.5 Discussion and Conclusions

The study aimed to check the accuracy and sensitivity of MODIS LST in registering the temperature changes across MDV by comparing the satellite LST with Ta measurements from AWSs. It was able to identify inconsistencies in daily average LST values due to undetected cirrus cloud and missing data, which require careful consideration and correction before utilizing the LST dataset for long-term study. The initial comparison between daily average Ta and LST shows spikes/drops in LST values that don't match with the typical trend. These anomalies were removed by replacing the values that represent the outliers with an average of preceding and succeeding day LST values. Furthermore, the data gaps were removed with an average of preceding and succeeding day LST values from the time series data. Both the techniques required the availability of LST data for at least 2 days of the observations. Missing data cannot be removed using these techniques for a long-term overcast due to data unavailability for a more extended period. Furthermore, outliers cannot be removed if there are only two continuous day values available out of 3. Both techniques, however, are successful in removing significant outliers and minor data gaps in the data.

The study aimed to check for the response of satellite derived LST values to meteorological changes in the valley, LST and Ta show a high correlation (>0.7 RMSE and 2-3 ℃ R square value) across MDV, some regions have better correlations than others. The correlation is better if the station is located on a homogeneous land surface type. MODIS LST products have a spatial resolution of 1km, and the LST acquired from the lake edge surface has reflectance from multiple surface types, including ice, land, and water bodies. LST acquired from the lake edges' mixed pixels have higher discrepancies from Ta than those from the pure pixel with the homogeneous surface type (land or snow). The AWS on the lake edge in the upper end of the valleys have a lower Ta. LST correlation than AWS at the lower end of the valley towards the Ross sea region. It could be due to the complex land surface and higher foehn frequency events experienced by upper valley regions. Bonney and Vanda register a more significant number of foehn events than any other stations in the MDV.

Data correction by removing the outliers, gap-filling the LST dataset increased the correlation between the LST and air temperatures and made the LST values more in synch with Ta. The daily average LST signal follows the Ta signal with an almost synchronous crest and trough. The difference in their value can be high for a few stations, but the trend remains the same. From the results of this study, it can be inferred that LST registers daily changes in temperature across MDV and is reliable for studying the surface temperature changes influenced by meteorology over larger spatial and temporal scales.

Chapter 3: Foehn detection and classification utilizing thermal remote sensing.

3.1 Introduction:

So far, the findings have highlighted the importance of foehn in modulating the MDV hydrological extremes. Foehn events play a significant role in controlling the valley floor air temperature and wind velocity over a large area (that can span multiple valley systems). Foehn can occur throughout the year, with higher frequencies during the winter since deeper low-pressure systems are prevalent. Though the summer experiences less foehn, they are more relevant for this study as they raise the valley's near surface Ta to near and above 0 °C, influencing the glacial melt, which has strong control on hydrology.

Foehn's timescale is typically from few hours to days and has been primarily studied using meteorological data across MDV (Speirs et al., 2013b). Yet using a sparse network of AWS across the MDV might not be instructive in the spatial heterogeneity of foehn's characteristics in this complex landscape (both at the valley scale and larger regional scale). Having a spatially dense dataset that can fill the significant gaps between the AWS locations is essential in studying this complex phenomenon.

In this chapter, we present a methodology to detect foehn events using satellite-based sensors that capture in the thermal band to measure Land Surface Temperature (LST) since, in the boundary layer, there is a tight coupling between air temperature and LST (Colombi et al., 2007; Vancutsem et al., 2010; Zhu et al., 2013; Meyer et al., 2016), the . This approach identifies the days when the foehn influenced the valleys' boundary layer and is spatially dense enough to provide a completer picture of foehn's dynamic characteristics.

Therefore, the objectives of this Chapter are:

- To develop a robust methodology for foehn detection from LST as measured by MODIS for the summer and winter periods across the MDV.
- To test the efficiency of this methodology in detecting foehn events by comparison with independently captured boundary layer data from the AWS network.

3.2 Context:

Previous studies debated over the nature (and nomenclature) of warm wind events experienced in the dry valleys. Some assert that the winds are katabatic in nature (Doran, McKay, et al., 2002; Lewthwaite

et al., 1990) and are responsible for major glacial melt and eventual flooding of the streams (Doran et al., 2008). Later, the wind systems were identified as being foehn in nature instead of katabatic (Speirs et al., 2010; McKendry & Lewthwaite, 1992). Speirs et al., (2010) studied these events, their genesis, and their correlation with the larger mesoscale events over the Ross sea region (Speirs et al., 2013a). They identified the influence of climatic events over the Ross Sea and the Amundsen region over MDV climatology.

Foehn impacts the atmospheric boundary layer significantly and substantially increases air and surface temperature and wind velocity in a particular way that can be used for identification through either in-situ data (AWS) or remote sensing data. A methodology was developed for detecting foehn events using meteorological data from AWSs, when they commence, end, and the duration (Speirs et al., 2010; Steinhoff et al., 2014). For this work, foehn onset is identified by an increase of wind speed above 5 m/s associated with a change to a south-westerly direction, the time-gradient in temperature (Ta) should be at least 1°C/ hr and for relative humidity a decrease of 5% /hr (Speirs et al., 2010; Steinhoff et al., 2014). The extent of the region affected by foehn is typically inferred by how many AWS stations simultaneously achieve the detection criteria. If it was detected by all 6 AWSs (Section 3.3.2), it is a valley-wide event affecting all the major valleys in MDV and, not a localized event that is experienced by mostly the up valley AWSs (Bonney and Vanda).

Though this methodology helped in studying the foehn events across MDV, it lacked in realizing the extent and effect of foehn events outside the observation points i.e., the location of the AWSs. The AWSs are not installed in all parts of MDV, and the previous methodology used for detecting foehn events depended on the availability of the data from the AWSs. The present work needs to develop a robust methodology that could detect foehn events even in the absence of any meteorological data from the areas where AWSs are not installed and also delineate the regions that show higher warming than the rest of the valley. Satellite data helps study the foehn events across MDV over a wider spatial and high temporal scale. Though satellite data do not provide high-frequency observation like AWS, they compensate for the drawback by providing wider spatial scale observations

3.3 Data

3.3.1 MODIS

MODIS sensors mounted on both Aqua (MOD11) and Terra (MYD 11) satellites provide two daytime LST and two night-time LST datasets every day (*MODIS Land Team Home Page*, n.d.). The LST products from these sensors are used for detecting foehn for our period of interest. The year 2015-16 summer (December -February) was used as a test year for summer foehn detection using satellite data. It is one of the recent flood seasons in MDV with available meteorological data. 2015 winter (April –

August) that leads to the summer flood season was chosen for winter foehn detection. Table 3.1 shows the time frame of satellite LST data collection for both summer and winter foehn detection.

LST dataset	From 1st April 2015 till 31st Aug 2015: 153 LST images	Winter foehn detection
LST dataset	From 1st Nov 2015 till 28th February 2016: 120 LST images	Summer foehn detection

Table 3.1 Time period of LST datasets collected for developing foehn detection technique for summer and winter period.

As foehn winds descend towards the valley floor, they warm up adiabatically, channel through the valley systems, and warm the valley floor boundary layer (Chapter 4 section 4.4.2.2). In the following chapter 4, it was identified that ridge tops are less affected by the foehn winds than the valley floor. Hence, the study only investigates the horizontal temperature signatures from the valley floor. Apart from satellite data, a Digital Elevation Model (DEM) with a spatial resolution of 40 m covering MDV is used to develop a knowledge of topography and demarcate MDV surface based on elevation into the valley floor and ridge top. component Digital Elevation Models (DEM) are arrays of regularly spaced elevation values referenced horizontally either to a Universal Transverse Mercator (UTM) projection or to a geographic coordinate system (Archuleta et al., 2017).

3.3.2 Meteorological data

Meteorological data from the 6 AWSs (Bonney, Brownworth, Fryxell, Explorer, Vanda, and Vida) across MDV are collected for independently identifying the foehn events from AWSs data. The foehn events detected from the AWSs are used to check the efficiency of the foehn detection methodology developed in this chapter. The data collected are those required for foehn detection, as discussed in chapter 1 (section 1.4.2).

- Air temperature
- Wind Speed
- Wind direction
- Relative humidity

3.4 Methodology

As foehn is established, a sharp increase in Ta can be observed due to adiabatic warming (Speirs et al., 2010). Results from chapter 2 showed LST follows the same trend and has a high correlation with Ta. Therefore, LST can be used as a proxy for Ta during foehn events, thereby increasing foehn's detection beyond the AWS network, providing a more comprehensive spatial dimension. Incoming Shortwave

Radiation (ISWR) has seasonal and diurnal control over the surface and air temperature fluctuation. However, the magnitude of Ta fluctuations is more pronounced in winter (in the absence of ISWR) and attributed to the changing synoptic pressure patterns that may cause foehn (Figure 3.1). Yet, in the presence of ISWR during summer, the boundary layer's temperature is much warmer, but the fluctuations flatten. Over the winter, roughly between the 1st of April till 31st of August, the ISWR is absent, and the air temperatures fluctuate between -10 to -40 °C.

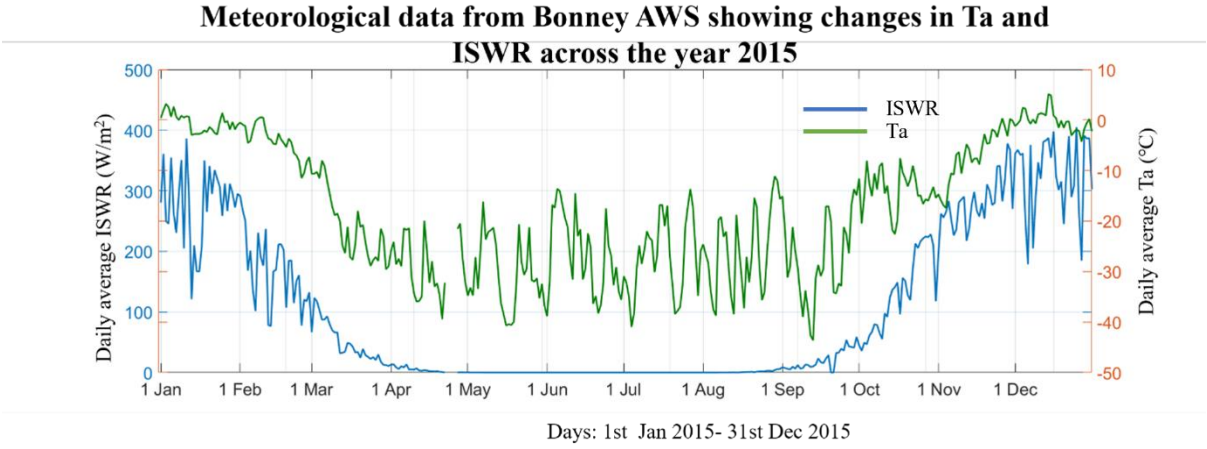

Figure 3.1 Changes in Ta and ISWR over the year of 2015 from Bonney AWS

During summer, the air and surface temperatures in MDV respond to solar forcing and foehn-induced warming (adiabatic). It is hard to identify the source of warming of the valley floor between the two causes. The more significant Ta fluctuations in winters make the detection of foehn easier since in the absence of radiative warming of boundary layer air (from ISWR), the adiabatic warming from the foehn is the only influence. The foehn detection technique developed in this study was first tested over the winter and then modulated for foehn detection over summer.

3.4.1 Foehn detection in winter

Foehn detection in winter uses 153 daily average LST images from 1st of April 2015 till 31st Aug 2015. The daily average LST is calculated by averaging the four LST images acquired from Aqua and Terra satellites - captured at a different time of day. Contour map generated from 40m DEM identifies 1200m contour line covering most of the valley floor in all 3 major valleys. Thus, the areas with an elevation greater than 1200m were cropped out from the LST images to avoid getting the ridge top pixels which show lesser response to foehn events. LST images provide information about the spatial distribution of surface temperature across the valley. Each pixel in the satellite LST image represents the daily average LST at a specific location. In a stack (3D matrix) of 153 LST images, a pixel at a particular location provides time-series daily average LST values for 153 days.

Strong foehn – as adopted here – are valley-wide in extent and last for a long duration (Speirs et al., 2010). Hypothesis: Due to the foehn wind's adiabatic warming, the heat transfer between surface and atmosphere causes the surface temperature to increase along with air. The imagery of the day when a foehn event occurred, most of the pixels in the imagery will show high LST values and an increase in temperature. Following above hypothesis, a foehn detection approach was developed based on temperature changes in the valley floor. The Algorithm for Detecting Foehn (ADF) checks the total number of pixels in an image showing positive deviation from their seasonal mean and determines if the image of the day shows any foehn-like conditions or not.

In the absence of ISWR, fluctuations in LST across MDV are direct results of either cold pool generation or foehn penetration in the valley floor. To detect warming due to foehn, a seasonal average LST image was generated by averaging 153 daily average LST images over the whole season, and then for each of the 153 images, the seasonal average LST image was subtracted from the daily average LST images, resulting in 153 images for each day where each pixel value represents the difference between daily average and seasonal average LSTs'. In an image, the areas affected by foehn winds show a positive deviation of LST from their seasonal mean. Strong foehn winds rapidly warm up almost the entire valley floor to higher-than-expected (without foehn) temperatures; thus, most of the pixel in an imagery representing a day with foehn shows a positive deviation from their seasonal mean.

The foehn detection algorithm considers the total number of pixels in the difference image which shows a positive deviation from their seasonal mean and determines if the image of the day has a foehn signature or not. The difference between daily average LST and seasonal average LST can be any small positive number, but this may increase the pixels' count with positive deviation, which can cause detection of false foehn signatures. Figure 3.2 shows the relation between the total number of pixels (in all the 153 imagery), indicating a positive deviation of greater than or equal to1 Kelvin from their seasonal mean and the foehn signal derived from the 6 AWSs across MDV. During a day when a foehn event occurred, there is a rise in the count of a total number of pixels showing positive temperature deviation from their seasonal mean. The total count of pixels showing positive deviation can be used as a metric xc for detecting foehn events from satellite data.

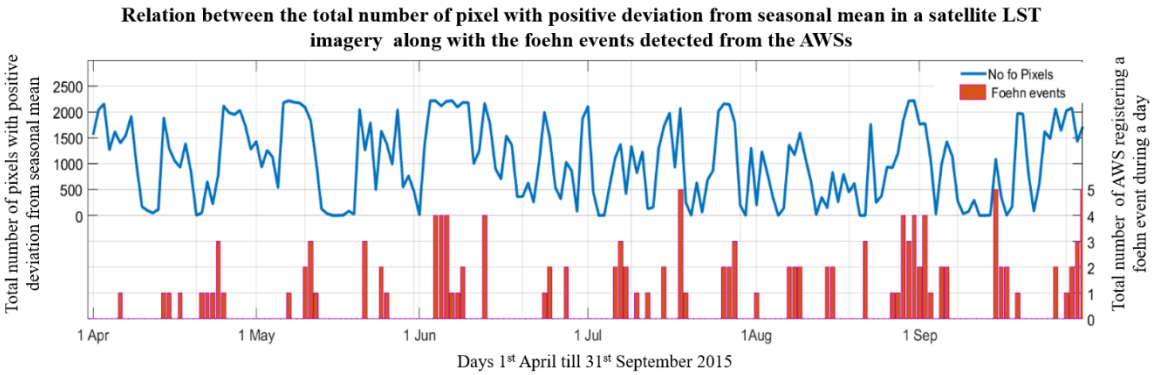

Figure 3.2 Relation between the total number of pixels with positive deviation from seasonal mean LST and the foehn events detected from the AWSs, the y-axis on the left represents the pixel count, whereas the y-axis on the right shows the number of stations registering a foehn event in MDV during a day.

Taking count of pixels with a small positive deviation value from the seasonal mean can cause false foehn detection as day-to-day differences of a few degrees are expected between images; on the other hand, if the pixels with high deviation value are only taken into count, it might cause missed detection of the foehn event as not many pixels register extreme temperature increase during a foehn event. A temperature difference threshold of 12 K for winters was determined by studying the deviation of daily average Ta from mean seasonal Ta for all the 6 AWSs, during a foehn event over 14 years of winter. A12 K threshold helped select the pixel, that had a significant difference between daily average LST and seasonal average LST values. The count of the total number of pixels in an image, showing deviation greater or equal to 12 K from their seasonal mean is higher in an image representing a foehn event. This helps determine the days with a foehn event with fewer chances of false detection or missed detection. The 12 K deviation allows us to detect higher magnitude foehn events that affect the valley floor for a long duration over a large area, which leads to a significant change in LST across the valley floor. Figure 3.3 shows the schematic diagram of the steps involved in the winter ADF algorithm. A summary of the steps involved are given below.

Step 1: Collect 153 daily average LST images over the winter and generate seasonal average LST.

Step 2: Subtract seasonal average LST from all the 153-daily average LST images resulting in 153 images with pixel values showing the difference between daily average LST and seasonal LST.

Step 3: Check for a threshold of 12 K and above in the difference image pixels value, if the pixel value greater than the threshold change values to 1 else change it to Null. Check the total number of pixels with value 1 in each image (image pixel value sum).

Step 4: Quantify the days with the highest number of pixels showing a positive deviation of 12 k and above from seasonal mean, those are the days with potential foehn event in MDV. If the total number of pixel is greater than 200 for >12K temperature rise, the day is considered a foehn event.

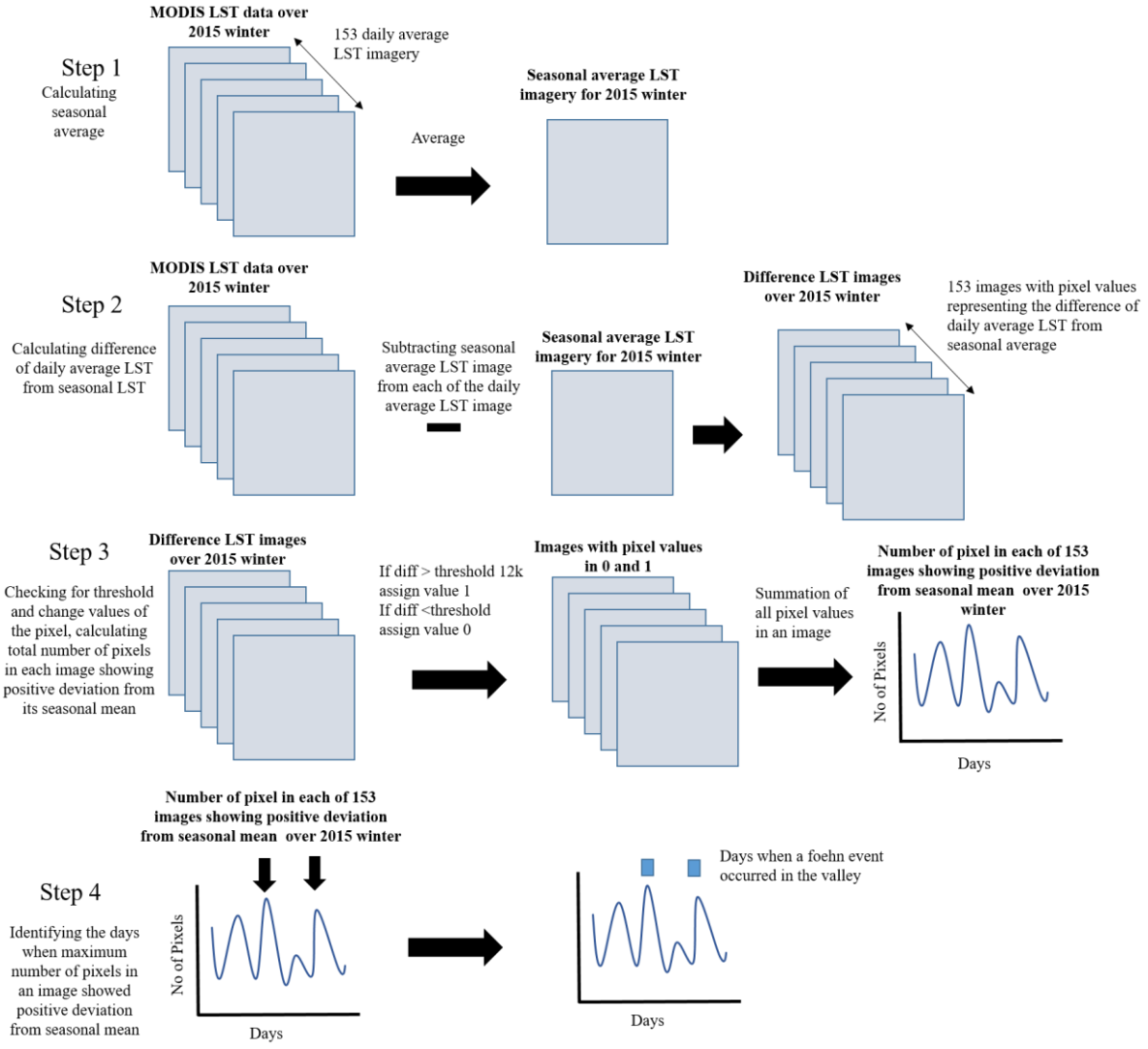

Figure 3.3 Steps involved in winter ADF for detecting foehn events from satellite LST datasets.

3.4.2 Foehn detection in summer

In summer, the temperature changes due to foehn events are less pronounced than in winter since the boundary layer air is much warmer and the synoptic pressure patterns that cause foehn are much weaker. In addition, the daily pulse of ISWR (radiative warming) can overwhelm warming trends from the adiabatic warming of foehn. Therefore, the ADF designed for winter needs modification for detecting summer foehn. The coupling between Ta and LST for summer is still tight, and Figure 3.4 shows the correlation between daily average Ta and daily average ISWR from Bonney AWS over the summer of 2015-16. Daily average Ta and average daily ISWR show a positive correlation, but the correlation may not be close as there are days when ISWR is low due to cloud cover, but Ta is high due to a foehn event occurring in MDV.

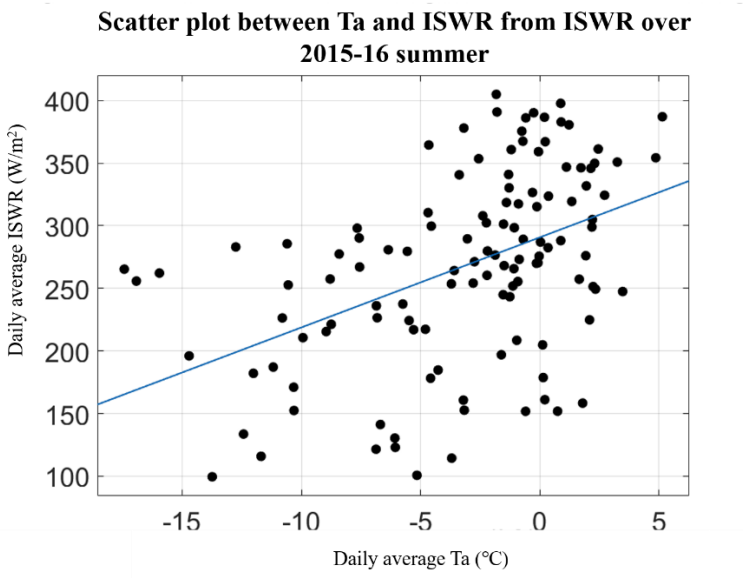

Figure 3.4 Scatter plot between daily average incoming shortwave radiation and daily average Ta over summer of 2015-16.

Due to the seasonal trend of increase and later decrease in the value Ta and LST during summer, the seasonal average LST value will be somewhere between the max and min values of daily average LST; thus, LSTs over peak summer (the period between mid-December will mid-January) will always be higher than the seasonal mean and the ones corresponding to the beginning and end of the season will be lower than the seasonal mean. A seasonal average LST calculated over summer, like what was done for winter ADF, cannot be used for the summer. ADF for summer needs a average LST value that changes across the summer and follows the pattern of daily average Ta. Individual average LST image is calculated for every image by averaging daily average LST images over 15 days window. The 15-day moving average LST is from 7 days before and 7 days after the observation day: thus, the seasonal average LST for each day changes with the seasonal trend in LSTs. A moving window was not used for the winter period as the winter temperature fluctuation were mostly between -10°C to -40°C and there are no significant seasonal fluctuations similar to summers. A 15-day window was chosen after carefully testing the datasets with various window sizes. For a smaller window, the seasonal LST sometimes show higher temperatures over the peak summer period and the increase in temperature due to foehn is lower than the seasonal average, causing missed detection of foehn; on the other hand, a larger window size causes the seasonal average to be lower than the day-to-day change in LST causing false detection of foehn. A balanced window is required to decrease the number of both missed and false foehn detection.

Like winter ADF, in summer ADF, the seasonal mean window LST image is subtracted from the daily average LST image for each day. A new 120-day time series dataset generated has every pixel representing the daily average LST difference from its 15 days window average. Similar to winter ADF, the deviation value considered as a threshold for summer was 6K. There is a trade-off between the

threshold and the foehn events detected; the low threshold value can cause many false foehn events to be detected, whereas a high threshold value leads to very few actual foehn events to be detected. The total number of pixels in each image showing a positive deviation from the 15-day mean was calculated. The days with number of pixels above threshold with a positive deviation greater than 6k and above are considered as a day when a foehn event occurred in the MDV. The summer threshold is lower than winter; this is because there is a low rise in temperature due to foehn in summer as the valley floor is already radiatively warmed up.

3.5 Results

3.5.1 Assessment of winter ADF performance in detecting foehn events.

The foehn events detected by ADF in winter are compared with the foehn events detected using meteorological data from the 6 AWSs to check for the methodology's efficiency in detecting foehn. The duration and time of onset of foehn event are different across the valley floor. To compile a singular foehn event information from the 6 AWS, a day with a strong foehn event was determined when 2 or more of the installed AWSs experienced a foehn event that lasted for more than 6 hours. Any foehn event that does not fall into the criteria is considered as a weak foehn event. The 6-hour threshold was chosen based on research by Speirs et al., (2013a), where a foehn day by any AWS is considered if it encounters six or more hours of foehn-like conditions in a day. Suppose a foehn event was only detected by one of the stations; in that case, the event is more likely to be a weaker foehn event that could not penetrate through the easterly wind flow and affect most of the valley, on the other hand, if all the 6 AWSs registered a foehn event it can be considered as a major event that had both intra and inter valley impact. As the 6 AWSs are sparsely located, a foehn signal detected by any two of the AWSs have a more extensive spatial coverage, and thus a spatial threshold of at least two stations was chosen.

The foehn events detected from the 6 AWSs are compared with the foehn events identified using winter ADF for 2015 winter (1st April till 31st Aug). Missing daily average LST values in an image representing foehn events can lower the total count of pixels with a positive deviation from their seasonal average. The lower number causes ADF to not detect the foehn events that occur during overcast. Thus, at least 75% of the pixels in an image must have daily average LST values, else they don’t add up to be greater than the threshold and not detect Foehn. A total of 26 foehn events was detected by ADF over the 2015 winter, out of which 17 corresponded to weaker foehn events (events that are detected by only one of the 6 AWSs and lasts for less than 6 hours) and one major foehn event, also identified by the AWSs. ADF may miss out on some significant events over the winter period due to LST data's unavailability because of overcast periods. Figure 3.4 shows the days with foehn events detected by ADF along with the days when the AWSs detected a foehn event.

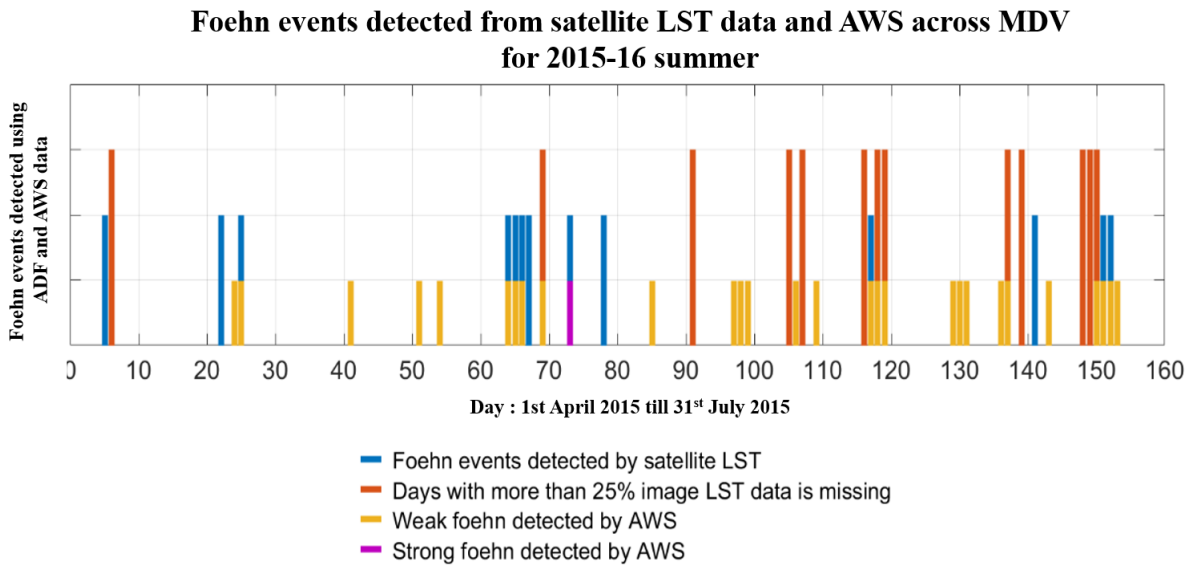

Figure 3.4 Foehn events registered by satellite LST and AWS across MDV during the winter of 2015 from 1st April 2015 till 31st Aug 2015. The y-axis represents the 153 days between the given period the foehn events occurred while the x-axis represents the foehn events detected by ADF and AWS.

The blue bars represent the days when a foehn event was detected by the ADF, whereas the yellow (weaker foehn events) and purple (stronger foehn events) bar show the foehn events detected from AWSs. When both the bars are coinciding, it indicates a day with foehn event that both ADF and AWSs detected. The red bar indicates days when 25% or more of the pixels in an LST imagery had missing values; the ADF cannot detect foehn events during those days.

ADF can detect stronger foehn events and is less sensitive in detecting the weaker foehn (Figure 3.4). LST data availability plays a significant role in the foehn detection process as ADF misses out on a few foehn events due to data unavailability over a substantial part of the image. The techniques discussed in chapter 2 (Chapter 2 Section 2.4.2) for removing missing data from the LST images cannot be used in this algorithm, as gap-filling over a long duration (>2 days) is not feasible, and the gap-filled LST values are always higher/ lower than the actual LST and a certain level of uncertainty is involved with filling up the LST over larger areas. Despite the limitation discussed din previous chapter gap-filling technique was applied on the satellite data for testing the performance of ADF, and the algorithm performed the same over the gap-filled data. For 2015, winter ADF was able to identify the significant foehn events, and further multiple-year analysis will help in better understanding the efficiency of winter ADF.

3.5.2 Assessment of summer ADF performance in detecting foehn events.

Foehn events detected from ADF are verified against foehn events detected using the AWS meteorological data for the 2015-16 summer (1st Nov till 28th Feb). The study applied conditions as for the winter ADF to quantify the foehn signature from all the 6 AWSs based on their duration and spatial

coverage. As ADF primarily concentrates on foehn events that have a more considerable spatial impact and result in extreme warming across MDV, the study required refining foehn signals representing stronger foehn events from the 6 AWSs. To compile a singular foehn event information from the 6 AWS, a day with a strong foehn event was determined when 2 of the installed AWSs experienced a foehn event that lasted for more than 6 hours. Figure 3.5 (a) shows the day with foehn events detected by the AWSs (blue) and the day with foehn events identified by the ADF (green) over the summer of 2015-16. Figure 3.5 (b) shows the number of pixels with missing data in the LST image for each day.

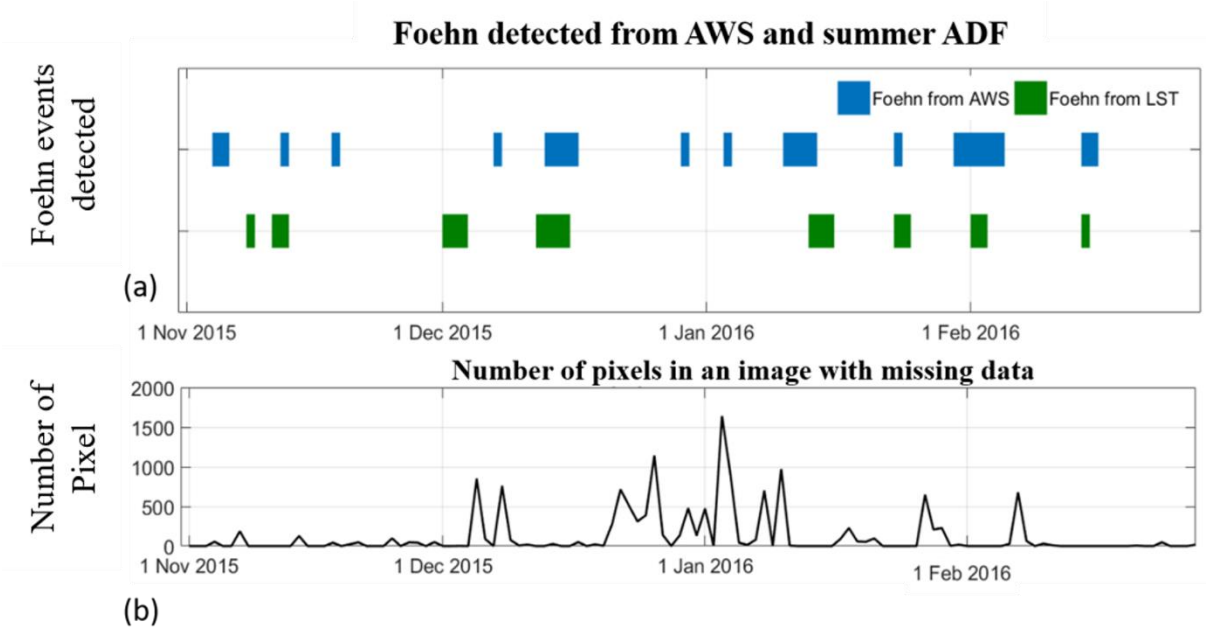

Figure 3.5 Foehn events detected using summer ADF and meteorological data from AWS over 2015-16 (a), along with the number of pixels in each image with missing data (b), the x-axis represents the days in the season from 1st Nov 2015 till 28th Feb 2016

The total number of foehn events detected by the AWSs is 28, whereas the summer ADF identified 33 foehn events (Figure 3.5) throughout the season; out of 28, 15 were detected by both AWS and ADF. 5 of the identified events are minor foehn events. Summer ADF over-estimated the number of days with foehn events; also, the efficiency was not high. Further studies are required to enhance summer ADF's performance in detecting foehn event.

3.5.3 Long term study:

Summer and winter ADF were applied on 14-year data to check for the methods' efficiency. The efficiency of ADF in detecting the foehn events is defined by the number of foehn events detected by ADF compared to the foehn events detected using the techniques developed by Speirs et al., (2010) from meteorological data. It is to check if the ADF can pick up as many days with a foehn event as were detected from the AWSs.

3.5.3.1 Winter foehn detection

Winter ADF was applied over 14 years of winters using the daily average LST images over the 1st of April till the 31st of August for each season. Table 3.2 shows the performance of winter ADF in detecting foehn events over 14 years.

Year	Total number of foehn events detected by ADF	Total number of long duration foehn events detected by AWS	Days with long duration foehn events detected by ADF and AWS (common events)	Days with short duration foehn events detected by ADF and AWS (common events)	Foehn events missed by ADF algorithm due to missing data	Foehn events not detected by ADF (events detected by AWS but not by ADF)	Efficiency of long duration foehn events detected by ADF with respect to AWS. (Percentage of long duration foehn events detected by AWS with respect to ADF)	Overall efficiency of foehn events detected by ADF with respect to AWS. (Percentage of all foehn events detected by AWS with respect to ADF)
2003	12	6	4	5	1	1	83.3	75
2004	11	5	4	7	0	1	80	100
2005	6	1	1	5	0	0	100	100
2006	16	5	2	13	3	0	100	93.7
2007	10	13	7	3	4	2	84.6	100
2008	15	5	2	11	3	0	100	86.6
2009	13	6	3	9	1	2	66.6	92.3
2010	7	1	0	2	0	1	0	28.5
2011	15	2	1	8	1	0	100	60
2012	18	10	9	8	0	1	90	94.4
2013	14	3	3	10	0	0	100	92.8
2014	23	10	6	9	2	2	80	65.2
2015	26	1	1	17	0	0	100	69.2
2016	15	5	4	9	0	1	80	86.6

Table 3.2 Winter ADF performance over 14-year data

Winter ADF showed higher efficiency in detecting foehn events for most of the years. In the years with very few to no foehn events, the efficiency reduced, and it can be seen for 2010 winter. The highest efficiency of winter ADF methodology can be as high as 100% and the lowest is 60% (without

considering the year 2010). Most of the events that winter ADF detected are major foehn events with 6 or more hours of foehn-like conditions experienced by 2 or more of the AWSs across MDV. The winter ADF also picked up on the minor foehn events. Winter ADF does not show high accuracy over the years with significantly fewer or weaker foehn events, though during these years, the number of foehn events detected by winter ADF is also low.

3.5.3.2 Summer foehn detection

Summer ADF was applied over 14 years of summer using the daily average LST images over the 1st of Nov till the 28th of Feb for each season. Table 3.3 shows the performance of summer ADF in detecting foehn events over the 14 years. Summer ADF shows low efficiency in detecting foehn events for most of the years. For the years with very few to no foehn events, the summer ADF identified a lesser number of foehn events. In contrast, the years with a higher number of foehn events, the number of foehn events detected by ADF was comparatively higher. The year 2014-15 was one of the years when there were fewer foehn events, and the summer ADF could not detect those events.

Year	Total number of foehn events detected by ADF	Total number of long duration foehn events detected by AWS	Days with long duration foehn events detected by ADF and AWS (common events)	Days with short duration foehn events detected by ADF and AWS (common events)	Foehn events missed by ADF algorithm due to missing data	Foehn events not detected by ADF (events detected by AWS but not by ADF)	Efficiency of long duration foehn events detected by ADF with respect to AWS. (Percentage of long duration foehn events detected by AWS with respect to ADF)	Overall efficiency of foehn events detected by ADF with respect to AWS. (Percentage of all foehn events detected by AWS with respect to ADF)
2003-04	35	10	3	1	1	6	30	11.4
2004-05	43	13	5	10	2	6	38.4	34.8
2005-06	49	13	5	10	2	6	38.4	30.6
2006-07	37	11	2	7	2	7	18.1	24.3
2007-08	35	15	11	9	1	3	73.3	57.1
2008-09	39	22	13	10	0	9	59.0	58.9
2009-10	37	18	7	7	3	8	38.8	37.8
2010-11	43	13	8	5	0	5	61.5	30.2
2011-12	47	14	11	9	1	2	78.5	42.5
2012-13	40	12	6	10	0	6	50	40

2013-14	45	24	13	13	0	11	54.17	57.7
2014-15	34	8	0	5	4	4	0	14.7
2015-16	33	28	15	1	4	9	53.57	48.4

Table 3.3 Summer ADF performance over 14-year data

The highest efficiency of summer ADF's is 78 %, and the lowest is 30 % (without considering the year 2014-15). Most of the events detected by summer ADF are major foehn events with 6 or more hours of foehn-like conditions experienced by 2 or more of the AWSs across MDV. Summer ADF is capable of picking up some of the minor foehn events. The summer ADF efficiency is less than winter ADF; the methodology overestimated the number of days with foehn events (detects false foehn). Summer ADF's lower efficiency is because of less pronounced changes in LST due to foehn compared to winter. Further development of the summer ADF will help increase the efficiency of foehn detection. The study could not dive further into developing this technique but aims to further enhance these techniques in the future using other datasets in conjunction with LST to reduce the dependency on AWS data for foehn detection.

3.6 Discussion and Conclusions

The chapter aimed to develop a methodology for automatic foehn detection using satellite LST data without using any *in-situ* measurements and was able to develop similar methodologies for summer and winter foehn detection. Winter ADF shows high efficiency in detecting the winter foehn events; this is because of the drastic increase in LST during winter foehn events, which are distinct from the winter period's typical colder temperatures. The summer ADF shows low efficiency in detecting foehn events due to its inability to distinguish between foehn and radiative warming signatures. The increase in LST value during winter due to foehn events is more evident than the summer fluctuations. The radiatively warmed valleys already have higher temperatures; thus, warming associated with summer foehn is less apparent and hard to detect using satellite LST.

The summer and winter ADF have a significant drawback in their inability to detect foehn events during an overcast period. Cloud cover results in the LST dataset’s unavailability for few pixels in the daily average LST imagery, which reduces pixel count with positive deviation from the seasonal mean, causing missed foehn detection from ADF during that period if any event occurred during that period. Techniques like data filling can be applied, as mentioned in the previous chapters. Still, the accuracy might not be as high, and the confidence in detecting foehn events using derived LST values will be low. Data filling was applied on some of the datasets, and both summer and winter ADF did not show much difference in detecting foehn events over the gaps-filled datasets. Though ADF techniques have

their limitations and efficiency concerns, winter ADF still shows some promising results. This foehn detection methodology identifies the pixels showing extreme warming (higher difference of daily average LST from the seasonal mean) indicating the regions with a higher degree of warming due to foehn winds for each day. The Summer ADF requires more refining to distinguish the temperature increase due to foehn from radiative warming of the valley floor, which will lead to more efficient foehn event detection over the summers. The methodology developed in this chapter can be implemented in other parts of Antarctica, where AWS support is limited. Though the methodology may require more refinement.

Chapter 4: Identifying the impact of foehn event across the MDV floor using satellite remote sensing data.

4.1 Introduction

Earlier research on the region's meteorology suggested the presence of individual microclimates at each location in MDV (Fountain, et al., 2002; Doran, McKay, et al., 2002; Riordan, 1982). The microclimates across the valley floor affect several physical processes in the valleys like weathering (Miotke.,1988), ablation (Oliphant, et al., 2015), climate change (Bokhorst et al., 2011). For a significant meteorological event like foehn that is influenced by synoptic-scale climate, most of its study across MDV is limited to point data from a few locations. The response of a location to foehn winds on the ridge top of a mountain will be different from a site on the valley floor .Furthermore when strong low-pressure systems force foehn in the MDV, each valley can exhibit different meteorological conditions, as the interaction between the foehn, the antecedent boundary layer condition, and the geometry of the landscape can influence the penetration of foehn into the valley system. Therefore, there can be large spatial heterogeneity in foehn characteristics that the current AWS network will not resolve. Past investigations into foehn genesis and their effects across MDV used data from Automatic Weather Station (AWS) and modelled meteorological data from Antarctic Mesoscale Prediction System, AMPS (Doran et al., 2008; Speirs et al., 2010; Steinhoff & David, 2006). Because of high variability in meteorology across the valleys, the data collected from a location cannot represent the meteorology of an adjacent site with similar geomorphic conditions (Colacino & Stocchino, 1981; Doran, McKay, et al., 2002), limiting the area of observation.

A comprehensive study of foehn events and their effects across MDV is required over a broader area to identify the shifts in meteorology across each location. Satellite remote sensing provides observation data over a wider spatial scale, which helps study meteorology over a larger area, even in lack of installed AWS. It will help study the effects of foehn events on the regions' surface temperatures even in areas that are not monitored by an AWS. Identifying and clustering the regions based on the temperature fluctuations during foehn events will aid in the study of glacial melt and the region's biodiversity. The present study utilizes satellite LST data to investigate summer foehn's effects on the valley floor temperatures and identify the regions that show a higher degree of warming during a foehn event in MDV.

Objectives of this chapter

- To study the influence of physical properties (elevation, land surface type, etc.) of the region on the LST values across various locations in MDV.
- To study the changes in valley floor horizontal temperature profile during a foehn event in MDV.
- To identify and cluster of warmer zones across MDV based on their warming due to foehn events.

4.2 Context

Microclimate is the climate of a very small or restricted area, especially when this differs from the climate of the surrounding area (Bechtel et al., 2012). A microclimate is distinguished from its surrounding by a sudden contrast in its micro-meteorological conditions from its immediate surroundings (Carlson & Traci Arthur, 2000). Previous research suggested a threefold microclimatic division based on climatic variation and terrestrial condition (Marchant & Head., 2005; Marchant & Head, 2007). In this classification system, the microclimates are classified into three zones, which include a coastal thaw zone (CTZ), inland mixed zone (IMZ), and a stable upland zone (SUZ). Each zone has an individual range of relative humidity, air temperature, precipitation, and hydrology. Though existing microclimatic divisions provide information on what sort of meteorology to expect at a particular region in MDV, the issue with this form of classification is the absence of precise geographic boundary and geomorphic landforms for each zone. A bulky classification of the regions into major groups undermines the individual microclimatic zones and their influence on the biological and physical processes across MDV.

The study uses satellite remote sensing data (Land Surface Temperature products from MODIS) to study the microclimates across the valley floor. It provides data over a broader spatial scale and areas that no AWS monitors. As discussed in chapter 2 (section 2.4.4), the LST response to the meteorological changes gives the study the confidence to utilize the datasets for investigating the temperature variability and effects of foehn events across various locations. As the research focuses on the study of foehn winds and their effects on MDV, the study identifies microclimates based on their response to the foehn events that lead to changes in their Land Surface Temperature (LST) values. The spatial range of microclimates in this study is between a few kilometres. MODIS LST data have a resolution of 1km, and a survey of microclimates using higher spatial and temporal resolution satellite datasets is currently not feasible.

4.3 Data

The 2015-16 summer period is considered for the present study. Among the recent years, 2015-16 summer showed unusual stream flow rates that are higher than the 18-year average. As explained in chapter 1 (section 1.5.2), the summers with extremely high flow rates compared to the 18-year average are considered flood seasons. They are often associated with a higher number of foehn events that last for long durations. Satellite data corresponding to the period is used for the study, along with meteorological data from the AWS. The different datasets used for the analysis are listed below:

- The MODIS LST data for the summer of 2015-16 from both aqua (MOD11) and terra (MYD11) satellites.
- Digital Elevation Model DEM data (40m).
- Landsat RGB band data in True Colour Composite (TCC) covering the region from LIMA.
- The meteorological data collected from 6 AWSs (Bonney, Brownworth, Fryxell, Explorer, Vanda, and Vida) over the 2015-16 summer.

LST data from MODIS is corrected for missing data and outliers based on the work done in chapter 2 (sections 2.4.2 and 2.4.3). For long-term study, 14 years of LST data collected between 2003 till 2016 summer was corrected for missing data and outliers.

4.4 Methodology and Results

The study investigates the horizontal temperature gradient across MDV and studies the region's physical properties' influences on the LST values. For the year 2015-16, 120 images corresponding to the region's daily average LST are used for the study. The daily average LSTs are calculated by averaging two daytime and two night-time instantaneous LST images for each day, acquired from the MODIS sensor mounted on Terra and Aqua satellites.

4.4.1 Influence of physical properties of MDV on the LST of the region

The location and terrain properties of the area play a significant role in determining its' LST values. These physical properties' influences on a region's temperatures are essential as these properties do not show significant change with time. The study explores how each location's surface temperature is different based on the location's physical characteristics. It provides a base for studying the temperature changes associated with foehn events in MDV. The physical properties selected for the study are listed below.

- Elevation
- Land surface type

- Proximity to Ross sea region

4.4.1.1 Elevation

The elevation of a place influences the temperature of that location. Lower Ta values are generally associated with higher elevation. The ridge top temperatures are different and comparatively colder than the valley floor temperatures. A contour map was generated from a 40m spatial resolution Digital Elevation Model (DEM). The contour map identified that the valley floor region roughly has an elevation between 0-800m. The MDV surface was divided into two groups: one comprising the valley floor with an elevation between 0-800 m (roughly), these also include some part of hill slopes at lower elevation, and the other region consisting of the mountain ridges, slopes and their tops with elevation above 800m. After dividing the MDV surface into two groups, the average LST value from all the pixels corresponding to each group was calculated from each image of 2015-16 summer; this generated a 120-day time series of daily average LST of each type. Figure 4.1 shows the daily average LST for the two groups over 120 days, one corresponding to the valley floor LSTs at a lower elevation (solid red) and the other representing ridgetop LSTs (solid blue).

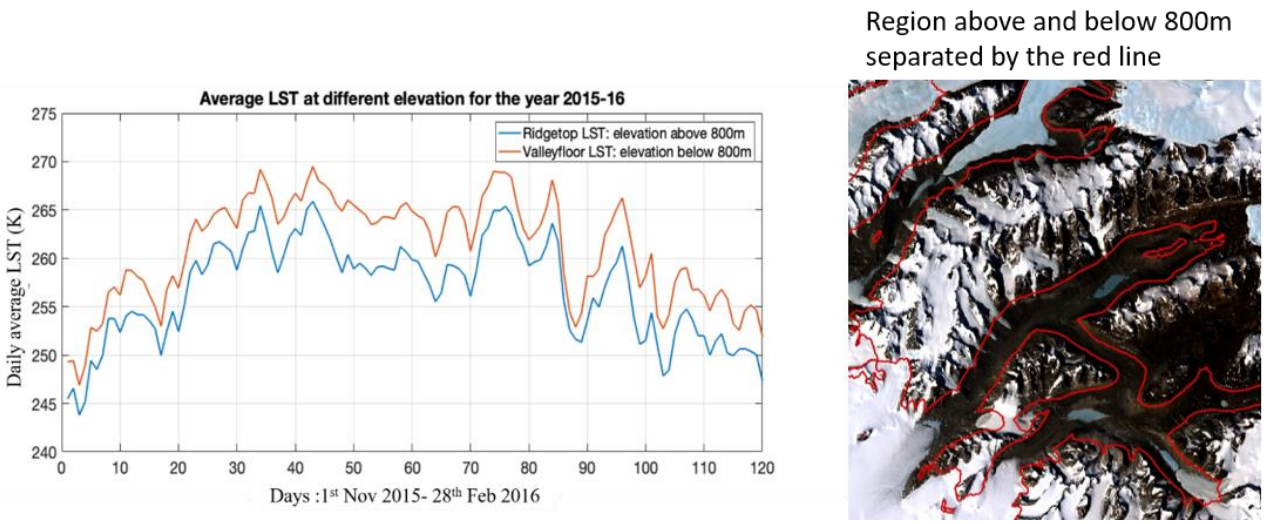

Figure 4.1 Daily average LST value of pixels at different elevations

From the graph, it can be identified that the LSTs at the ridge tops are always lower than the valley floor, indicating warmer valley floors during the summers. The daily average LST difference between the ridge top and valley floor is within a range of 1-7 Kelvin across the summer of 2015-16. This value may vary between years depending on the meteorology of each year. Inter and intra valley floor temperature variability cannot be observed from the above graph; the large-scale spatial variability of LST across MDV can help better understand inter and intra valley differences between locations.

Figure 4.2 shows the map of seasonal average LST across MDV for 2015-16 summer. It can be identified that the ridge top pixels have a lower seasonal average LST compared to valley floor pixels. The LST values vary between the three valleys and within each valley. The map shows that some of the regions on the valley floor are warmer than their neighbouring areas, highlighted inside the green ellipses. The image provides a rough idea of the horizontal temperature gradient of the LST values over different locations in MDV. LST across MDV fluctuates a lot over multiple temporal scales (diurnal, seasonal, and inter-annual); though the seasonal average LST image shows which regions have been warmer throughout the season, it does not provide information on the day to day temperature fluctuations.

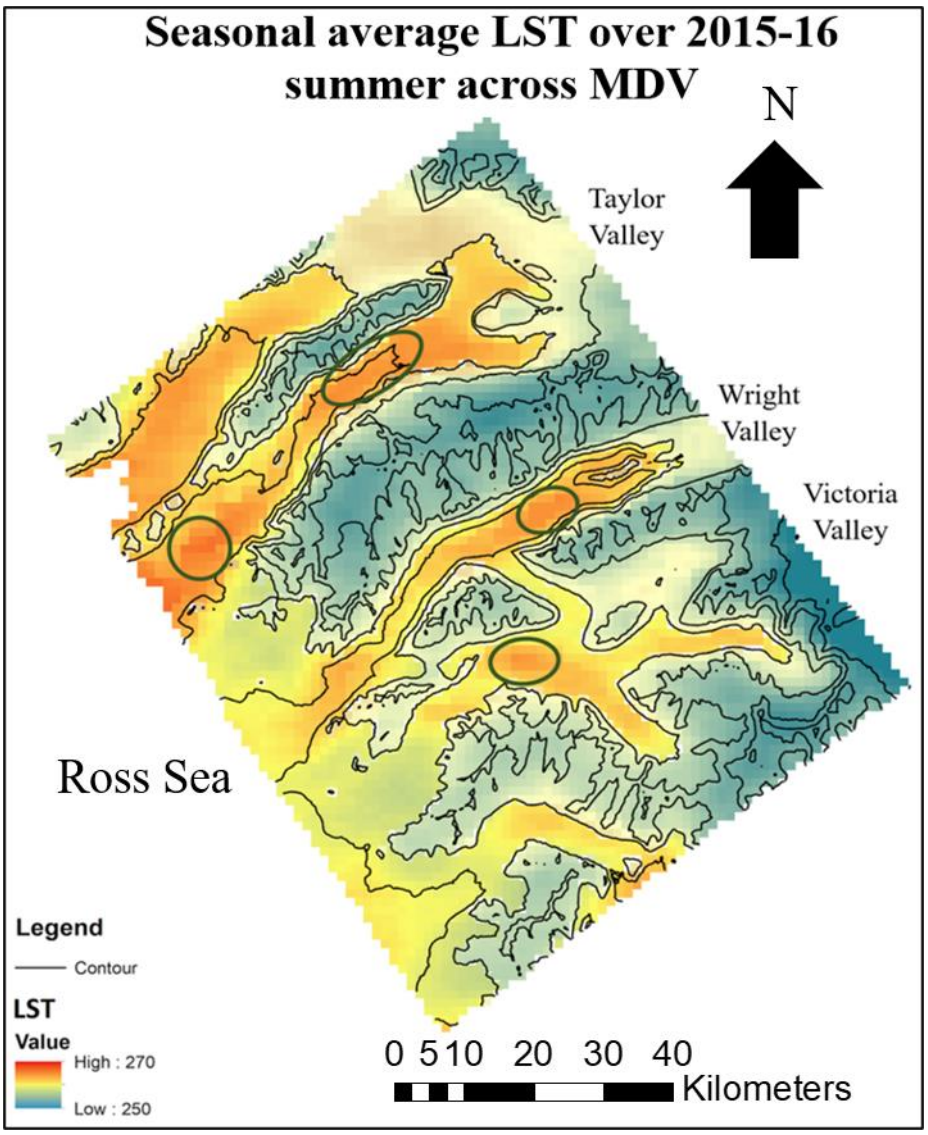

Figure 4.2 Seasonal average LST across MDV over 2015-16 summer, the regions showing higher temperature in comparison to the rest of the valley floor are highlighted.

4.4.1.1 Land surface type

Land surface type plays a significant role in controlling a region's surface temperature; snow and ice-covered area typically have lower temperatures than barren land. The incoming shortwave radiation (ISWR) from the sun is the primary energy source for the earth and its atmospheric system. The earth's surface reflects 29% of the total ISWR to space, and out of the rest of the 71 %, 23% is absorbed by the earth's atmosphere and 48% by the surface (Lindsey, 2009). The outgoing shortwave radiation is dependent on the ISWR, $R_s \downarrow$ and surfaces' albedo α_s which is the ratio of total incoming and outgoing shortwave radiation.

$$\alpha_s = R_s \downarrow / R_S \uparrow$$

The albedo of the surface controls how much energy is available for surface warming after some of the incoming ISWR is reflected. Like snow cover areas, the region with higher albedo reflects most of the incoming radiation, causing less energy to be available for warming up of the surface; on the contrary, water bodies having low albedo absorb most of the radiation, and a minimal amount of the ISWR is reflected. Thus, the heating up of a location on Earth's surface dramatically depends on the surface type's albedo (T.R.OKE, n.d.). MDV surface is no exception to this; each location in MDV is warmed up differently based on the albedo of the surface . Snow and ice-covered glaciers and ridgetops warm up differently from the barren land on the valley floor.

A unsupervised classified image of two different surface types was generated from Landsat Image Mosaic of Antarctic (LIMA). The classified images includes two major groups: one with snow and the ice-covered surface type and the other with the barren land. The ridgetop and valley floor pixels are divided into two major groups based on the surface types. Average LST of pixels representing these two surface types at different elevations is calculated for each image of 2015-16 providing a 120-day time series of daily average LST of the two surface types at two different elevations. Figure 4.3 shows the daily average LST of the two major surface groups' pixels at two different elevations. The valley floor-land surface type is the warmest among the four groups and is followed by the valley floor-snow and ice surface type. The temperature difference between the two groups can be as high as 3-4 Kelvin or lower than 1Kelvin. The snow and ice pixels at the MDV floor surface include mostly warmer lakes, glacial ablation zone, and smaller isolated patches of snow. Both ridge top snow and ice-covered surface and bare land surface have lower daily average LST than the valley floor pixels. The ridge top barren surface has higher temperatures than the snow and ice-covered regions due to low albedo leading to higher radiative warming. The temperature difference between ridge top and valley floor pixels can be as high as 10 kelvin.

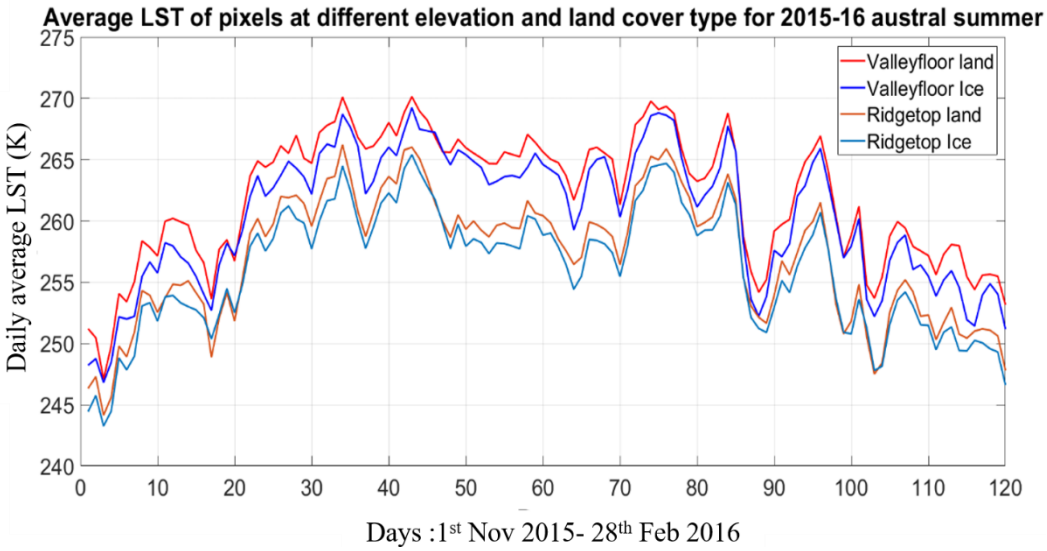

Figure 4.3 Average LST value for various land surface types at different elevations; the x-axis represents the days across 2015-16 summer, and the y-axis represents daily average LST.

The valley floor mainly comprises bare land surface type, and these have warmer temperatures due to radiative warming because of the low albedo. The snow and ice surfaces on the valley floor are warmer than the barren soil and snow and ice surface of the ridge top. The snow and ice surface on the valley are located at a lower elevation and are surrounded by barren land surfaces covering larger areas. The larger patches of barren soil result in higher absorption of the ISWR and increase the overall temperature of the surface.

The ridge tops are mostly covered by snow and ice and have very few barren soil patches; these regions are colder due to their higher elevation and albedo. The snow and ice cover regions on the ridge tops have a high albedo and reflect most of the ISWR, making them colder than the valley floor. Valley floor surfaces are also more vulnerable to foehn events. The valley floor, both barren land and snow, and ice cover surface are more exposed to foehn winds as they descend from the Transantarctic mountains and channel through the valleys, which cause the higher temperature of the valley floor surface types compared to the ridge top.

4.1.3 Proximity to Ross sea region

The regional geography of MDV between the relatively colder Transantarctic Mountains and warmer McMurdo Sound/Ross sea air masses influences the air temperatures and winds of the region (Steinhoff et al., 2013). The Transantarctic Mountains act as a barrier in preventing the Ross sea region's moisture-bearing weather systems from moving inland (Speirs et al., 2008), causing MDV to have very low precipitation. The westerly winds descending in the valleys from the direction of the Transantarctic mountains are warmer and less frequent than the easterlies from the direction of the Ross sea region. The present work explores the seasonal LST trends of pixels covering MDV based on their proximity

to the Ross Sea region. A Euclidean distance raster file of 1km spatial resolution showing each pixel's distance from the Ross Sea was generated. Seasonal average LST was calculated from 120-daily average LST images over 2015-16 summer. The seasonal average LST of each pixel was compared with its distance (proximity) from the Ross Sea region. Figure 4.4 shows the scatter plot between seasonal average LSTs of the pixels covering MDV (a) and their distance from the Ross Sea region. Figure 4.4(b) and (c) show the trends in ridgetop and valley floor pixels individually.

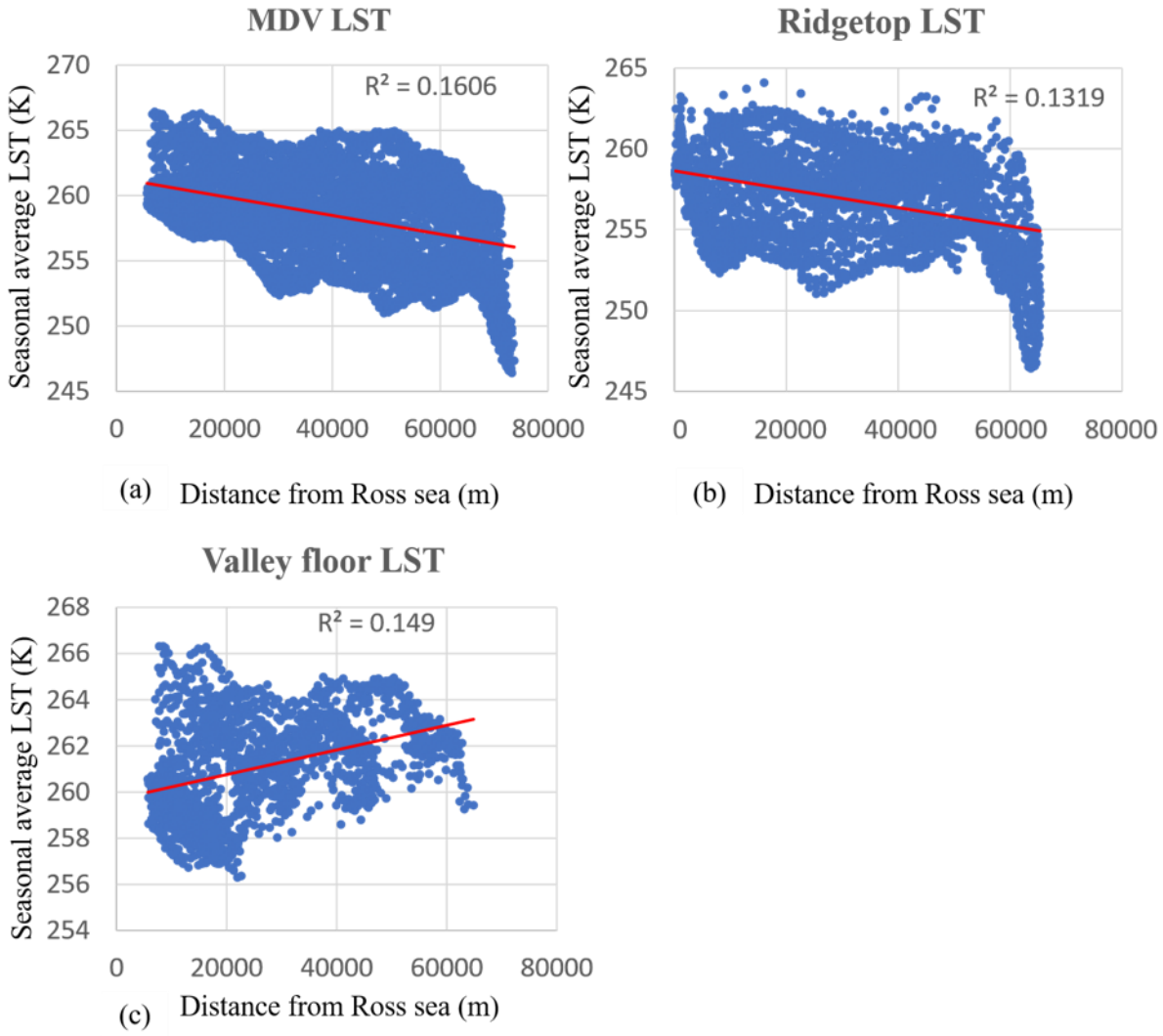

Figure 4.4 Scatter plot between seasonal average LST of each pixel and its distance from the Ross Sea, (a) covering the whole MDV region, (b) ridgetop pixels and (c) valley floor pixels, the x-axis represents the distance from the Ross Sea, the y-axis represents the seasonal average LST.

The trend across MDV shows a decrease in LST with an increase in distance from the Ross Sea region. The MDV pixels are divided into two groups based on their elevation: valley floor and ridgetop pixels. The scatter plot between ridge top pixels' LST and their distance from the Ross sea region shows similar tendencies as the whole of MDV; there is a decrease in the ridge top LST values with distance from the Ross Sea. While the whole of MDV and the ridge top pixels' LST show a negative trend with an

increase in distance from the Ross Sea, the scatter plot between valley floor pixels' LST and their distance from the Ross Sea show an opposite trend. The valley floor pixels' LST increases with distance from the Ross sea region. The trend in valley floor LST indicates a warmer upper valley region near the Transantarctic Mountains compared to the lower valley region towards the Ross Sea area, which may be a result of high-frequency foehn induced warming as registered by the upper valley AWSs .Trends in ISWR (radiative warming) show that lower valley AWSs receive higher radiation than upper valley regions, which contradicts the low temperatures in the lower valley region as compared to the upper valleys. The upper valley temperatures are mostly contributed to the high frequency foehn rather than the radiation induced warming.(Chapter 1, section1.5.4.1). The valley floor LST trend may vary inter annually depending on how frequent foehn events occurred during each season.

4.4.2 Study of foehn and its effects on MDV surface temperatures

The importance of foehn winds in modulating the valley-wide metrological conditions was discussed in the previous chapters. Due to limited observational data, studying these events' effects across MDV was limited to a few locations. The present study investigates the impact of the foehn events across MDV over a large spatial scale using satellite-derived Land Surface Temperature (LST) data. It provides a fresh perspective into foehn study across MDV from a more extensive spatial scale observation.

4.4.2.1 Foehn events: Meteorological study

The 2015-16 years also had a higher frequency of foehn events (Chapter 1, section 1.5.2). The foehn events commencement and cessation are determined from the meteorological data collected from all the 6 AWS (Bonney, Brownworth, Explorer, Fryxell, Vanda, and Vida) across MDV. Foehn identification conditions discussed in chapter 1 (section 1.5.2) were applied to the meteorological data to identify the events occurring during the 2015-16 summer. Figure 4.5 shows the duration of foehn events registered by the 6 AWSs. It can be identified that between week 6 and 7 (highlighted inside the box), there had been a foehn event that was registered across all the 6 AWSs, that lasted for several days, indicating an event that had a significant impact on the valley floor meteorology over a long duration and across a large spatial scale. The present work takes the period between 11 Dec 2015 till 17 Dec 2015 as an ideal case for studying a long-duration foehn event with extensive spatial coverage. Figure 4.5 shows that not all AWSs experience equal number and duration of foehn events.

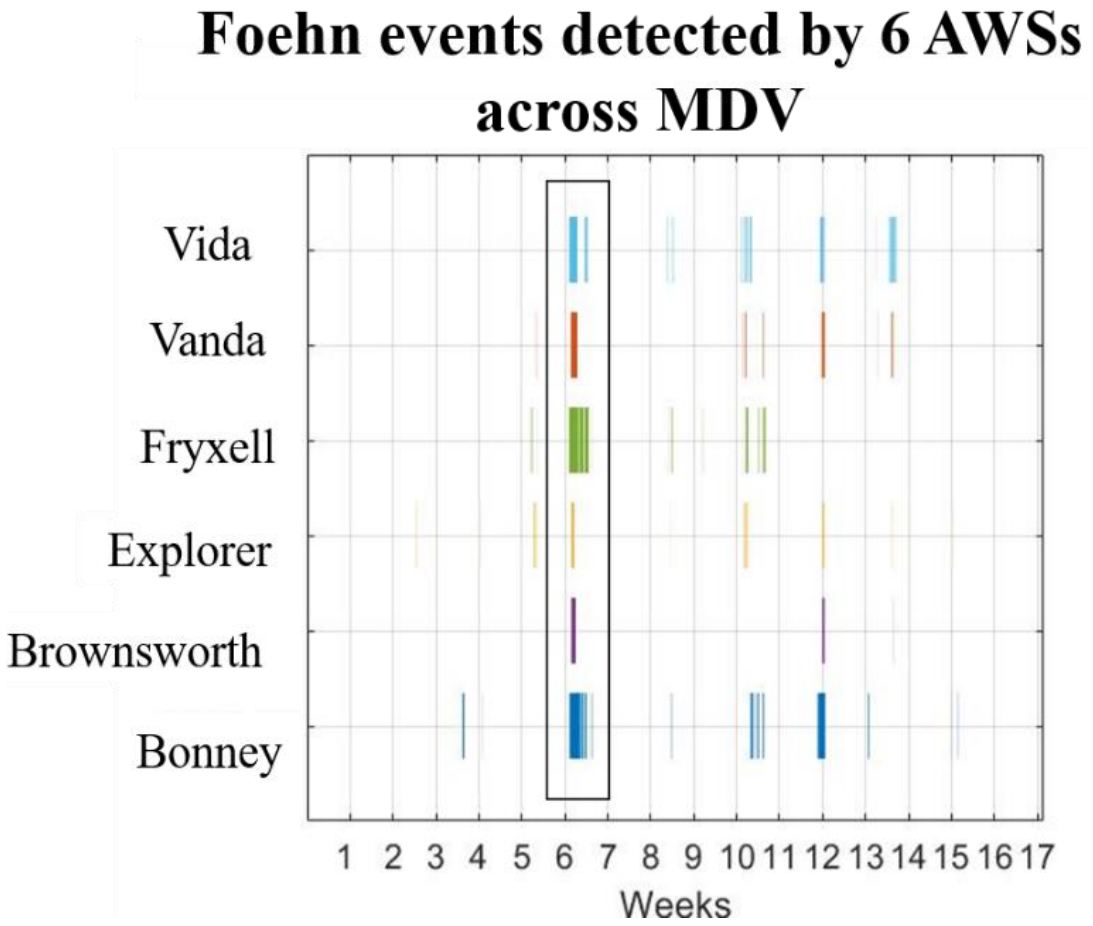

Figure 4.5 Foehn events registered by the AWSs across MDV over summer of 2015-16; the x-axis represents the weeks in the summer season from 1st Nov 2015 till 28th Feb 2016, while the y-axis represents foehn events detected by each station.

The location of the AWSs in MDV plays a significant role in the number of foehn events it experiences. Figure 4.6 shows the total foehn hours experienced by each of the AWSs over 7 days from 11th of Dec 2015 till 17th of Dec 2015. On the 11th of Dec 2015, no foehn was registered by any of the 6 AWSs. On the 12th of Dec 2015, with the foehn's genesis, 4 out of 6 AWSs registered the event. On the 13th, 4 AWSs reported 24 hours of foehn winds, and the rest 2 experienced more than half a day of foehn winds. On the 14th, the foehn event's intensity gradually starts to decrease, with 2 out of 6 AWSs reporting 21 hours of foehn winds, and the rest were negligible. On the 15th, foehn intensity further reduced with 3 out of 5 AWSs registering the events with a maximum of 18 and a minimum 9-hour duration. On the 16th, the foehn event ceased after being reported by 2 of the AWS for 3 hours.

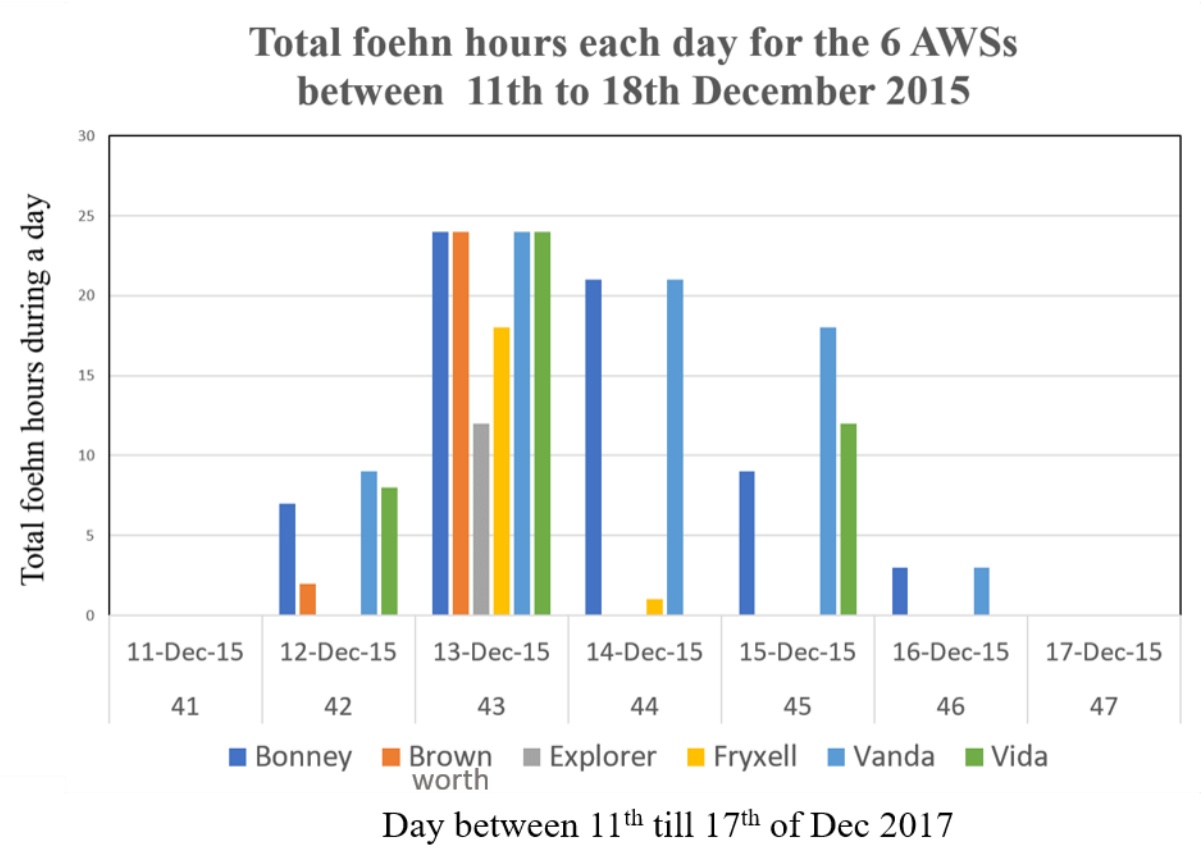

Figure 4.6 Total foehn hours experienced by each AWSs across 7 days, the y-axis represents the number of foehn hours registered by each AWS, the x-axis represents the days from 11th Dec till 17th Dec 2015.

It can be identified from Figure 4.6, the AWSs located at the inner end of the valley (Bonney, Vanda) towards the Transantarctic Mountains were among the first to get affected by the foehn winds as the event began, and the wind gradually descended to the lower end of the valley towards Ross sea region. Brownworth and Vida, located at the lower end and centre of the Wright and Victoria valley respectively, were affected on 12th Dec 2015 when the foehn wind descended into these two valleys. On the other hand, Taylor Valley had foehn winds descend to the lower end of the valley on 13th Dec 2015. On 14th Dec of 2015, when foehn wind's intensity started to decrease, the lower valley AWSs were the first to show foehn cessation while the upper valley AWSs were still experiencing foehn winds. Gradually the foehn event started to reduce and altogether ceased on 16th of Dec 2015. This case study of one of the many foehn events occurring in the valleys, and each event has different dynamics and affects the valley floor temperatures. AWSs located in the upper valley were the most affected. The AWSs situated at the lower end were late in experiencing the foehn winds and experienced lesser foehn hours, especially in Taylor valley. Taylor's natural barrier, Nussbaum Riegel, delayed the foehn winds to reach the Taylor Valley's lower end.

4.4.2.2 Foehn events: Study using remote sensing data.

Daily satellite imagery helps study the day-to-day meteorological changes in the valley floor and study each area's response to the foehn events in MDV. Figure 4.7 shows the MDV surface's daily average LST from 11th Dec 2015 till 17th Dec 2015. The satellite images help study the spatial and temporal variability in LST in response to the foehn events across MDV.

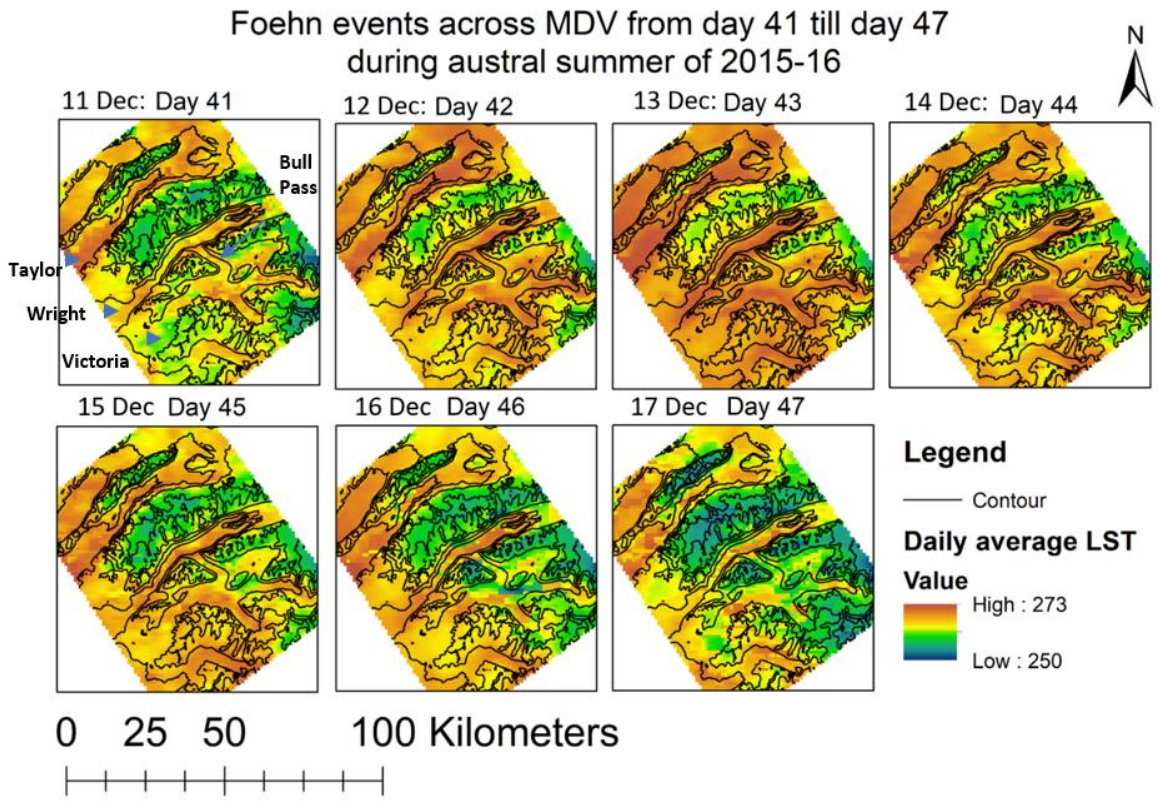

Figure 4.7 Changes in daily average LST in Kelvin across MDV from 11th Dec 2015 till 17th Dec 2015, when a significant foehn event lasted for 5 days.

During the 11th and 17th of Dec 2015, the days with no foehn events; it can be observed that valley floor temperatures are distinctly warmer than the ridge tops. For Taylor valley, the upper valley region towards the Transantarctic Mountains is comparatively colder than the Ross Sea's lower valley. On the 12th of Dec 2015, when the foehn events commenced, a contrast in LST value from the previous day can be observed across the valleys. The lower elevation ridges and the valley floor show warmer temperatures associated with foehn winds. On the 13th, when the foehn events magnitude is at its highest with 4 stations recording 24-hours of foehn winds, the average daily LST shows maximum warming across the valley floor and the ridges. The higher elevation ridgetops show an increase in temperature but are still colder than the valley floor and are less affected by foehn warming compared to the valley

floor and low elevation ridges. On the 13th, even warming occurs across Taylor and Wright valley. Parts of Victoria valley show some variability in temperatures across its valley floor surface. Bull Pass and upper Victoria valley are colder in comparison to the lower end of the Victoria valley. On 14th Dec 2015, as the foehn events start to recede, the ridge tops cools down faster than the valley floor. LST across MDV is lower than that on 13th but is still high as the foehn events lasted for more than 12 hours for most of the stations. On the 15th of Dec 2015, the temperature was reduced compared to previous days, and Victoria valley can be seen cooling down faster than Taylor and Wright. However, the lower end of Victoria was still warmer than the upper end. On the 16th of Dec 2015, with negligible hours of foehn winds observed by 2 of the AWSs, upper Victoria valley temperatures drastically reduced compared to Wright and Taylor Valley. Each location in MDV showed different levels of warming because of foehn winds, and there is high variability in warming patterns among the valleys and within the valleys.

The effect of foehn event on the valley floor LST distribution

As seen in Figure 4.7, the LST values across MDV change drastically during a foehn event. The valley floor LSTs show more even (homogeneous) warming during a foehn day than on a non-foehn day. Histogram of LST values across MDV can better explain the changes in temperature distribution across different days during a foehn event. Figure 4.8 shows the histogram distribution of daily average LST across MDV from 11th Dec 2015 till 17th Dec 2015.

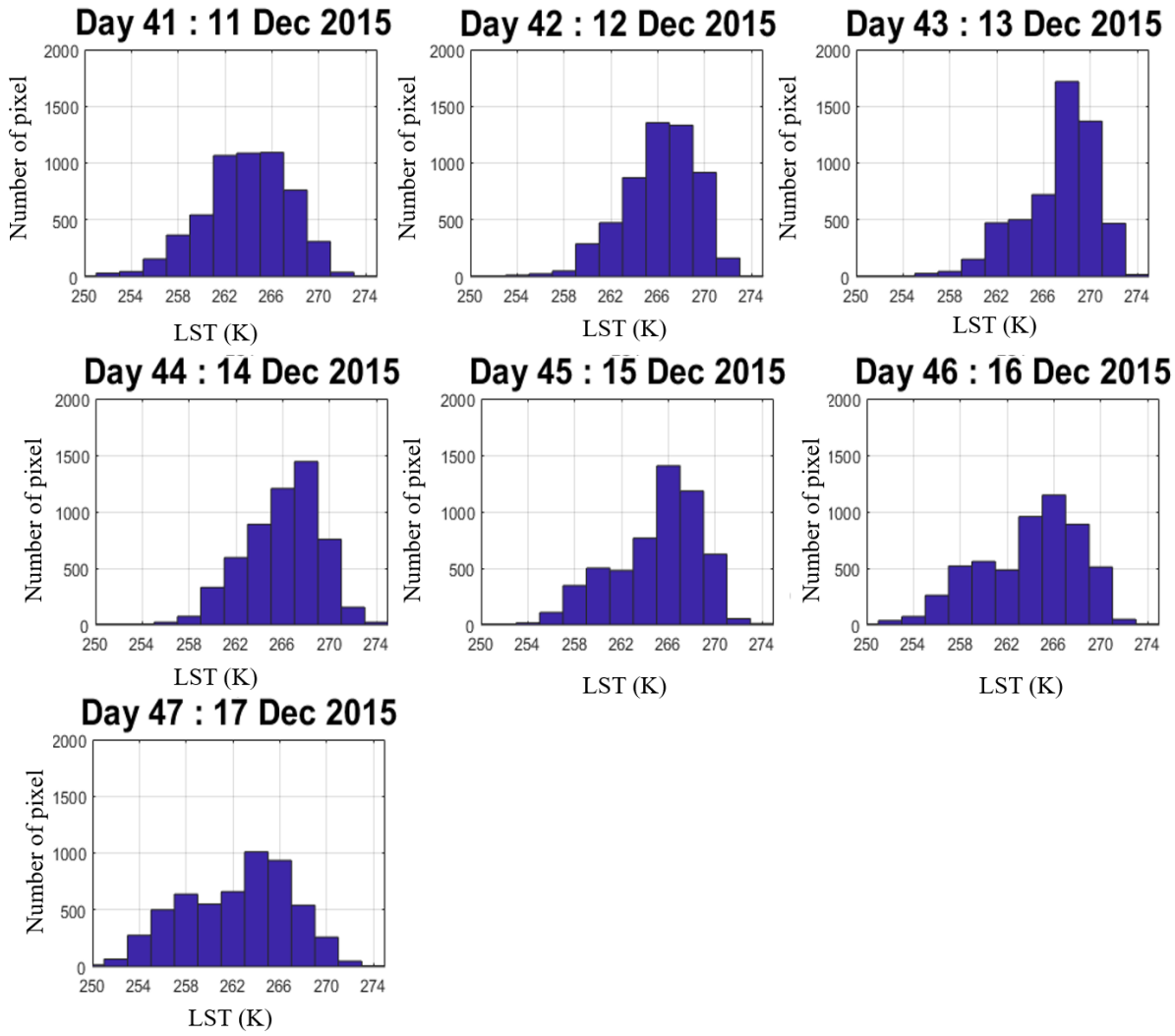

Figure 4.8 Histogram of LST covering the whole MDV region across the 7 days from 11th Dec 2015 till 17th Dec 2015. The y-axis represents the number of pixels in each category; the x-axis represents the LST group.

The histograms show on 11th, most of the LST distribution is between 255K and 270K. With foehn onset on the 12th, the distribution gets concentrated between 260K and 270K, with most of the pixels having LST values ranging from 265K to 270K. On the 13th of Dec 2015, when foehn magnitude was maximum, the distribution clustered more, with most pixels having LST values ranging from 265K to 270K. As the foehn events started receding on 14th, the LST distribution gradually spread out with a reduction in foehn intensity. On the 17th, the distribution of pixels is over a more extensive range of temperatures, and the pixels register lower temperatures than the days when there was a foehn event.

MDV low elevation valley floors are susceptible to higher temperature changes due to foehn events than the rest of the region. Taylor valley was chosen for studying the valley-wide distribution of daily average LST during the foehn events from 11th Dec 2015 till 17th Dec 2015. Figure 4.9 shows the

histogram plots of daily average LSTs of the pixels covering the Taylor valley floor during the 7-day foehn event.

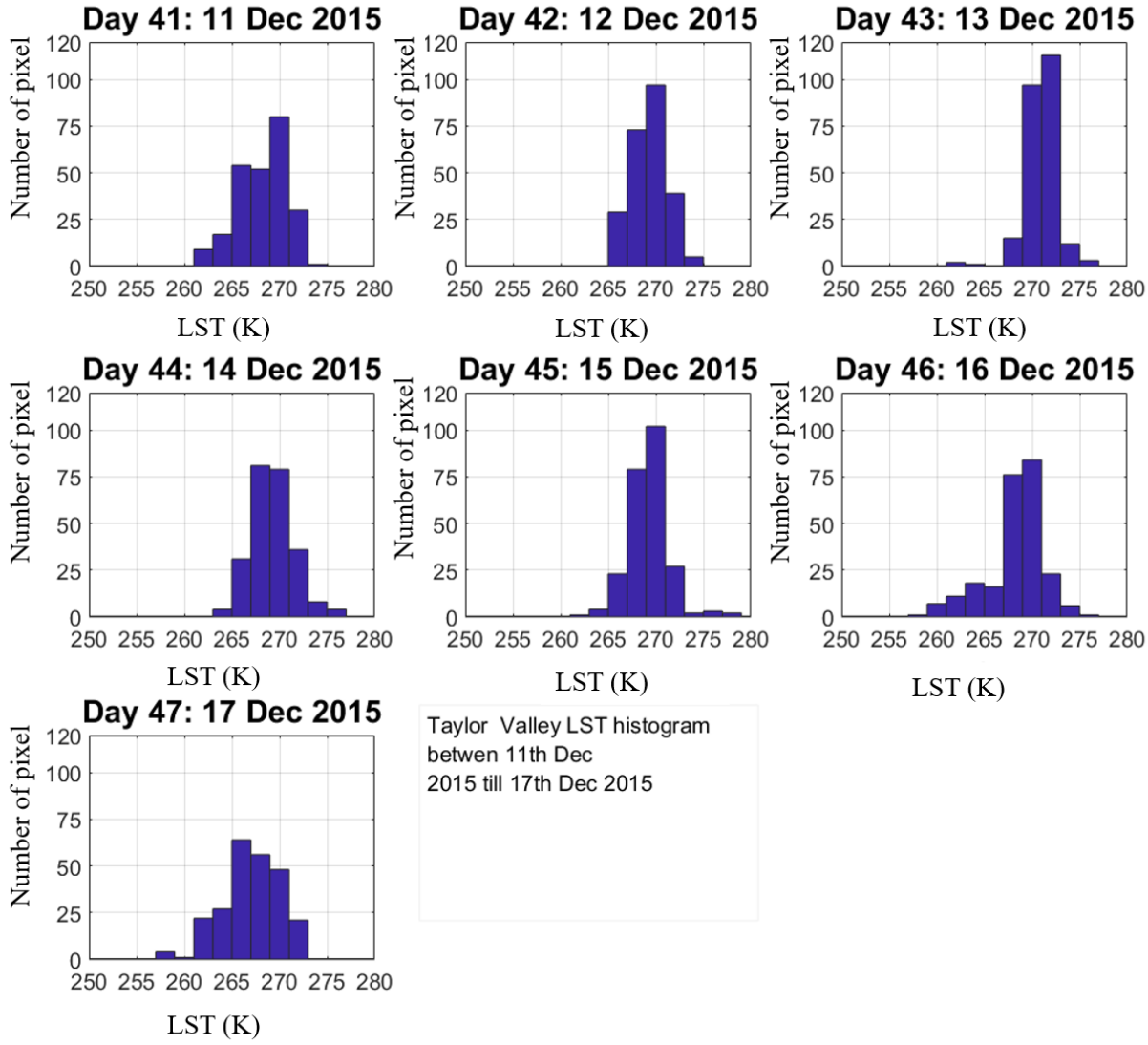

Figure 4.9 Histogram of LST covering the Taylor valley across the 7 days from 11th Dec 2015 till 17th Dec 2015. The y-axis represents the number of pixels in each category; the x-axis represents the LST group.

The daily average LST temperature on the 11th is distributed between 260K and 275K. As the foehn event commences, there is a gradual growth in LSTs' magnitude over 12th to 13th Dec 2015; the temperature distribution clusters between 265K to 275K range and is highly concentrated between 270k to 273k when the foehn event is at its highest magnitude on 13th Dec 2015. The distribution gradually spreads out to lower temperature groups as the foehn event's intensity reduces in magnitude following the trend across the whole of MDV.

During summer, the MDV heats up radiatively; the LST values vary among lower temperature groups as the radiative heating depends on the surface types' albedo and the region's elevation. The ice and snow-covered areas heat up differently from the dry, barren surfaces or the wet riverbeds, and thus the LST distribution is over a wider group of temperatures. When warm westerly winds descend into the valley floor during foehn, warming shifts from radiative to predominantly adiabatic warming of the valley floor boundary layer. The heat transfer between the atmosphere and valley floor surface is even despite the land surface type. Long-duration convective heating due to foehn lasts over 24 hours, resulting in a rise in temperature and the valley floor having similar temperature ranges despite their surface type. The clustering of LST values into a higher temperature group results from this phenomenon. As the foehn events magnitude reduces, the warming of the valley floor gradually shifts to radiative warming, and the temperature distribution spreads out to the lower temperature groups as the valley floor cools down.

Changes in horizontal temperature gradient from the upper end (towards the Transantarctic Mountains) towards the lower end (towards the Ross Sea region) of the valley during a foehn event.

The wind regime strongly influences the temperatures across the valleys in MDV. The bimodal wind regime of westerly and easterlies cause the temperatures at the two ends of the valley to be different. During a typical day, without foehn events, the upper valley temperatures are colder than the lower end, which are more susceptible to warm easterlies from the Ross sea region. Figure 4.10 shows the changes in LST profile across the valley from the upper to the lower end of the Taylor valley (Base of the Taylor glacier till the end of the valley at Ross sea region) from 11th Dec 2015 till 17th Dec 2015.

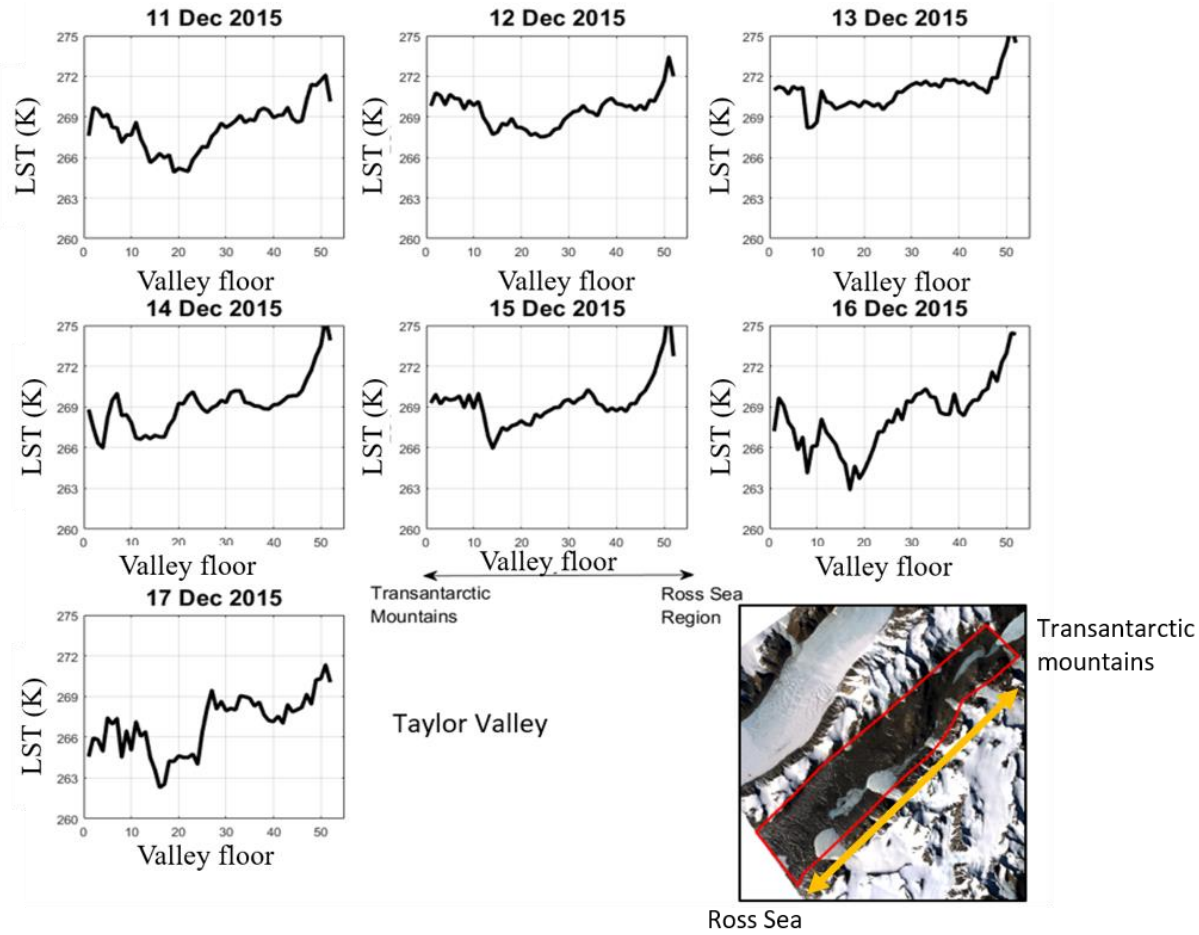

Figure 4.10 Average LST along the valley from the upper end to the lower across the 7 days from 11th Dec 2015 till 17th Dec 2015, the y-axis represents the average LST, and the x-axis represents the distance from the inner end of the valley to the outer.

The daily average LST values at the upper end of the Taylor valley are lower than the lower end. The temperature fluctuates across the length of the valley from the upper end to the lower end. Figure 4.10 shows on the 11th, the temperature gradually reduced with distance from the upper end of the valley, then it increases with proximity from the Ross sea region. There are fluctuations in daily average LST values across the valley's length when there are no foehn events as the valley is predominantly warmed radiatively. At the onset of foehn, there is a gradual increase in LST values along the valley. The fluctuations in LST along the valleys' length flattens, and the temperatures show similar ranges along the valley floor. As the foehn magnitude gradually starts decreasing and finally the event ceases, the fluctuations in LST values increase progressively and reach a typical state like those on 11th and 17th of Dec 2015, before and after the foehn event. As the foehn winds traverse along Taylor valleys' length, it increases the temperature almost evenly; the temperature fluctuation resulting from differential radiative warming dampens, and the valley floor warms up evenly across its' length.

4.4.3 Response of MDV floor to foehn events

MDV valley floor warms up because of the combined effects of radiative warming from solar radiation and adiabatic warming of foehn winds during summer. The idea of using satellite data to study the foehn events is to understand the more considerable spatial scale impact of foehn events on the MDVs. A few location in the MDV are more susceptible to foehn events than others, and the rise in temperature due to foehn in those areas is more substantial than the others.

The present work cannot discriminate the warming due to foehn from that of solar radiation over summer for which, it investigates only the days when a foehn event was identified by the AWSs and the associated climatic that are favourable for higher temperatures across the valleys. All the days experiencing summer foehn events between the years 2003 and 2016 were categorized into four different groups based on the duration and spatial impact of foehn winds along with the intensity of the ISWR (Chapter 1 section 1.5.3). The details of each day's event and their grouping is provided in Table 2 of the appendix and the clustering can be seen in Figure 1.12. The four major groups include.

- Group 1: days with 6 or fewer hours of foehn winds during low ISWR <250 W/m^2.
- Group 2: days with 6 or fewer hours of foehn winds during high ISWR >250 W/m^2.
- Group 3: days with 6 or more hours of foehn winds during high ISWR >250 W/m^2.
- Group 4: days with 6 or more hours of foehn winds during low ISWR < 250 W/m^2.

Group 1 and 4 represent foehn events that occurred when the ISWR was low; these include days over the beginning or end of summer or during an overcast period when clouds attenuates ISWR. The availability of LST images during these periods is low, primarily due to cloud cover. The study will focus on groups 2 and 3 when ISWR is high (clear sky days), and the foehn duration varies between days. The two groups are associated with conditions that are favourable for glacial melt. Not all AWS across MDV provide net radiation information available for warming, hence, the study relies on ISWR measurements to understand how much energy is available for warming, depending on each surface types' albedo.

Daily average LST images corresponding to a foehn event in each group were stacked together. The images were pre-processed to remove missing data and outliers (Chapter 2, section 2.4.2 and 2.4.3). The stacked images from groups 2 and 3 had 34 and 37 satellite LST images across 15 years respectively. Each image in the groups represented a day when there was a foehn event in MDV. Group 2 had daily average LST images of the days with foehn events that lasted for less than 6 hr and occurred in the presence of high ISWR above 250 W/m^2. Similarly, Group 3 had daily average LST images of the days with foehn events that lasted for more than 6 hours and occurred in the presence of high incoming solar radiation above 250 W/m^2. The daily average LST of each day varied from the other;

one day is warmer or colder than the other depending on the strength of the foehn events and prevailing meteorological condition during that day. The study's purpose is not to find which day is warmer than the other, instead to find the hotspot zones that showed exceptionally high warming relative to the rest of the valley. To compare one region's warming to another, the LST of a pixel needed to be compared with a standard value. A spatial average of all the pixels in the image is calculated to get an image mean. The image mean is subtracted from each pixel's LST value to check how much warmer or colder each pixel is from the image average. Subtracting image average LST from each pixel's value normalizes the temperature difference between images and only concentrates on the difference warming of each zone in each image.

The difference in temperature between the image means and the daily average LST values indicate which areas are warmer and cooler by how many degrees from the rest of the valley's average LST, highlighting the areas where temperature deviates from the mean. It was done for both the groups, resulting in a stack of groups 2 and 3 where the pixel in each image shows the difference between daily averages LST from the image mean.

As the study focuses specifically on the warming trends across the MDV to identify areas that experienced higher temperature rise than the rest of the valley, the pixels with negative deviation were not considered. The positive difference values (temperature difference between daily average LST and image mean LST) of the pixels in each group ranged from 0 to 12 K. The temperature range is divided into 3 categories, representing different levels of warming.

- Pixels with 0 to 4 K temperature difference represent low warming.
- Pixels with 4 to 8 K temperature difference represents moderate warming.
- Pixels with 8 to 12 K temperature difference represents high warming.

The pixels belonging to each category of warming were isolated in each group's stacks; after calculating the stack sum, density maps are produced for each group and with different levels of warming. The density map shows the number of occurrences of each category of warming at different locations in MDV. Each pixel value in the density image represents the number of days over the 14 years the pixel experienced each category of warming. For example, a pixel with a value of 5 in group 2, category 3, experienced 5 days with a high degree of warming ranging between 8 to 12 K over a period with fewer than 6 hours of foehn and ISWR above 250w/m^2. The higher the pixel value, the higher the number of days the region experienced that category of warming. Figures 4.11 and 4.12 show the clusters in the valleys that are affected by different warming levels from the two groups, groups 2 and 3, respectively.

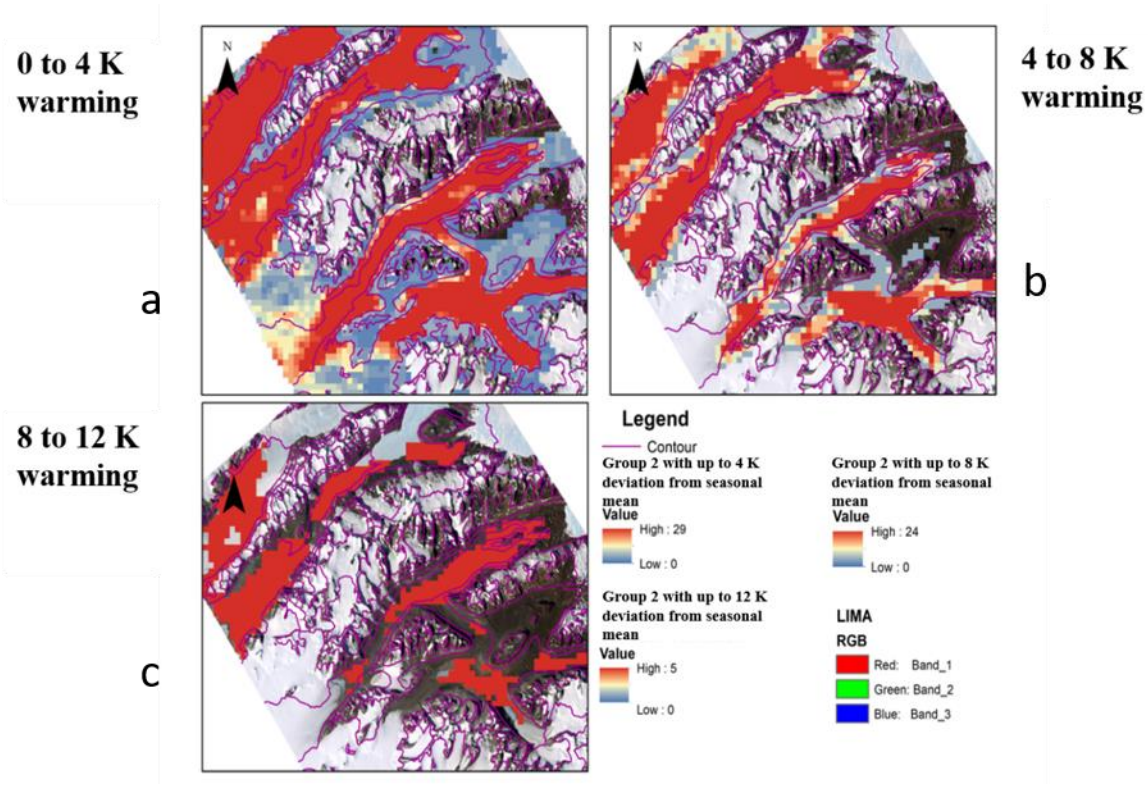

Figure 4.11 Group 2 highlighted regions with different warming levels in kelvin when the solar radiation was high and foehn duration was low. a) shows the pixel with deviation between 0-4K, b) shows deviation between 4-8K, c) shows deviation between 8-12K from the valley mean.

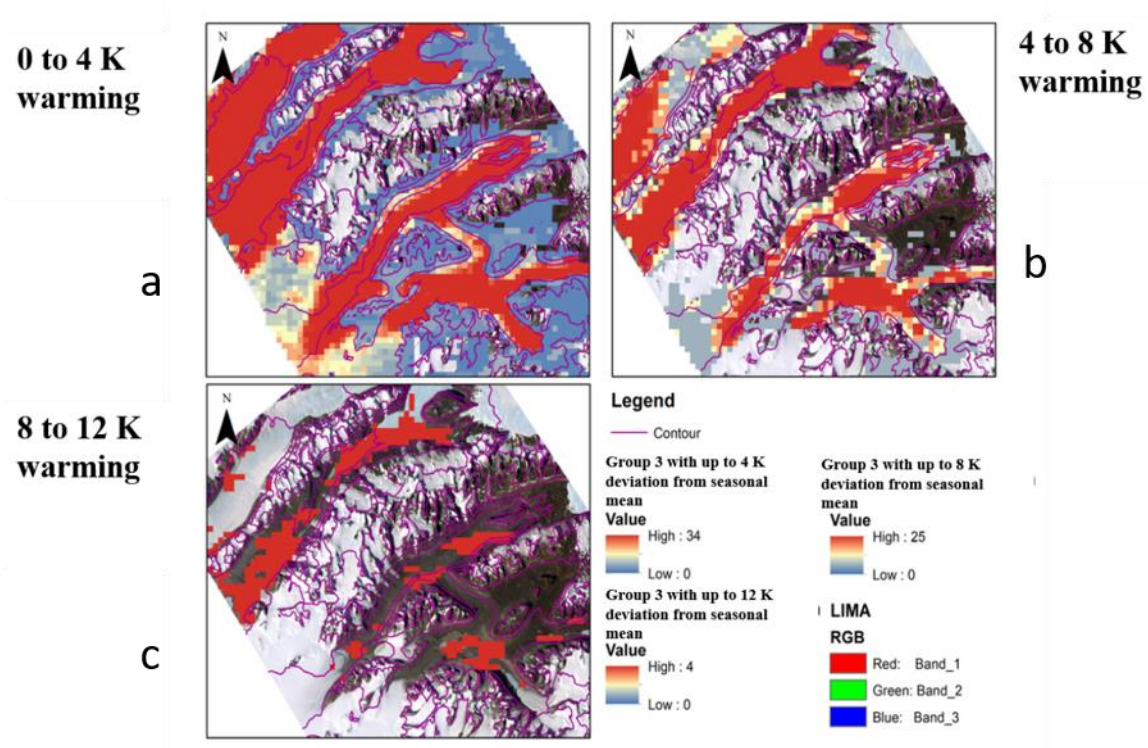

Figure 4.12 Group 3 highlighted regions with different warming levels in kelvin when the solar radiation was high and foehn duration was high. a) shows the pixel with deviation between 0-4K, b) shows deviation between 4-8K, c) shows deviation between 8-12K from the valley mean.

Figures 4.11 and 4.12 show that a lower level of warming from 0 to 4 K in both groups occurred across the valley floor. In group 2 though, the lakes (Fryxell & Bonney) in Taylor valley seem colder than the nearby region; in group 3, the whole valley can be seen warming up; even the lakes show lower-level warming. The low elevation ice-covered region is warmed up negligibly. For the category of warming representing moderate warming with a temperature difference from 4 to 8 K, it can be identified that in Wright valley, higher elevation ridges and parts of Bull pass show lower warming days than the rest of the valley floor groups. It is interesting to find the moderate warming is concentrated in half of the valley lengthwise, due to the higher elevation on the other half of the valley, seen from the DEM contour lines.

For the category of warming representing high warming with temperatures difference between 8 to 12 Kelvins, it can be identified the warming is concentrated on the smaller areas for both group. The upper and lower end of Taylor valley experienced this warming but are divided by Nussbaum Riegel. In Wright valley, group 2 – high warming category covers a larger area than that of group 3, and the warming is concentrated around the lake Vanda region. For Victoria valley, the center region heated the most compared to the valley's upper and lower regions.

In Taylor Valley, as previous studies suggested, the presence of Nussbaum Riegel causes the upper and lower end of the valley to experience different meteorological conditions. It can be seen in the present study that the Nussbaum Riegel, not only physically divides Taylor Valley into two parts but also creates two different meteorological regimes (Fountain and others, 1999), disrupt the higher temperatures across the MDV during a foehn event. For a higher degree of warming, its effects can be seen distinctly (category b and c), where the warming is concentrated in the two halves of the valley divided by the partition. The Wright valley area around the lake Vanda is more affected by foehn winds than the rest of the valley. The lower Victoria valley shows the most warming for higher categories.

4.4.4. Relation between warming and elevation

A higher degree of warming is observed in smaller areas in certain areas of the Valleys. The pixel value representing the number of days of each category's occurrence in each group was compared with the pixel's elevation. Figures 4.13 and 4.14 show the scatter plot between the pixel values of the density plot image, representing the number of days of the occurrence of a category of warming in each group with the pixels' elevation value.

For both groups, lower level warming from 0 to 4 Kelvins can be observed across all the regions irrespective of the locations' elevation. As we move to a higher degree of warming from 4 to 8 K, a pattern can be observed. The region (pixels) that experiences a higher number of days with moderate to high warming has a lower elevation. All the pixels in the analysis represent all the valley floors, and

among them, the pixels with the lower elevation show a higher number of days with moderate to high warming events. The lower elevation areas having a higher degree of warming due to foehn could be because the winds descend from a higher altitude to the lower elevations causing higher adiabatic warming of air parcel. An atmospheric temperature profile could provide more information on this process.

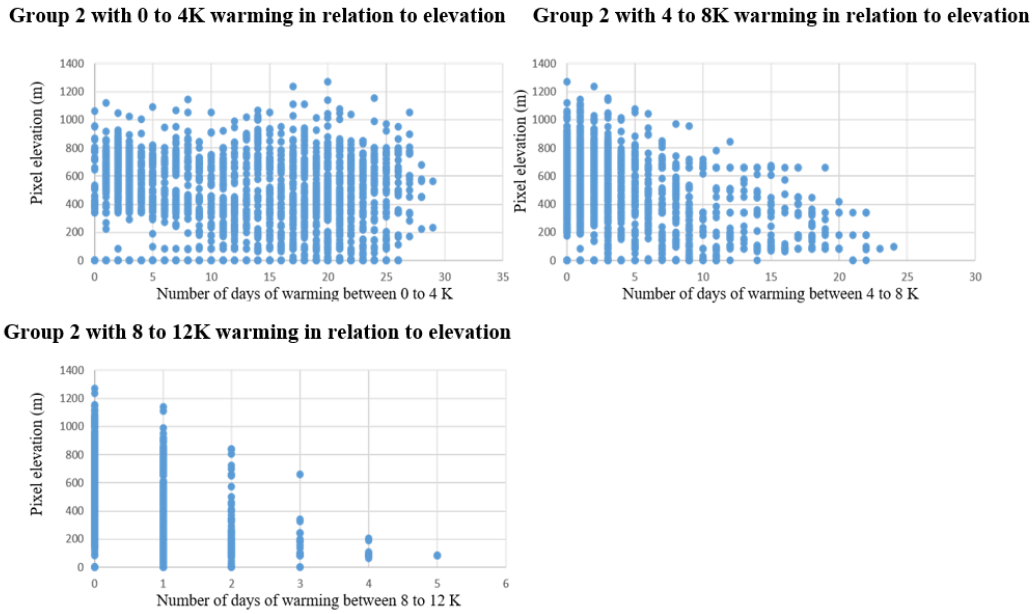

Figure 4.13 Scatter plot between elevation and event frequency for group 2 categories when the solar radiation was high and foehn duration was low.

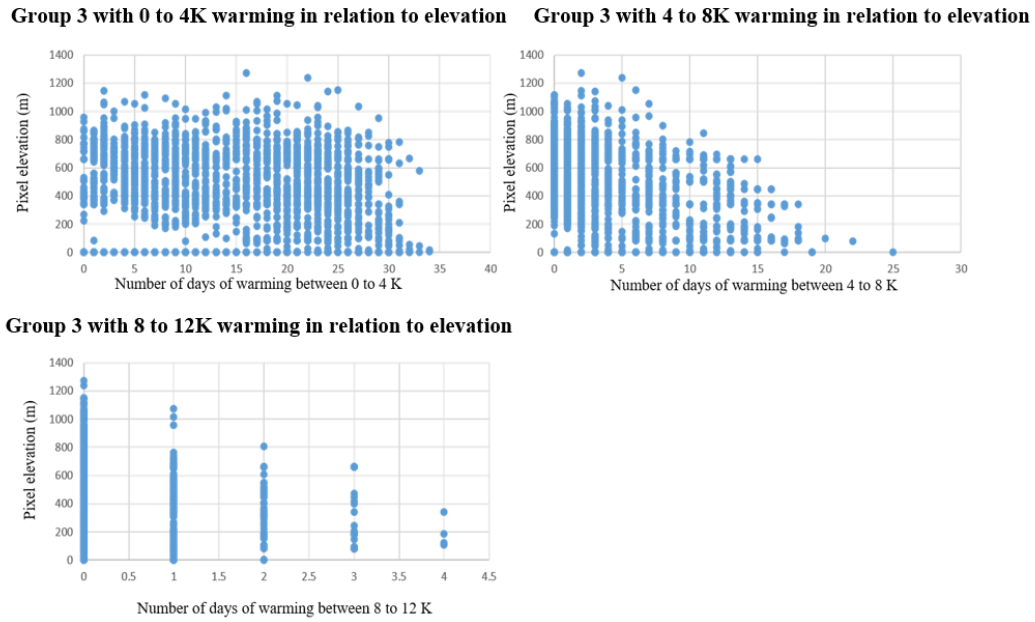

Figure 4.14 Scatter plot between elevation and event frequency for group 3 categories when the solar radiation was high and foehn duration was high.

4.4.5. Relation between warming and location.

The location and elevation of a region's pixels in the MDV play a major role in determining the region's response to foehn events. From the previous analysis, it can be concluded that regions close to the Transantarctic Mountains with lower elevation experience higher warming than the pixels close to the Ross sea and lower elevation. The major warming regions were mostly concentrated towards the upper valley region for Wright and Victoria, whereas for Taylor valley the warming is distributed across the valley and is divided by Nusbaum Riegel. For confirming the trend, the daily average Ta from the AWSs for the group 2 and group 3 events were plotted. Figures 4.15 and 4.16 show daily average Ta for group 2 and group 3, respectively. It can be observed that the temperatures in group 3 are higher than that of group 2 because of high-intensity radiative warming along with longer duration foehn events in group 3. The low elevation of the areas near the Transantarctic Mountains warm up more than the areas with similar elevation that are away from the mountains

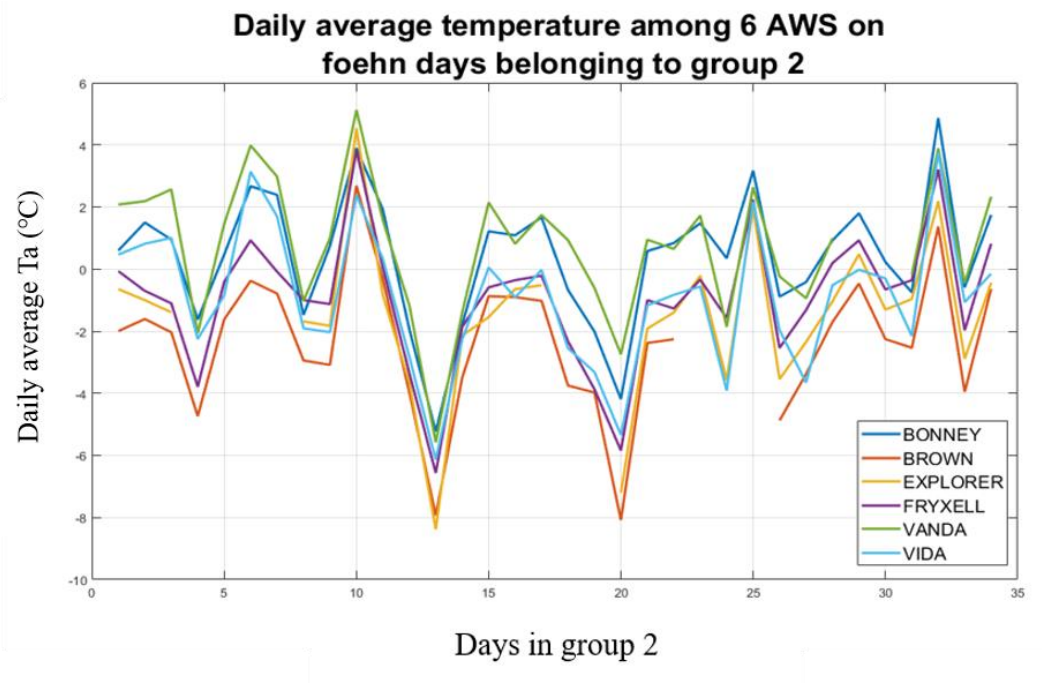

Figure 4.15 AWS daily average air temperature during foehn events for group 2 when the solar radiation was high, and foehn duration was low. x-axis represents the days that are in the group, whereas y-axis represents the daily average Ta recorded by the AWSs in those days.

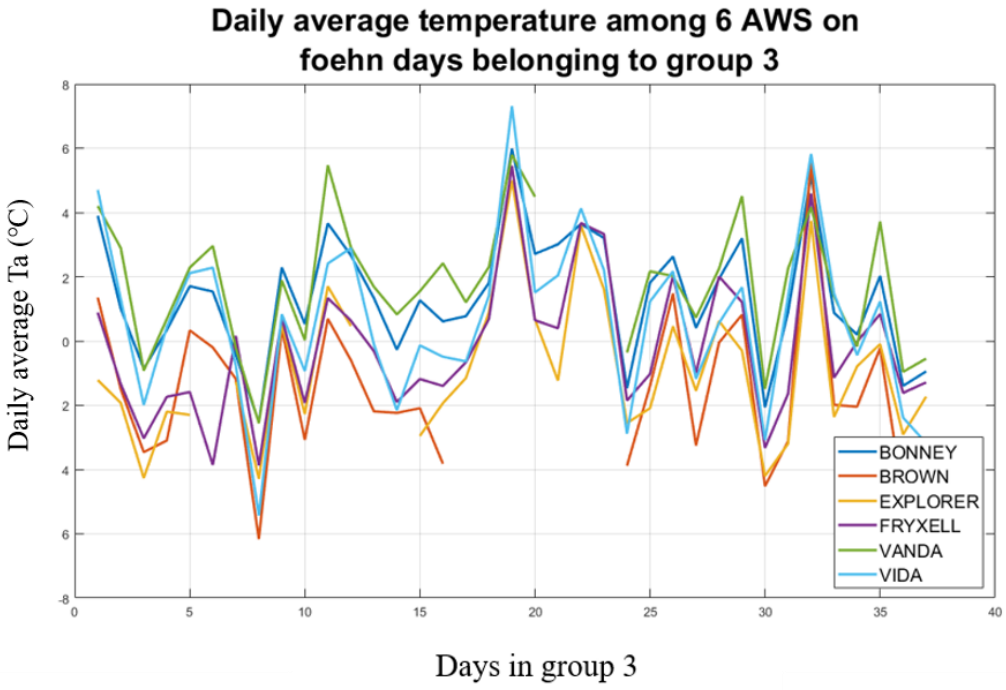

Figure 4.16 AWS daily average air temperature during foehn events for group 3 when the solar radiation was high, and foehn duration was high. x-axis represents the days that are in the group, whereas y-axis represents the daily average Ta recorded by the AWSs in those days.

From the Figures 4.15 and 4.16 it can be identified that for both the groups AWSs located at the upper end of the valley showing higher warming than the lower end of the valleys. Fryxell and Explorer are neighbouring stations located at the lower end of the Taylor Valley. These two stations show lower warming than Bonney for both the groups. Fryxell elevation is lower than Bonney, but due to Bonney's proximity to the Transantarctic mountains and due to the barrier effects of Nussbaum Riegel, it receives higher frequency foehn events and is warmer than Fryxell. Fryxell AWS with an elevation of 19 m and explorer 25.7m, Fryxell shows more warming than Explorer in the two groups. Vanda AWS in Wright valley is in a region with less constriction to the flow of foehn winds as compared to Brownworth and is warmer; it is also located near to the Transantarctic Mountains and has a lower elevation (Chapter1 Section 1.4)

4.5 Discussion and Conclusion

The chapter aimed to explore the larger spatiotemporal changes in LST occurring in MDV during foehn events and also identify the areas in the region that are more susceptible to foehn-induced warming. From the above analysis, we can conclude that the warming associated with foehn events changes LSTs gradient along the MDV. The pixels' surface temperatures covering the valley floor register higher temperature groups during a foehn event, indicating higher and more even warming across the valley

floor. In contrast to a foehn day, the LST distribution of the typical days when there is no foehn is over a more extensive range of temperatures which include lower temperature groups, indicating differential radiative (radiative) warming based on the surfaces' albedo. The valley floor is almost evenly warmed during an intense foehn event, and the fluctuation in temperature across the valley floor's length reduces, showing even distribution of high LST values across the whole length of the valley. The convective exchange of heat between the turbulent boundary layer warmed during a foehn event and the cooler valley floor evenly warms up the valley floor regardless of the land surface type and is not controlled by the diurnal cycle.

The regions with the lower elevation are more susceptible to warming due to foehn winds. These regions have a higher degree of warming than the rest of the valley floor and can also be considered potential zones for high glacial melt, as the valley floor includes glacial ablation zones. During stronger foehn events, the upper valley toward the Transantarctic mountains becomes warmer than the lower end (which was previously observed from AWS data), which is reverse to a typical day without any foehn event. The warmer easterlies from the Ross sea region heat the lower end of the valley during a typical summer day, but when a long-duration foehn occurs and as it descends into the valleys, it warms up the upper valley region more than the lower. Also, the stronger foehn events last longer over the upper valley region than the lower end causing extreme warming of the region.

The regions identified in the study will help develop strategies for future research expeditions to concentrate their study on the regions that are more susceptible to warming due to foehn wind. Unavailability of satellite data due to the overcast period is one of the drawbacks for the analysis; also, 1km spatial resolution of satellite LST data can be too low for studying the finer scale microclimatic changes in the valley floor. The regions identified in the study showed higher warming during a foehn event but these regions do not necessarily have higher LSTs throughout the summer as the warming is mostly controlled radiatively in absence of foehn. Chapter 5 tries to identify the regions in MDV that have high-temperature values throughout the summer.

Chapter 5: MDV hydrology

5.1 Introduction

Seasonal changes in meteorology result in higher temperatures and incoming solar radiation during summers across the MDV surface. The radiative warming during summer is sufficient enough to raise the temperatures across the valley to cause glacial melt in the valleys, even in absence of adiabatic warming due to foehn wind. The glacial melt varies between locations depending on the amount of direct solar radiation the region receives (Conovitz et al., 1998). The glacial melt during a year with weaker foehn events (2000-01) is lower than the years with a higher number of strong foehn events (2001-02) (Doran, et al., 2002). The occurrence of foehn events in the valley directly controls the amount of glacial melt occurring during the season.

Figure: 5.1 shows the average discharge rate of all the MDV monitored streams during 2000-18. For some of the years, the seasonal average discharge rate is distinctly higher than the 18-year average (red line). The year 2001-02 shows extreme discharge rates and is considered a flood season (Doran, et al., 2002). Like 2001-02 summer, 2008-09, 2010-11, 2011-12, 2013-14, 2015-16- and 2016-17 year show discharge rates that are higher than the average.

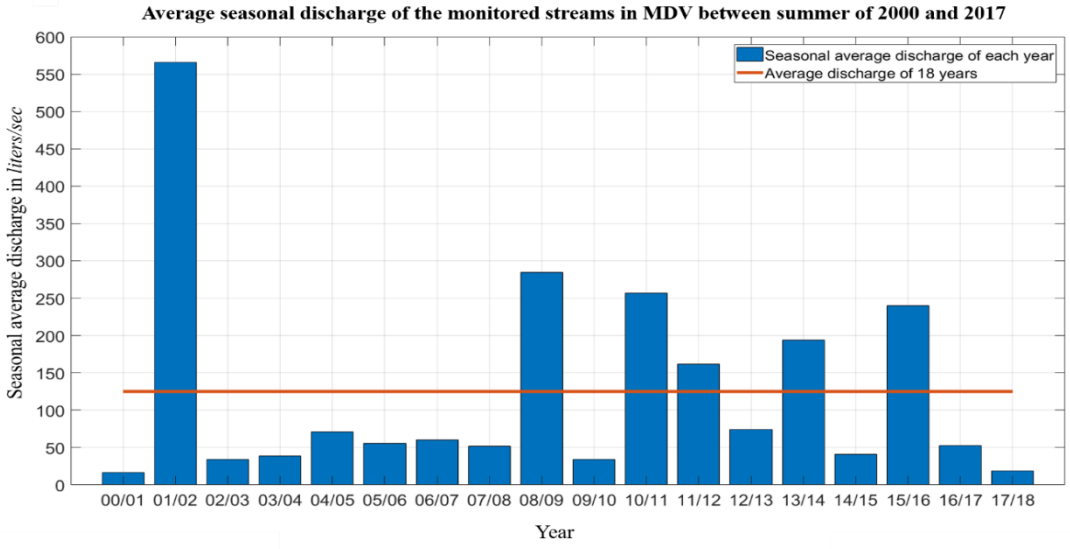

Figure 5.1 Average discharge rate of all the monitored streams over the 18 year of summer; the x-axis represents the summer seasons while the y axis represents the average seasonal discharge.

The maximum inflow to the lakes in MDV from glacial melt occurs over 8 weeks of summer, between December and January. The glacial melt ceases during winter, and there is no streamflow and the only way the water mass is lost during winter is by sublimation. Ablation rates during summer vary considerably within MDV because of the control of topography on the wind, ISWR, and Ta (Ebnet,

Fountain, & Nylen, 2005). There is high variability in melt across the valleys during the summer; the water input from melting snow varies between sites and ranges from 1.7–3.4 cm per year (Hunt et al., 2010). The vertical terminal cliffs on the glaciers can have higher or lower melt rates than the horizontal surfaces based on the differences in ISWR they receive (Hoffman et al., 2016). The glacial mass balance is affected by the Surface Energy Balance (SEB) equation's residual energy, which causes sublimation and melt of the glaciers during summer (A G Fountain et al., 2006) Chapter 1, section 1.3.2)). The diurnal variability in the flow rates of the MDV streams shows they respond to solar radiation forcing; the time of maximum flow rates during a day for most of the streams is around 1400Hrs (NZST) when ISWR is highest (Conovitz et al., 1998).

The only way of measuring the long-term glacial melt right now is by measuring the flow rates of the streams. Due to the distant installation of stream gauges from the source, the presence of hyporheic zones along the streams, and topographic shading and terrain structure, the meltwater from glacial melt gets disrupted from reaching the stream gauges which delays or lower the readings of total liquid water generated from the melt (Conovitz et al., 1998). The lag and flow attenuation make it is hard to study the stream discharge's response to meteorological changes across the valley floor.

In Chapter 4, satellite data helped find the regions that are more susceptible to warming during a foehn event; still, the glacial melt in those areas does not necessarily have to be high as it depends on many other factors like the size of the source glacier, aspect of the region, and elevation. The present study aims to utilize satellite-derived LST values to study the influence of meteorological changes in the valley on the hydrology of the region.

Objectives of this chapter

- Investigate the influence of the LST near a source glacier on the flow rates of the streams.
- To determine the zones in Dry Valleys that have temperatures favorable for glacial melt.
- Investigate the control of foehn and ISWR on stream discharge.

5.2 Context

MDV has limited life forms and is devoid of vascular plants and vertebrate species. The life forms that dominates the region are microbial and can be seen flourishing during the summers. During the summer, the glacial melt results in ephemeral streams, which support photosynthetic cyanobacterial mats and associated heterotrophs (Takacs-Vesbach, Zeglin, Gooseff, Barrett, & Priscu, 2010; Zeglin, Sinsabaugh, Barrett, Gooseff, & Takacs-Vesbach, 2009). Despite the harsh conditions prevailing in the valley, MDV harbors cyanobacteria, diatoms, heterotrophic bacteria and mosses in the streams,

phytoplankton in the lakes, and heterotrophic bacteria, nematodes, tardigrades, and rotifers in the soils (Andrew G Fountain et al., 1999).

MDV receives minimal precipitation. The streams that harbor microbial life forms are generated by to glacial melt during the summer. The streams contribute to the inflow of water into the lakes of MDV. The stream's flow rates in MDV are highly susceptible to the changes in meteorological and terrestrial conditions in the valleys (Conovitzl et al., 1998). Due to the strong control of meteorology on MDV hydrology and the eventual biodiversity dependencies on the glacial melt, it is essential to study the effects of summer meteorology on the region's hydrology.

5.3 Data

Multiple datasets are used for the long-term study of valley floor meteorology's effects on the region's hydrology. The various datasets used are listed below.

5.3.1 Satellite data

The MODIS LST data for 13 years of summers between the years 2003 till 2015 was collected. Four LST images per day from Aqua and Terra satellite taken during different overpass at a different time of the day are used to generate daily average LST for all the 120 days of 13 years of summer. Daily average LST image is generated from the 4 instantaneous images during a day for the assessment. The LST images were cleaned for missing data and outliers using techniques discussed in chapter 2 (section 2.4.2 and 2.4.3).

5.3.2 Stream gauge data

The streams in MDV are monitored using stream gauges installed by LTER. Most of the streams in MDV contribute an inflow of glacial meltwater to the lakes during summer. To quantify the inflow due to glacial melt, which leads to lake level rise, the stream gauges are often located near the lake rather than the source glacier. For studying the stream discharge rates response to meteorological changes in the valleys, streams whose stream gauges are located near the source glacier are selected for the study. The streams chosen for the study are listed below, along with the name of the stream gauges (Table: 5.1)

Name of stream gauge	Stream	Contributing inflow to Lake
house_h2	House Stream	Lake Hoare
lawson_b3	Lawson Creek	Lake Bonney

Onyx_Wright	Onyx River	Lake Vanda
santafe_b2	Santa Fe Stream	Lake Bonney
andrsn_h1	Andersen Creek	Lake Hoare
canada_f1	Canada Stream	Lake Fryxell
green_f9	Green Creek	Lake Fryxell

Table 5.1 Stream gauges installed across different streams in MDV

Figure 5.2 shows the map of all the installed stream gauges across MDV and the monitored streams.

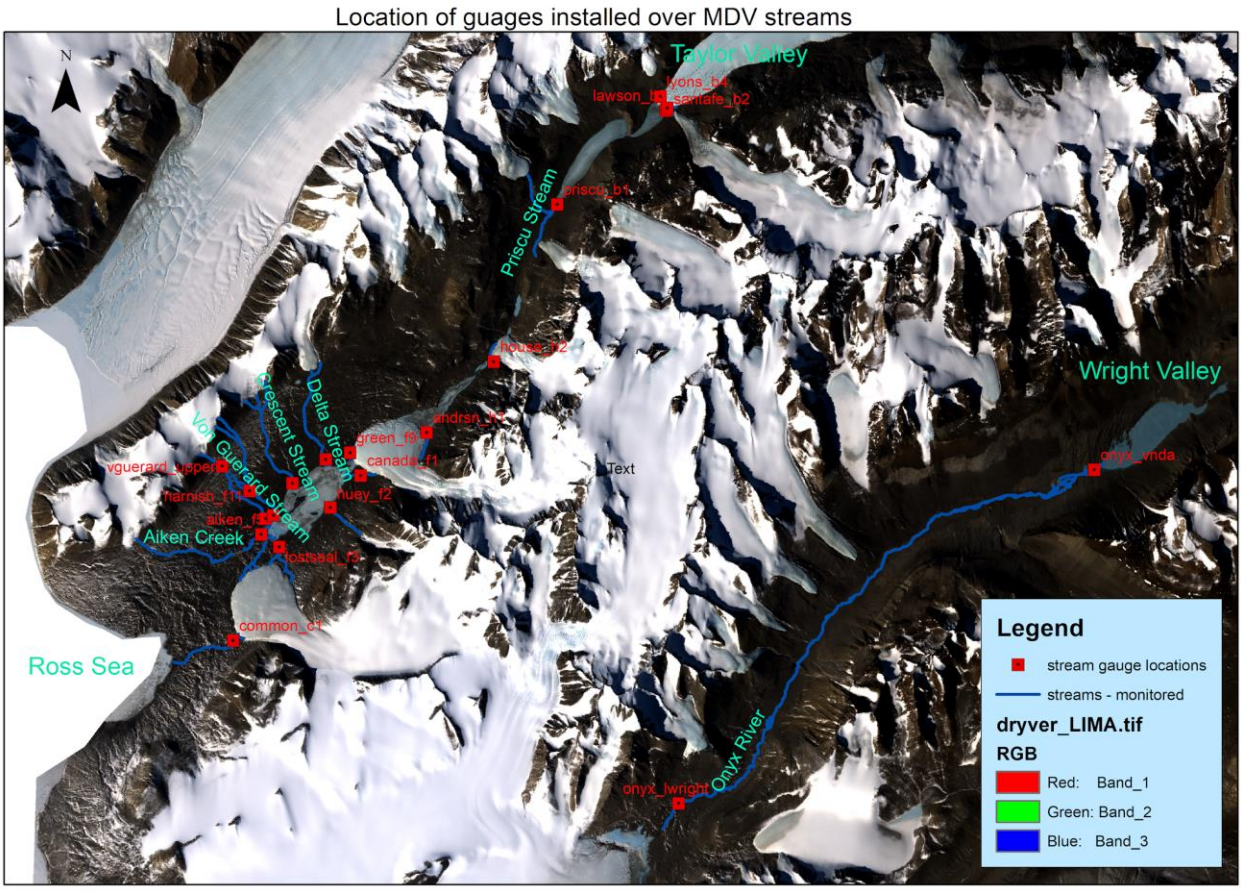

Figure 5.2 Map showing the locations of all the stream gauges installed over the streams across MDV.

5.3.3 AWS data

Meteorological data were collected over 120 days (1st Nov -28th Feb) of summers between the years 2003 to 2015 from 6 Automatic Weather Stations (AWS), which were installed across MDV as a part of McMurdo Dry Valley Long Term Ecological Research (LTER) Network. Three AWS were selected

from Taylor valley: Bonney, Fryxell, and Explorer; two AWS were selected from Wright: Vanda and Brownworth; and only Vida AWS was selected from Victoria valley.

5.4 Methodology and Results

The study investigates the response of glacial melt to meteorological change in the valley by looking into the fluctuations in stream discharges in relation to the daily average LST changes across the glacial ablation zone in the valleys.

5.4.1 Effect of higher LST values on the glacial melt and stream discharge

The daily average flow rate from all 7 stream gauges was collected over 13-years of summer between 2003 till 2015. Some of the streams have missing streamflow data for a few days or over the entire period of summer. Daily average LST was collected from pixels surrounding the glacial ablation zones. For studying the impact of meteorological change on the stream flow rates, the daily average LST of the glacial ablation zones are compared with the daily average flow rates registered by the stream gauges of that stream. Figure 5.3 shows the scatter plot between daily average flow rates of the 7 streams over the 13-year of summers in relation to the daily average ablation zone LST.

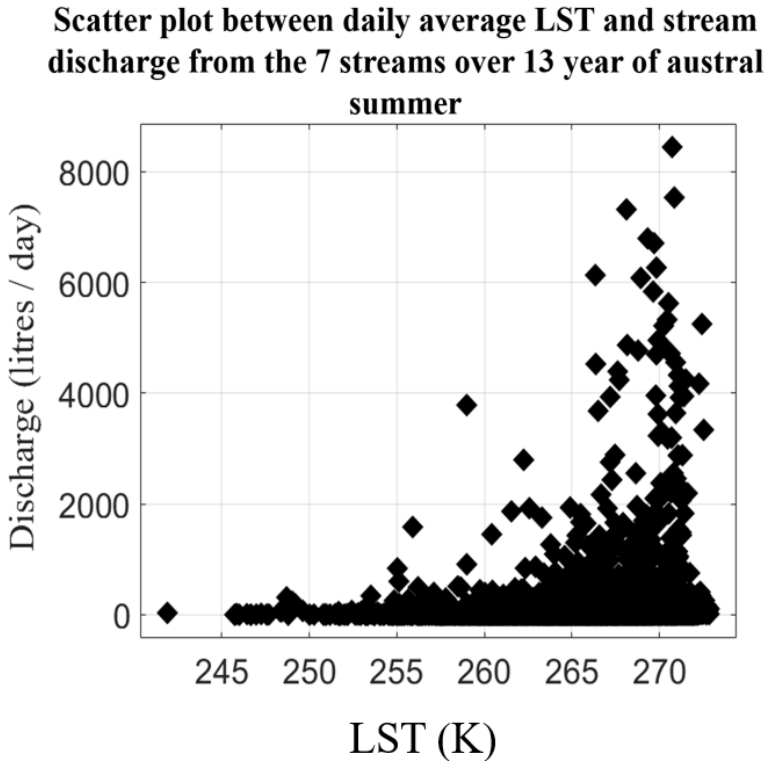

Figure 5.3 Scatter plot between average daily flow rates of a stream to the corresponding daily average LST of the region around the source glacier. The x-axis represents the daily average LST and the y- axis represents the daily average discharge.

It can be observed that with an increase in daily average LST, the daily average flow rates increase, indicating the influence of warmer temperatures around the glaciers in producing higher meltwater. The daily average LST above 265 Kelvin showed higher flow rates than the LST below that; the flow rates increased rapidly when the daily average temperatures were above 265 Kelvin.

5.4.2 Identifying the zones favourable for glacial melt in the MDV.

The LST of a location can reach 273.15 Kelvin and higher during a day when the satellite imagery is acquired. However, the night-time temperatures are lower than the daytime LST; thus, when the study averages the 2 day-time and 2 night-time LST for generating an average daily LST, the higher temperature values during the day gets dampened. Even if the daytime LSTs are high, the daily average LST might not reflect it. High daily average LST values are not necessarily achieved only during foehn events; it can be the result of extreme radiative warming during the peak summer (between mid-Decembers till mid-January).

This chapter identifies the regions in MDV where the surface temperatures were high for most of the summer; this can help identify the region experiencing the most warming (temperatures above 273.15 Kelvin) because of either adiabatic warming due to foehn event or radiative warming due to ISWR. The daily average LST equal to or above 273.15 Kelvin is an obvious choice for a favourable glacial melt temperature of a region, but due to the averaging of 4 instantaneous LST observations at different times of the day to generate daily average LST, the LST value of a region where the temperatures were 273.15 Kelvin or higher during a day is reduced. The study needed to determine a range of daily average LST values indicating a day when the daytime LST was higher than 273.15 Kelvin.

5.4.2.1 Determining a daily average LST threshold suitable for glacial melt.

Figure 5.3 showed that the stream discharge increases drastically when the daily average LST value is around 265 Kelvin or higher. The stream gauges are located near the source glaciers, thus the effects of increased temperatures around the source glacier, on the glacial melt are directly observed on the stream discharge. The study takes 267 Kelvin, daily average LST as a threshold indicating if the pixel experienced temperatures above 273.15 Kelvin during the day.

For verifying that the temperature 267 Kelvin can be used as a threshold, air temperature (Ta) data from the 6 AWSs located across MDV was collected from 2003 to 2015 summer. During the 120 days of the summer from 1 November till 28th February, the daily average Ta was calculated for all the years from the 6 AWSs. Also, the total number of hours when temperatures were above 273 Kelvin was calculated for each day for every season from the 6 AWSs. Figure 5.4 shows the scatter plot between the daily average Ta of a day with the total number of hours in a day when the average hourly Ta was above or equal to 273.15 Kelvin.

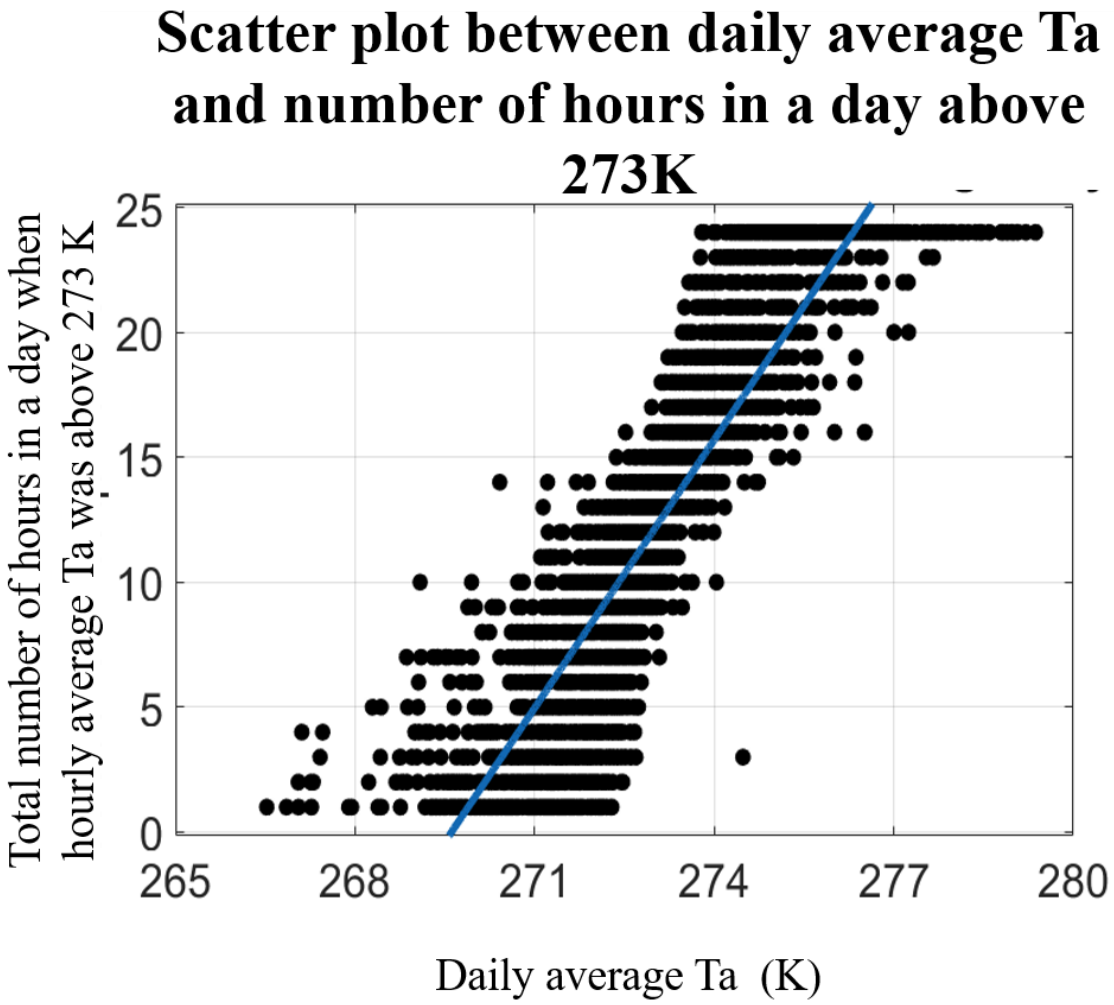

Figure 5.4 Scatter plot between daily averages Ta and total hours when daily average Ta was above or equal to 273.15 K for all the 6 AWS over 120 days for all the summer between the years 2003 to 2015.

The scatter plot shows how the daily average Ta from a station is related to the total number of hours it experiences temperature above 273.15 Kelvin on that day. It can be observed that if a day experiences 1 hour of temperature above 273.15 Kelvin the daily average Ta can range from 267 to 272 Kelvin. As the number of hours in a day above or equal to 273.15 Kelvin increases, the daily average Ta range also increases. For a day when the hourly average Ta was above 273.15 K throughout the day (24 Hr) the daily average Ta ranges roughly from 273 to 279 Kelvin. From the above scatter plot, we can roughly estimate that the daily average Ta of 267 Kelvin will have one or more hours of temperatures above 273.15 Kelvin. Thus, the study uses 267 Kelvin as a daily average LST threshold to determine if a pixel is having a favourable temperature during a day for glacial melt or not.

5.4.2.2 Identifying the zones in the MDV valley floor, which have temperatures favorable for melt.

The study investigates the valley floor (roughly, also include hill slopes in some area) temperatures up to an elevation of 1200m. The valley floor does not include the higher elevation glacial patches but includes the low-level glaciers and glacial ablation zones in the MDV. The following analysis might not explain the glacial melt at higher elevation during summer but helps in understanding control of higher temperatures near the glacial ablation zones and their effects on the melt.

Daily average LST image covering MDV floor was generated for 120 days of the summers between 2003 and 2015. A stack of 1680 images of daily average LST was generated. Pixel values in every image were checked for the threshold and if the pixel value was greater than equal 267 Kelvin the pixel value was changed to 1, and if it was below 267 Kelvin the value was changed to 0. Finally, a stack sum was calculated from all the 1560 images, where each pixel value represented the number of occurrences of days when the LST was equal to or above 267 Kelvin over 120-days of the 13 summer years. A higher number in the pixel value indicates the region had a higher number of days when the daily average LST was above or equal to or above 267 K and the pixel had favorable conditions for melt

Figure 5.5 shows the image covering the MDV floor with pixel values representing the number of days when daily average LST was above 267 Kelvin at each location in the valley floor. It can be identified that the region surrounding the major lakes in Taylor, Wright, and Victoria valley experienced a higher number of days when the daily average LST is above 267 Kelvin. For Taylor valley, Lake Bonney on the upper half of the valley, and Lake Fryxell on the lower half of the valley experienced a greater number of days with temperatures above 267 Kelvin. In Wright valley, the pixels with a higher number of days above 267 Kelvin are concentrated near Lake Vanda. The Onyx River generated from Brownworth Lake has the highest discharge among all the streams, but the region has less frequency of temperatures above 267 Kelvin in comparison to the Lake Vanda region. The 267 K can be considered with a bias of 2K as LST and Ta bias ranges between 2K. Brownworth glacier has a large surface area and acts as an enormous source of meltwater, though the temperatures above 267 Kelvin are less frequent around Brownworth than Vanda. Whenever the area reaches temperatures suitable for melting, a large surface area is subjected to glacial melt and producing an enormous amount of liquid water which gets accumulated in Brownworth Lake. Also, the calving of large glacial chunks during the summer contributes to the meltwater of the river Onyx. This phenomenon was observed during one of the field trips to Lake Brownworth for the 2016-17 summer when the research team witnessed large glacial calving on the edge of the Brownworth glacier. The discharge of a stream depends on the size of the source and the total surface area of the glacier that contributes to the melt. A short duration of temperatures above 273.15 can also cause high amounts of glacial melt for a large source.

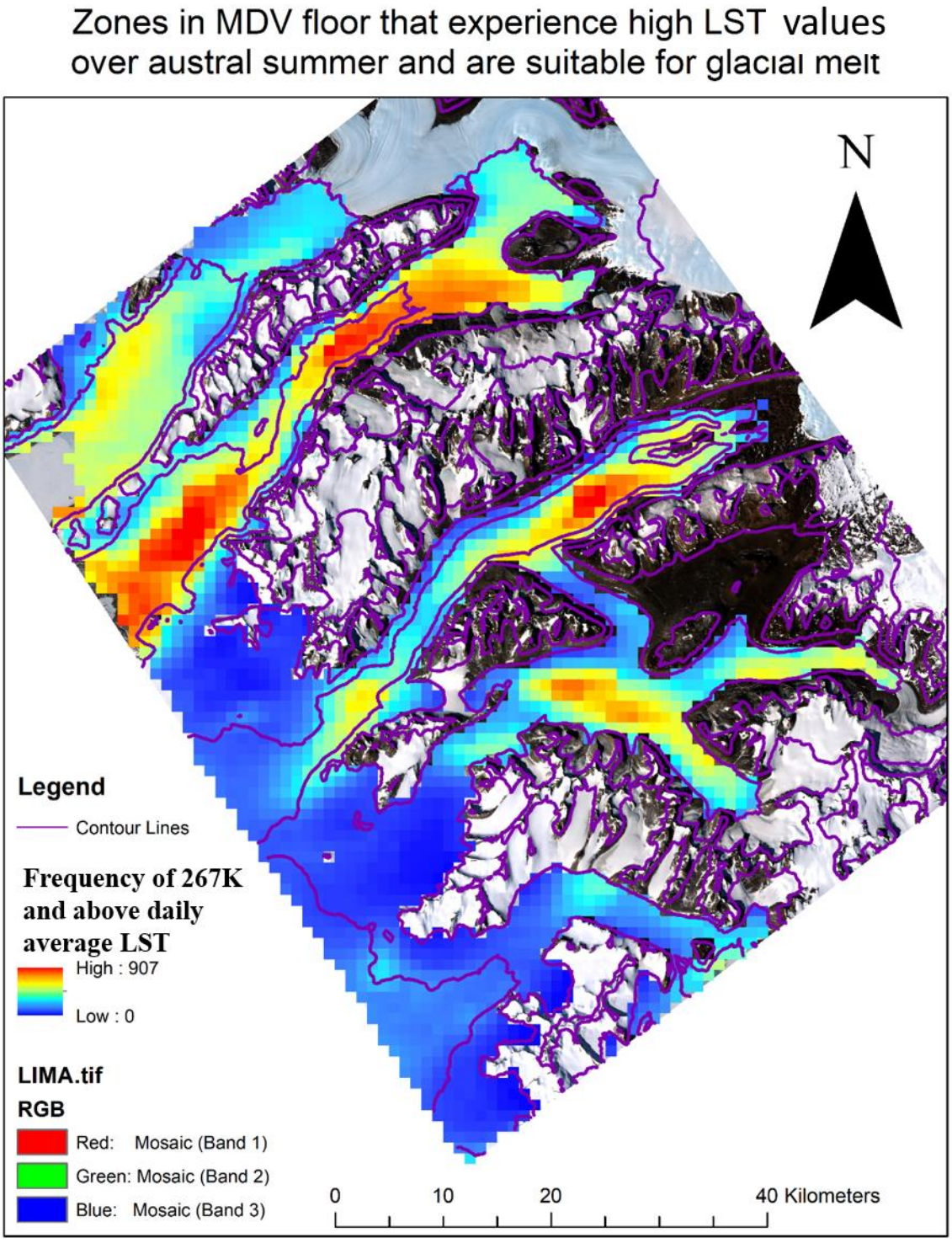

Figure 5.5 Number of days with temperatures above melting point experienced by each pixel covering MDV floor over 13 years of summers.

5.4.3 Foehn and net SWR control on hydrology

The glacial melt during the summer is controlled by warming due to ISWR and foehn events. The stream discharge is highest during the peak summer due to radiative warming from ISWR. During that period, the foehn events add to the warming of the valley floor and eventual glacial melt. The temperature increases at a location in MDV depend on the net energy it receives from incoming and outgoing longwave radiation. The net radiation depends on the albedo that varies between land surface types in MDV. Very few AWSs record the net radiation values and thus it limits the use of net radiation as a parameter to investigate the warming pattern across the AWSs sites, for which the research is only concentrated on how much incoming short-wave radiation a region received to understand the warming pattern based on the available energy for warming.

For studying the response of MDV hydrology to the meteorological changes, the year 2015-16 was chosen as a study period. Out of the 7 stream gauges selected for long-term study in this thesis, the discharge rates from only four of them were recorded during this year. The stream data of the following four streams were selected.

- Anderson
- Canada
- Green
- Onyx

The daily average discharge rate of the 4 streams was calculated and the daily average LST was collected from the streams' source glacier. Table: 5.3 shows the streams in MDV with their max and mean discharge along with the max and mean daily average LST around the source glacier over the summer.

Stream	Max LST (K)	Mean LST (K)	Max discharge (litres/sec)	Mean discharge (litres/sec)
Anderson	271.75	262.16	121	24.5
Canada	271.99	264.49	10.35	1.71
Green	272.81	265.34	149.73	28.37
Onyx wright	271.17	263.17	7321.4	1122

Table 5.3 MDV streams with their discharge and LST near the source glacier.

Onyx River shows a visibly higher discharge rate than the other streams over the summer, though the mean and max LST is not the highest. Canada has the lowest discharge among all the streams whereas Anderson and Green have comparatively higher discharge rates.

The meteorological data from 6 AWSs were used to determine the days when there was a major foehn event with a large spatial impact on the MDV floor, i.e., at least 2 of the AWSs experienced the foehn event on a day. The daily average stream discharge changes are compared with daily average LST around the source glacier, along with the foehn events over the summer, to study the effects of the foehn events and solar radiation on the daily average LST and discharge rates. Figure 5.6 shows the changes in daily average LST around the source glacier stream flow rates along with the foehn events occurring over 2015-16 summer. Onyx stream is not included as the flow rates are too high tom compare with the other stream gauge's discharge.

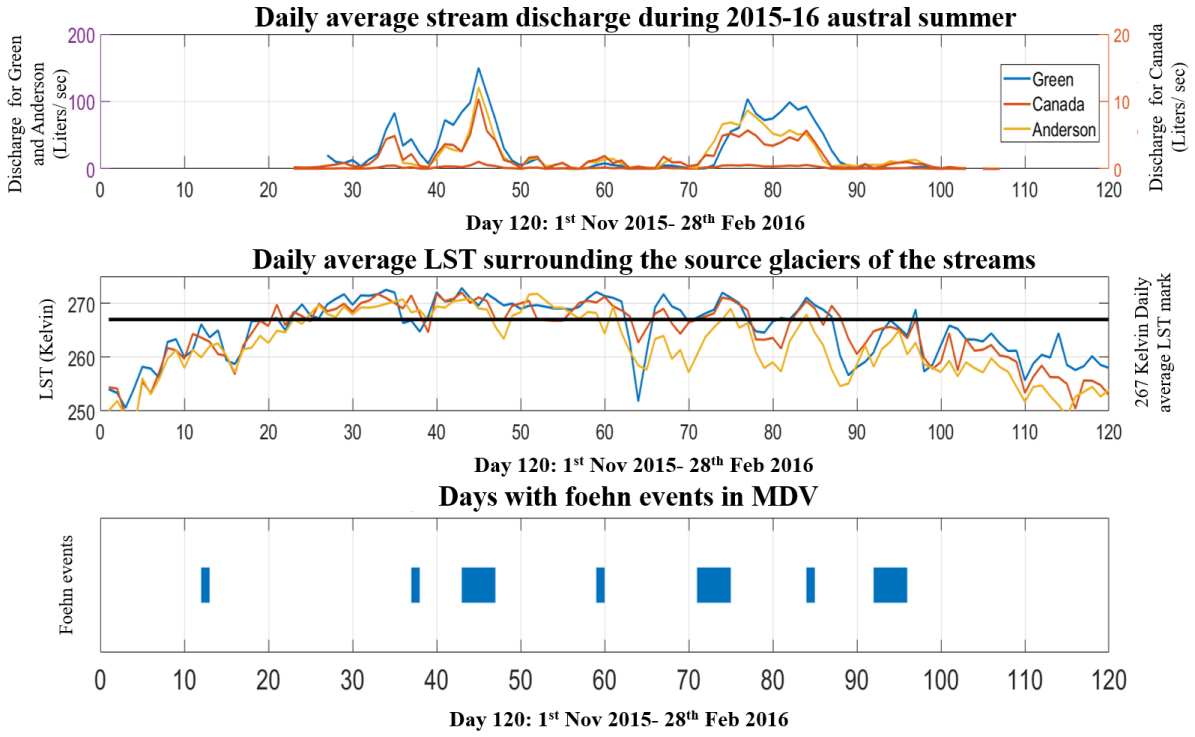

Figure 5.6 Influence of radiative warming and foehn events on the daily average LST and stream discharge

It can be identified that the major discharge from the streams occurred in beginning to mid of December (day30-daya50) and in mid of January (day70 -day90) for all the 3 streams. During these periods, the daily average LST was above 267 k for most of the days, although there were a few dips (between day 75 and 85) in the temperatures, which might have been due to overcast.

The period between the beginning of December and the end of January (Day:31-92) is when the solar radiation is maximum, and the valley is radiatively warmed to its highest temperatures. During this period, generally in absence of foehn winds the glacial melt is solely driven by radiative warming.

Period between day 50 and 70 the melt is mostly driven by solar radiation, though a small foehn vent on day 59, did increase the melt to a very small amount.

During a foehn event between day 40 and 45 there was a sudden rise in discharge rates, also the daily average LSTs were high during that period. The glacial melt during this period is mostly driven by foehn induced warming. During that even though the foehn events seized and the temperatures dropped there was gradual drop in discharge but it still was comparatively high compared to rest of the period. The glacial melt is a complex process and often a discharge can be expected after a very warm period even when the event seizes.

Unlike diurnal radiative warming from ISWR that varies within a day, foehn warming is continuous, and high glacial melt can be expected during the hours when there is low ISWR. At day 70 and 75 there was a foehn event that lasted for around 5 days, during that period the discharge increased again and as it was about to recede there was another short foehn event on day 83 which kept the discharge high for a few days, but it eventually receded as the daily average LST dipped below 267 k after day 87. On day 92 a major foehn event occurred which lasted for days though it increased the LST for a short duration, it was not strong enough to cause high glacial melt. Due to low ISWR, the valley floor surface temperature becomes colder, and even if a long-duration foehn event occurs at the end of the summer season, sometimes they are not strong enough to raise the valley floor temperatures high enough to cause glacial melt. This is one of the case studies and the foehn dynamics may vary between years.

The discharge in the MDV streams is due to seasonal radiative warming of the glaciers and the valley floor surrounding the glacial ablation zones. During this period, the valley floor and glaciers are already warmed enough due to radiative heating to cause glacial melt, thus when a foehn event occurs during this period it adds to the warming of the valley floor and further increases the temperatures resulting in higher glacial melt and eventual discharge rates. The LST around the glacier ablation zone shows a rise in temperature during the foehn events. The warming depends on the strength of the foehn event (the duration and the spatial coverage of the event). Foehn event accompanied by high incoming solar radiation can cause high glacial melt across the MDV floor.

5.4.4 Comparison of 2008-09 and 2013-2014 summer

2008-09 and 2013-14 were flood seasons with higher stream flow rates than the average of the 18 years (Figure 5.1) over the summer. They are also associated with a higher number of foehn events during the summer season in comparison to a non-flood season. While analysing the long term foehn events over 18-years of summer (chapter 1, section 1.5.2) and their associated stream discharge, it was found that for 2008-09 summer, even though there was lower number of foehn events in comparison to 2013-

14, stream discharge was higher for the season. Figure 5.7 shows the foehn events registered by the 6 AWSs across MDV over the summers of 2008-09 and 2013-14.

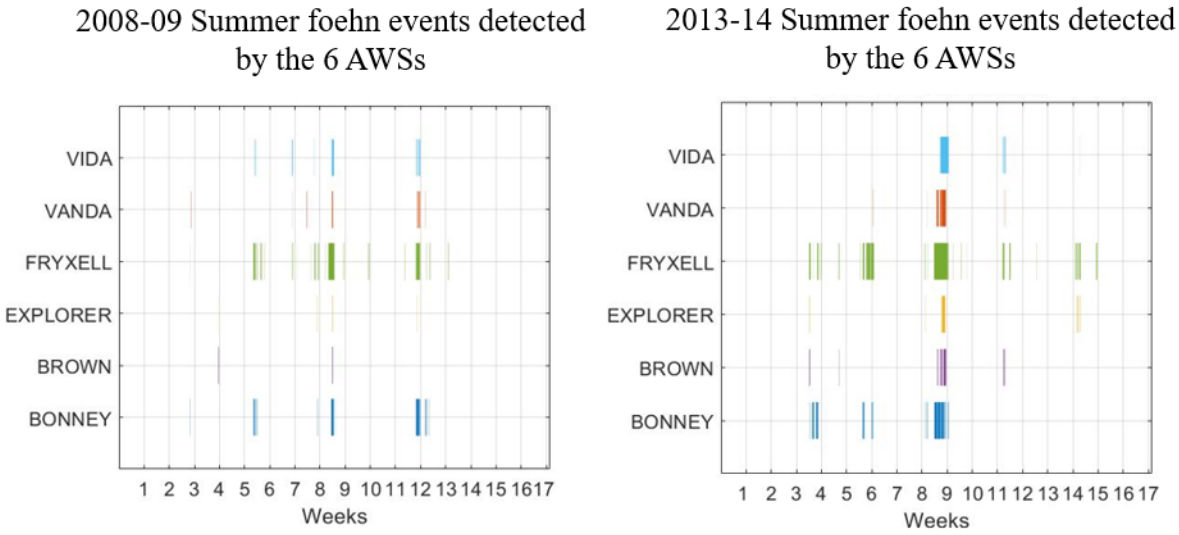

Figure 5.7 Foehn events registered by the 6 AWSs across MDV over the summer of 2008-09 and 2013-14, the x-axis represents the week in the summer from 1st Nov till 28th Feb of the season, while the y-axis shows the foehn events detected by all AWSs across MDV.

The year 2013-14 shows a higher number of long duration foehn events compared to 2008-09 and though the meteorology of 2013-14 is more favourable for glacial melt, the discharge rates of 2008-09 are higher than 2013-14

5.4.4.1 Meteorology

To investigate further into the discrepancy, the differences between the meteorological conditions of the seasons and the discharge rates from the streams needs studying. Table 5.4 shows a comparison between the meteorological conditions across the 2 flood seasons 2008-09 and 2013-14. It was found that the total number of foehn hours experienced by all the AWS are higher for the year 2013-14 in comparison to 2008-09, also 2013-14 experienced higher seasonal average Ta for all AWSs. The average seasonal wind speed experienced by all the AWS for both seasons is similar, as is relative humidity. The average seasonal ISWR experienced by the 6 AWSs in the year 2008-09 is higher compared to 2013-14 except for Explorer which experienced just 8 units less ISWR for the year 2008-09 as compared to 2013-14. It can be stated that the summer of 2008-09 was sunnier with less cloud cover in comparison to 2013-14.

	Years	Bonney	Brown	Explorer	Fryxell	Vanda	Vida
Average seasonal Air temperature in℃	2008-09	-4.66	-7.19	-7.03	-6.42	-3.92	-6.66
	2013-14	-3.38	-5.98	-5.61	-4.2	-2.79	-5.95
Average seasonal Wind speed in m/s	2008-09	4.58	3.97	3.66	3.52	5.76	4.98
	2013-14	4.87	4.04	3.75	4.71	5.69	4.84
Average seasonal Incoming radiation in W/m^2	2008-09	288.69	293.23	269.34	281.21	251.97	279.25
	2013-14	267.18	260.36	277.51	264.43	234.89	168.12
Average seasonal Relative humidity in %	2008-09	51.99	60.52	66.16	68.46	41.91	52.11
	2013-14	49.58	60.98	62.68	61.79	41.61	53.69
Average seasonal Soil temperature in ℃	2008-09	1.43	-2.66	0.36	-0.52	-1.68	-3.09
	2013-14	2.69	-1.33	-0.68	0.31	-0.72	-5.39
Total seasonal precipitation in mm	2008-09	52.40	-	88.70	-	-	-
	2013-14	137.10	-	261.30	-	-	-
Total number of foehn hours throughout the season	2008-09	89	48	14	16	171	60
	2013-14	131	71	49	65	278	76

Table 5.4 Meteorological data comparison between 2 flood seasons of 2008-09 and 2013-14

Table 5.5 shows the seasonal average discharge rate in liters/seconds collected from the 12 stream gauges installed over the monitored streams across MDV. Out of 12 stream gauges, 7 stream gauges show higher discharge rates for the year 2008-09 compared to the year 2013-14. The major difference in discharge rates is visible over the streams gauges installed across Onyx river at its' two ends in the Wright Valley. The Onyx_Wright stream gauge is located near the source of the river and shows extremely high discharge rates from Brownworth glacier. There is an increase in the discharge as the river reaches Onyx _Vanda stream gauge near the lake Vanda. It is due to the increase in the number of tributaries contributing more inflow to the river as it reaches toward Lake Vanda. The discharge rates for Onyx in the year 2008-09 are higher in comparison to other streams during the same season and also the discharge rate of 2013-14.

The Brownworth AWS located near the source of River Onyx registered the highest seasonal average ISWR among all the AWSs, also it was highest between the two seasons. Brownworth, though experienced lower foehn hours and lower Ta for the year 2008-09, the discharge rate of Onyx was

higher for 2008-09 in comparison to 2013-14, which was more cloudy year compared to 2008-09 summer.

Stream gauges	2008-09	2013-14
Aiken	99.71 litres/sec	113.45 litres/sec
Anderson	61.24	44.61
Canada	79.17	60.23
Common	92.57	103.64
Crescent	26.85	52.73
Delta	75.17	41.24
Green	52.73	66.86
Harnish	11.37	23.4
Lawson	53.36	37.59
Onyx_Vanda	1915.18	878.74
Onyx_Wright	1416.78	1074.15
Vguerard	49.94	22.95

Table 5.5 Stream gauge discharge data of all the 2008-09 and 2013-14

Onyx River has the highest discharge rates between the two seasons, making it an ideal case study for observing the meteorological differences between the two seasons and their influence on the discharge rates.

5.4.4.2 Onyx stream flow rates

Onyx River is generated from the accumulation of glacial melt over a large area of the lower Wright glacier into Lake Brownworth. Brownworth AWS was selected for studying the influence of meteorological changes on the hydrology of the seasons, and Onyx_wright stream gauge data was used to study the stream discharge for both seasons as it was installed close to the source.

Significant summer glacial melt occurs over 6 weeks, between mid-December till the end of January. The climatic conditions during these 6 weeks are critical in influencing the glacial melt over the summer. Figure 5.7 shows the stream discharge data from Onyx_wright stream gauge along with hourly average Ta, hourly average ISWR, and foehn events experienced by Brownworth AWS for the summer of 2013-14. Between the 8th to 9th weeks of the summer, the foehn event that occurred at Brownworth lasted for about half a week leading to an almost instantaneous increase in Ta above 0°C. This condition of high Ta lasted till the mid of the 9th week though the foehn event ceased by the beginning of the ninth week. There is a gradual increase in the flow rates from mid of 8th week, but a significant increase was noted from the beginning of the 9th week which lasted for a week and gradually started receding. Though the foehn event had instantaneous effects in increasing the air temperature which lasted for an extended period even after cessation, there were no significant changes observed in discharge rates at the time of

commencement of the foehn event. The time lag between the beginning of foehn and steep increase in discharge was about half a week. The increase in discharge rates was observed after the cessation of foehn events. This delay between the change in meteorological conditions and increase in stream discharge is very high. Glacial melt takes time to respond to sudden meteorological changes in the valley, also the glacial melt generated due to higher temperatures requires time to get collected in the lakes and reach the stream gauge which is roughly around 1.5 km from the source lake Brownworth. The delay between the change in meteorological condition and increase in discharge rates needs to be studied more along with the complex process of glacial melt and stream discharge reaching the stream gauges. It is hard to confer if the melt is due to the preceding foehn events or is a result of summertime heating when the daily average ISWR of greater than 600 W/m^2 over the period.

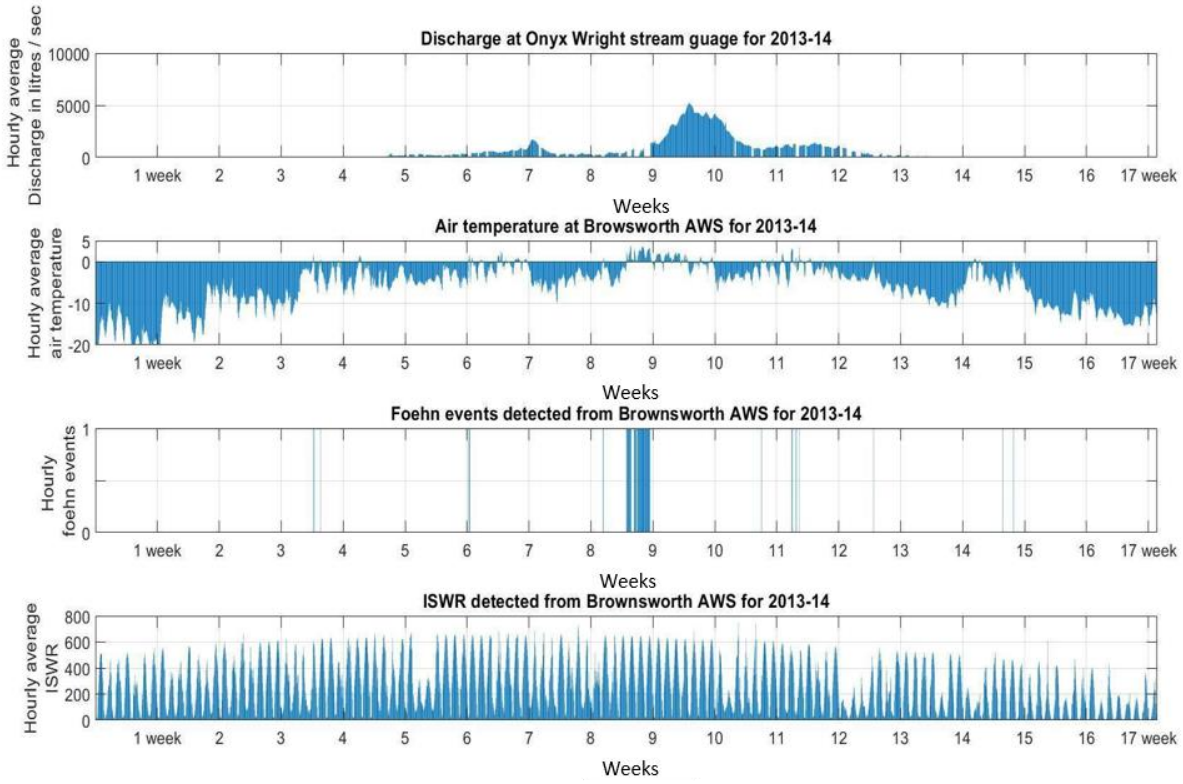

Figure 5.7 Stream gauge response to meteorological changes in lower Wright region for 2013-14

Figure 5.8 shows the stream discharge data from Onyx_wright stream gauge along with daily average Ta, daily average ISWR, and foehn events experienced by Brownworth AWS for the summer of 2008-09. The higher temperatures for this season lasted from the beginning of the 7th week till the end of the 9th week. During the period, discharge rates increased gradually from the 7th week and peaked at the beginning of the 9th week, and gradually decreased by the end 10th week. With the decrease in Ta and ISWR, the discharge rates decreased gradually as well. During this period few short-duration foehn events did spike the temperatures to higher Ta, but they lasted for a short period and did not cause any

distinct increase in discharge rates. Despite lesser foehn events, the discharge rates in the summer were up to 10^4 litres per second. The only distinct meteorological factor that was higher between the two seasons was the high ISWR for 2008-09 in comparison to 2013-14. The stronger foehn events occurring at the beginning of the 12th week did increase the temperature for a short duration but did not cause any significant change in discharge rates.

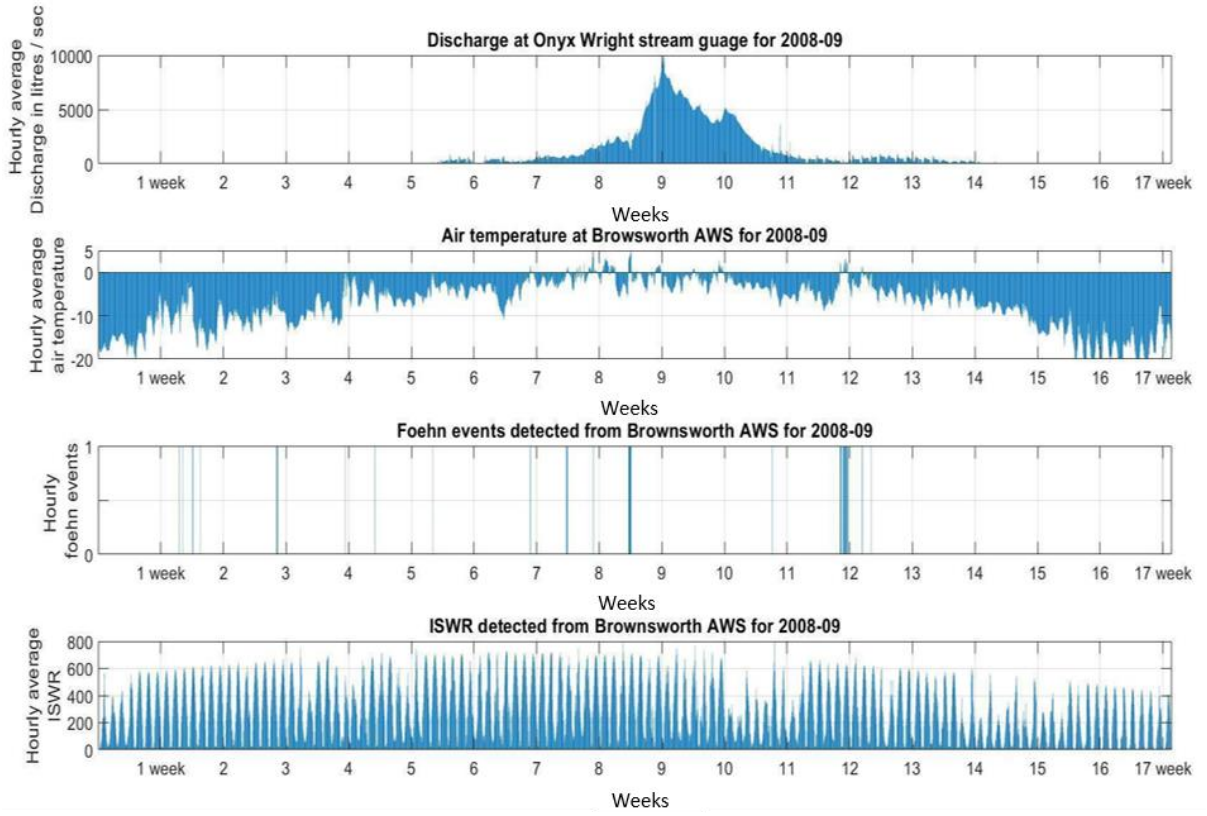

Figure 5.8 Stream gauge response meteorological changes in lower Wright region for 2008-09

The meteorological data collected from Brownworth AWS for 6 weeks of the summer between the beginnings of the 6th week (13th Dec) till the end of the 11th week (23rd Jan) show that for the year 2008-09 Brownworth received additional 676.70 W/m^2 of ISWR for the period in comparison to the year 2013-14. The daily average Ta difference between the two seasons was -0.84°C showing the seasons had similar air temperatures during the peak summer. The year 2013-14 received 32 foehn hours more than 2008-09 during the same period but had a lesser glacial melt. From the above analysis, it can be justified to say that the foehn events are not solely responsible for higher discharge rates. Higher ISWR for a long duration over the peak summer of 6 weeks can cause extreme flooding in MDV streams.

5.5 Discussion and Conclusions

The chapter aimed to understand MDV hydrology with help of LST datasets from satellite and later identify the region in MDV which experience temperatures favourable to glacial melt. The study also aimed to highlight the importance of radiative and foehn induced warming on the hydrology of the region. The study was able to identify the region in MDV that experienced a higher number of days when the temperatures are above the melting point. The regions identified, experienced a higher degree of warming as a result of both radiative and foehn-induced warming. These areas have temperatures favourable for melt which may affect the neighbouring glaciers and also the MDV biodiversity.

The study highlighted the importance of ISWR warming during summer, which when associated with foehn events can cause flooding of the MDV streams. Larger glaciers like Brownworth in lower Wright region on receiving higher ISWR can cause high glacial melt due to the large surface area being exposed to radiative warming. It is contrary to the popular belief that a higher number of foehn events lead to a higher temperature and glacial melt, though foehn events increase the valley floor temperatures during the summer it might not be enough to raise the temperatures above the melting point on its own and cause high glacial melt. The occurrence of foehn events during the peak summer in presence of high ISWR result in rapid glacial melt in the valley floor surface and cause the flooding of the streams.

Key Findings

The following section summarizes some of the major findings in each chapter of this thesis.

Chapter 1

- The long-term (18 years) study of the meteorological data across MDV showed the stations located towards the Ross sea region had different meteorology from those located towards the Transantarctic Mountains. Also, the seasonal and diurnal fluctuations in meteorology across MDV show significant inter-annual variability.

- Stronger foehn (> 6 Hr duration) events during summer tend to occur mostly during clear sky (high ISWR) days. Short duration foehn events (< 6 Hr) when associated with high ISWR (>250W/m^2, daily average) can raise the valley floor temperatures above the melting point on the other hand if they occur during low ISWR, they are mostly not capable of raising the temperatures above 0°C. Long duration foehn (> 6 Hr) occurring during low ISWR can cause extreme warming of the valley floor (section 1.5.3, group 3).

- The stark difference in the stream discharge between a flood and a non-flood season is mostly influenced by the foehn events during the season rather than the average meteorological conditions at daily to monthly scales. The meteorology associated with the two seasons might not have much difference between them, but the foehn events cause warming of the valley floor which leads to intense melt and eventual flooding of the MDV streams during flood seasons.

Chapter 2

- Daily average Land Surface Temperature (LST) data and air temperature (Ta) across MDV show a high correlation (R-square>0.7 and RMSE <3°C).
- Removing outliers and data gap filling increases the correlation between daily average LST and Ta. The locations near the Transantarctic mountains have a larger difference in the value of LST and Ta compared to the one located near the Ross sea region also, the LST from a pixel representing a mixed pixel (multiple land surface type) has a lower correlation with Ta compared to a pure pixel (single land surface type).
- Due to the high correlation between Ta and LST, MODIS-derived LST has utility in providing a spatially comprehensive picture of the foehn dynamics in the MDV, for both during summer and winter.

Chapter 3

- An algorithm for detecting foehn events is developed using long-term satellite data for both the summer and winter seasons, which does not require *in-situ* measurements.
- The algorithm works on determining the number of pixels showing an increase in temperatures in an image during foehn events, identifying these pixels helps demarcate the regions that are most and least affected due to foehn-induced warming.
- The winter algorithm has higher efficiency in detecting foehn events compared to the summer algorithm, because of the more pronounced changes occurring in the LST across MDV due to foehn in absence of radiative warming. Summer foehn detection algorithm will require more refinement for better performance.

Chapter 4

- Elevation and surface type control the LST of a location in MDV such that valley floor barren surfaces are warmer than the ridgetop ice and barren surface by up to 6-7 ℃, and valley floor snow and ice cover surface up to 4℃ throughout the summer season (2015-16).
- The seasonal valley floor LSTs tend to increase as the distance from the Ross Sea increase, i.e., the temperature towards the Transantarctic mountains tends to be higher than the Ross sea region. This trend is opposite to the overall trend of the MDV region and the ridge top pixels, which show lower LST towards the Transantarctic Mountains as the distance from the sea increases, i.e., the temperature towards Ross sea is higher than those near to the Transantarctic Mountains. The valley floor temperatures across the upper valley region are high due to more frequent foehn events experienced by the region due to its proximity to the Transantarctic Mountains.
- During a foehn event, the valley floor warms up more than the ridge top, the valley floor temperatures show higher values than the ridge top throughout the whole duration of a foehn event. The ridge tops cool down faster than the valley floor as the foehn intensity reduces. Also, the valley floor temperature shows uniform warming due to the continuous exchange of heat between the valley floor surface and the adiabatically warmed air parcel due to foehn. During a typical day without any foehn event, the uneven temperature distribution across the valley floor is due to differential radiative warming of the valley floor depending on the land surface type.
- The regions with a higher degree of foehn-induced warming are identified. Higher degree of warming often occur in areas with lower elevation in the MDV region. The low degree warming can be seen across the valley floor, but the number of days with a higher degree of warming occurs mostly in the areas of the valley floor that have low elevations.

- The stream flows across MDV are responsive to the LST changes across the glacial ablation zones. A daily average LST threshold is determined to identify when a pixel experiences temperature above the melting point during a day. The regions having a higher number of degree-days above freezing are identified across the valley floor.
- For the 2015-16 summer, it was identified foehn events occurring at the beginning or during the end of the summer season are not capable of raising the temperature of the glacial ablation zones significantly to cause high melt. High radiative warming (peak summer seasons), when associated with foehn-induced warming causes high melt rates in the region.
- On comparing two flood seasons with different foehn hours, the research highlighted the importance of summer ISWR on causing high melt rates in the region. High ISWR can cause high melt rates during summers despite lower foehn hours. Large sources like the Lower Wright glacier can cause high discharge rates because of radiative warming of a larger span of the glacial surface.
- It is conferred that though summer foehn frequency massively influences the stream flow and glacial discharge, it is important that the foehn events occur at a time of high ISWR which provides necessary condition to increase temperature above melting to cause the extreme melt and discharge in MDV.

Limitations and future scope

Though the present study opened paths for the use of satellite remote sensing datasets for studying the meteorology of MDV, more detailed studies are required to have an in-depth analysis of the meteorological dynamics that are responsible for controlling the valley floor temperatures. MODIS dataset though is useful in studying the day-to-day changes in temperature across MDV, the study is limited to days that are devoid of cloud cover, i.e., clear sky days. The study was unable to explore the spatial temperature distribution across MDV during an overcast period. MODIS datasets provide LST data in 1km resolution, which is low spatial resolution data, there is much more variability in temperatures across the 1SqKm area covered by 1 MODIS pixel, which gets generalized. Using higher resolution satellite data from Landsat with 30m resolution is a viable option, but its low temporal resolution makes it less useful in studying the day-to-day temperature changes. The foehn detection technique over the summer developed in the study was less efficient in detecting foehn events cross

MDV, this technique can be modified using more satellite data for a more efficient future foehn detection across the summers. Future studies with satellite datasets that provide high temporal resolution like MODIS and high spatial resolution as Landsat will be able to explore more extensively the variability in spatial temperature distributions across the valley floor and highlight the difference in meteorology between locations. LST dataset from MODIS at multiple time of the day will help in understanding the diurnal LST changes occurring in the valley that was not addressed in the study, also help study the LST changes associated with foehn events at different hours of the day and analyze the progress of the event.

Appendix

Table 1 The number of days with missing data for different meteorological parameter from each of the AWSs over a period of 18 years

Air Temperature																		
STATION	2000	2001	2002	2003	2004	2005	2006	2007	2008	2009	2010	2011	2012	2013	2014	2015	2016	2017
BONNEY	16	0	0	0	0	0	0	24	0	0	0	0	0	0	0	0	16	49
BROWN	0	0	0	0	0	47	40	0	0	0	101	86	0	0	0	0	0	0
EXPLORER	0	0	0	0	56	120	26	0	0	48	8	0	39	19	0	0	0	0
FRYXELL	0	0	0	0	0	0	0	0	0	0	0	0	0	0	0	0	3	0
VANDA	0	0	0	0	0	0	0	0	0	0	0	19	0	0	0	50	0	0
VIDA	0	0	0	0	0	0	3	0	0	0	0	0	0	0	1	0	0	0
Soil Temperature																		
STATION	2000	2001	2002	2003	2004	2005	2006	2007	2008	2009	2010	2011	2012	2013	2014	2015	2016	2017
BONNEY	16	0	35	84	0	0	0	24	0	0	38	50	0	0	0	0	16	49
BROWN	0	0	0	0	0	47	40	0	0	0	101	86	0	0	0	0	0	0
EXPLORER	0	0	0	0	56	120	71	0	0	48	8	0	39	19	0	0	0	0
FRYXELL	0	0	0	0	0	0	0	0	0	0	0	0	0	0	0	0	3	0
VANDA	0	0	0	0	0	0	0	0	0	0	0	19	0	0	0	50	0	0
VIDA	0	0	0	0	0	0	3	0	0	0	0	0	0	0	1	0	0	0
Wind Speed																		
STATION	2000	2001	2002	2003	2004	2005	2006	2007	2008	2009	2010	2011	2012	2013	2014	2015	2016	2017
BONNEY	16	0	0	0	0	0	0	24	0	0	38	50	0	52	15	0	16	49
BROWN	0	0	0	0	0	47	40	0	0	0	101	86	0	0	0	0	0	0
EXPLORER	0	0	0	0	56	120	26	0	0	48	8	0	39	19	0	0	0	0
FRYXELL	0	26	0	0	0	0	0	0	0	0	0	0	0	0	9	0	3	0
VANDA	0	0	0	86	0	0	0	0	0	21	0	19	0	0	0	50	0	0
VIDA	0	0	0	0	0	0	3	0	0	0	0	0	0	61	1	0	0	0
Wind Direction																		
STATION	2000	2001	2002	2003	2004	2005	2006	2007	2008	2009	2010	2011	2012	2013	2014	2015	2016	2017
BONNEY	16	0	0	0	0	0	0	24	0	0	38	50	0	52	15	0	16	49
BROWN	0	0	0	0	0	47	40	0	0	0	101	86	0	0	0	0	0	0
EXPLORER	0	0	0	0	56	120	26	0	0	48	8	0	39	19	0	0	0	0
FRYXELL	0	26	0	0	0	0	0	0	0	0	0	0	0	0	9	0	3	0
VANDA	9	0	0	86	0	0	0	0	0	21	0	19	0	0	0	50	0	0
VIDA	0	0	0	0	0	0	3	0	0	0	0	0	0	61	1	0	0	0
Short Wave Incoming Radiation																		
STATION	2000	2001	2002	2003	2004	2005	2006	2007	2008	2009	2010	2011	2012	2013	2014	2015	2016	2017
BONNEY	16	0	0	0	0	0	0	24	49	31	0	0	0	0	0	0	16	49
BROWN	0	0	0	0	0	47	40	0	0	0	101	86	0	0	0	0	0	0
EXPLORER	0	0	0	0	56	120	26	0	0	48	8	0	39	19	0	0	0	0
FRYXELL	0	27	0	0	0	0	0	0	0	0	0	0	0	0	0	0	3	0
VANDA	0	0	0	37	0	0	0	0	0	0	0	19	0	0	0	50	0	0
VIDA	0	0	0	0	0	0	3	0	0	0	0	0	0	0	1	0	0	0
Relative Humidity																		
STATION	2000	2001	2002	2003	2004	2005	2006	2007	2008	2009	2010	2011	2012	2013	2014	2015	2016	2017
BONNEY	16	0	0	0	0	0	75	24	0	0	0	0	0	0	0	0	16	49
BROWN	0	0	0	0	0	47	40	0	0	0	101	86	0	0	0	0	0	0
EXPLORER	0	0	0	0	56	120	26	0	0	48	8	0	39	19	0	0	0	0
FRYXELL	0	0	0	0	0	0	0	57	0	0	0	0	0	0	0	0	3	0
VANDA	0	0	0	37	0	0	0	0	0	0	0	19	28	0	0	50	0	0
VIDA	0	0	0	0	0	0	3	0	0	0	0	0	0	0	1	0	0	0

Table 2 Days with long-duration foehn events in MDV over18 years of austral summers along with the number of foehn hours registered by each station along with the daily average incoming shortwave radiation during the period

Date	Foehn hours BONNEY	Foehn hours BROWN	Foehn hours EXPLORER	Foehn hours FRYXELL	Foehn hours VANDA	Foehn hours VIDA	Total station detecting foehn	ISWR at BONNEY	ISWR at BROWN	ISWR at EXPLORER	ISWR at FRYXELL	ISWR at VANDA	ISWR at VIDA	Avg	Group
2000-2001															
6/11/2000	0	9	8	3	0	8	4	NaN	97.94	62.52	69.79	108.97	119.29	91.7	4.00
12/11/2000	0	1	2	0	1	0	3	NaN	269.13	270.06	272.71	264.60	285.19	272.3	1.00
23/11/2000	0	4	7	1	9	0	4	245.11	248.09	202.42	221.19	251.10	273.13	240.2	4.00
28/11/2000	0	1	11	0	17	1	4	183.82	188.68	113.62	139.20	228.76	235.02	181.5	4.00
23/01/2001	9	5	0	0	15	13	4	328.29	326.08	316.86	331.70	344.87	374.65	337.1	3.00
24/01/2001	20	18	0	0	24	21	4	322.17	340.60	326.39	356.98	311.76	343.56	333.6	3.00
7/02/2001	19	8	7	13	15	0	5	253.79	261.88	267.68	254.54	274.69	277.40	265	4.00
2001-2002															
14/12/2001	0	10	6	1	20	3	5	173.16	134.65	112.37	142.85	140.83	140.20	140.7	4.00
15/12/2001	0	18	20	10	24	22	5	192.65	159.53	183.10	185.41	174.50	146.97	173.7	4.00
16/12/2001	0	0	0	1	18	5	3	173.93	171.72	135.48	146.96	187.48	182.28	166.3	1.00
29/12/2001	16	2	0	0	20	21	4	384.14	404.26	415.88	438.17	419.01	418.08	413.3	3.00
30/12/2001	23	24	8	15	24	23	6	371.59	385.98	422.64	423.70	381.63	408.09	398.9	3.00
31/12/2001	5	5	1	1	9	7	6	302.33	350.99	370.08	369.92	338.57	365.48	349.6	3.00
1/01/2002	2	1	0	0	20	16	4	377.63	372.90	381.81	374.91	425.28	412.86	390.9	3.00
2/01/2002	5	16	18	4	22	15	6	377.16	376.45	321.60	346.56	399.85	368.94	365.1	3.00
3/01/2002	1	2	12	3	22	15	6	254.92	208.27	142.87	164.61	238.77	254.26	210.6	4.00
5/01/2002	18	2	0	0	16	11	4	374.08	388.76	416.54	423.29	407.07	394.39	400.7	3.00
6/01/2002	4	0	0	0	6	4	3	371.37	387.39	414.12	422.55	411.11	392.75	399.9	2.00
10/01/2002	9	13	5	4	17	19	6	364.84	378.75	403.65	411.66	395.64	378.71	388.9	3.00
11/01/2002	19	24	16	15	24	23	6	356.71	378.62	406.28	415.05	392.16	378.93	388	3.00
12/01/2002	14	10	2	6	22	15	6	353.52	371.46	399.17	407.48	386.41	374.68	382.1	3.00

16/01/2002	1	0	0	0	1	7	3	353.63	331.99	347.19	357.88	364.68	346.65	350.3	2.00
17/02/2002	0	1	2	0	1	0	3	169.23	170.68	165.01	177.19	165.65	201.82	174.9	1.00
2002-2003															
17/11/2002	0	1	1	1	0	1	4	313.59	350.60	326.54	355.49	338.68	235.68	320.1	2.00
4/12/2002	3	1	0	0	8	0	3	351.01	361.10	291.31	328.06	365.94	359.84	342.9	2.00
6/12/2002	11	1	0	0	13	4	4	363.70	388.83	392.28	416.76	404.94	398.60	394.2	3.00
13/12/2002	2	1	0	0	10	1	4	382.08	422.97	413.81	434.61	418.47	430.51	417.1	2.00
19/12/2002	0	1	3	0	8	0	3	220.21	208.85	198.03	199.74	202.54	197.15	204.4	1.00
20/12/2002	0	2	5	0	4	3	4	158.43	149.45	101.95	81.74	206.22	209.90	151.3	1.00
2/01/2003	3	2	0	0	2	11	4	359.89	394.64	382.56	393.41	378.45	427.51	389.4	2.00
8/01/2003	4	1	2	0	0	0	3	307.44	262.73	251.81	234.23	302.91	289.01	274.7	1.00
21/01/2003	0	1	3	3	3	0	4	85.44	130.97	36.29	35.93	69.79	83.91	73.72	1.00
2003-04															
1/12/2003	0	2	3	0	0	6	3	161.58	206.55	201.59	202.30	NaN	203.78	195.2	1.00
2/12/2003	1	4	5	3	0	3	5	84.79	110.23	86.75	67.82	NaN	73.98	84.71	1.00
9/12/2003	16	4	0	3	0	15	4	374.21	391.66	401.24	426.59	406.09	398.49	399.7	3.00
10/12/2003	4	1	0	0	0	9	3	334.93	318.37	364.39	392.11	292.48	306.11	334.7	2.00
26/12/2003	2	1	0	0	0	1	3	396.18	391.90	375.02	394.79	385.05	384.71	387.9	2.00
2004-05															
9/11/2004	0	2	2	1	0	0	3	266.25	271.41	274.03	254.65	277.42	270.01	269	1.00
12/11/2004	0	2	2	0	0	1	3	261.66	291.02	258.50	241.84	290.36	284.34	271.3	1.00
13/11/2004	1	1	1	0	0	0	3	242.11	281.71	262.46	251.18	245.82	291.15	262.4	1.00
20/11/2004	3	2	0	0	15	4	4	288.33	343.50	335.39	305.90	314.02	310.13	316.2	3.00
21/11/2004	6	2	0	3	3	5	5	325.19	355.33	354.53	343.05	311.81	283.39	328.9	3.00
30/11/2004	6	4	0	2	11	2	5	254.24	272.29	265.79	268.93	251.04	259.47	262	4.00
20/12/2004	11	0	0	0	10	15	3	395.49	397.34	430.21	402.53	406.55	417.02	408.2	3.00
21/12/2004	10	11	0	0	23	15	4	384.18	418.68	419.52	412.79	389.25	405.13	404.9	3.00
5/01/2005	1	3	0	0	15	9	4	225.56	235.46	NaN	162.19	257.75	212.89	218.8	4.00
2005-06															

3/11/2005	1	0	0	0	1	1	3	173.00	156.60	NaN	127.69	187.14	184.27	165.7	1.00
27/11/2005	2	0	0	0	7	6	3	313.46	355.07	NaN	362.03	339.79	342.34	342.5	2.00
6/12/2005	1	0	0	0	2	1	3	330.31	332.81	NaN	379.89	297.43	344.53	337	2.00
8/12/2005	1	3	0	1	0	8	4	204.33	247.91	NaN	271.94	230.96	286.53	248.3	1.00
15/12/2005	3	7	0	0	10	0	3	351.28	392.20	NaN	382.79	395.03	397.06	383.7	3.00
20/12/2005	1	2	0	0	1	3	4	294.05	354.38	NaN	336.52	281.76	302.04	313.8	2.00
29/12/2005	3	0	0	0	9	4	3	354.98	396.37	NaN	382.66	404.22	419.71	391.6	2.00
2006-07															
30/12/2006	0	2	1	0	12	5	4	315.61	333.36	374.43	322.66	369.84	410.72	354.4	2.00
31/12/2006	0	10	8	1	11	10	5	317.44	358.08	413.23	379.89	355.89	398.73	370.5	3.00
1/01/2007	0	0	0	1	19	3	3	159.75	162.11	134.27	122.14	153.35	173.21	150.8	1.00
2/01/2007	0	1	0	0	17	20	3	324.10	372.44	372.44	348.45	372.88	355.24	357.6	3.00
5/01/2007	0	2	3	1	21	14	5	233.21	240.87	204.99	204.13	250.46	271.30	234.2	4.00
14/01/2007	0	1	7	0	2	1	4	334.50	333.82	352.33	334.98	287.23	299.10	323.7	2.00
20/01/2007	0	0	0	3	20	7	3	249.50	NaN	251.09	246.94	262.97	263.35	254.8	4.00
2007-08															
15/12/2007	6	0	3	0	5	0	3	355.25	373.12	372.60	366.34	384.09	329.64	363.5	2.00
23/12/2007	13	5	1	0	13	14	5	376.02	387.62	372.50	412.32	369.87	359.89	379.7	3.00
24/12/2007	2	3	0	0	3	4	4	362.91	403.22	407.68	427.09	377.76	411.10	398.3	2.00
15/01/2008	6	0	0	0	3	1	3	326.27	397.29	369.93	393.23	360.66	357.01	367.4	2.00
16/01/2008	1	0	3	0	5	0	3	233.21	282.98	226.26	237.78	218.48	244.81	240.6	1.00
2008-09															
11/11/2008	1	2	0	0	1	2	4	264.70	319.80	288.48	308.25	294.19	280.88	292.7	1.00
20/11/2008	4	2	0	2	2	2	5	272.93	362.42	332.05	357.68	324.22	299.69	324.8	2.00
28/11/2008	0	1	3	5	0	0	3	230.11	231.88	198.61	219.36	194.20	192.69	211.1	1.00
29/11/2008	1	0	1	0	2	0	3	218.26	277.03	195.39	224.25	254.92	262.85	238.8	2.00
8/12/2008	12	1	0	0	14	6	4	352.98	417.82	407.36	421.37	392.66	384.38	396.1	3.00
19/12/2008	0	2	0	0	7	6	3	359.52	422.24	413.48	424.82	384.18	404.24	401.4	2.00
23/12/2008	1	4	0	0	1	0	3	347.95	369.46	351.80	355.29	351.28	348.68	354.1	2.00

26/12/2008	4	1	3	0	8	1	5	351.26	415.96	401.77	414.89	392.36	391.93	394.7	3.00
30/12/2008	17	8	4	5	23	16	6	355.35	409.09	411.09	422.78	392.24	447.51	406.3	3.00
31/12/2008	3	0	0	0	1	1	3	346.19	383.51	401.07	409.64	298.14	411.57	375	2.00
22/01/2009	7	3	3	0	9	6	5	NaN	367.27	333.04	349.55	333.65	369.92	350.7	3.00
23/01/2009	19	14	0	1	20	14	5	NaN	346.84	332.02	344.29	318.53	359.30	340.2	3.00
25/01/2009	7	2	0	0	4	0	3	NaN	326.56	307.99	327.48	317.53	358.78	327.7	2.00
26/01/2009	3	1	0	0	5	0	3	NaN	332.58	299.86	315.19	311.47	352.48	322.3	2.00
2009-10															
13/11/2009	3	6	2	2	12	1	6	NaN	146.37	115.76	115.40	108.91	131.49	123.6	4.00
14/11/2009	0	1	2	2	3	1	5	NaN	74.22	58.16	42.31	51.59	78.97	61.05	1.00
16/11/2009	10	6	0	3	17	10	5	NaN	336.32	301.62	315.12	303.55	334.66	318.3	3.00
19/11/2009	0	2	1	1	0	1	4	NaN	326.96	323.70	348.46	318.18	355.47	334.6	2.00
25/11/2009	0	1	1	0	0	1	3	NaN	341.84	337.84	356.13	287.28	296.41	323.9	2.00
30/11/2009	1	2	3	0	8	3	5	NaN	294.00	270.06	303.28	286.72	314.36	293.7	1.00
1/12/2009	11	0	0	0	3	7	3	NaN	355.42	345.03	379.51	347.66	370.30	359.6	3.00
2/12/2009	7	0	0	0	5	1	3	460.09	384.04	375.46	400.82	362.13	401.56	397.3	2.00
5/01/2010	1	0	0	0	5	3	3	265.94	329.73	271.36	296.24	267.28	319.33	291.6	1.00
20/01/2010	3	1	0	0	1	0	3	306.55	346.98	NaN	364.57	330.14	367.97	343.2	2.00
21/01/2010	6	2	0	0	13	13	4	303.52	344.22	NaN	360.22	326.57	361.26	339.2	3.00
7/02/2010	7	3	0	1	2	7	5	240.48	250.92	NaN	261.13	247.41	274.66	254.9	4.00
8/02/2010	3	4	0	1	0	3	4	229.36	261.80	NaN	267.74	252.40	278.69	258	1.00
2010-11															
1/11/2010	0	0	0	1	2	1	3	214.55	246.11	NaN	245.72	229.59	261.16	239.4	1.00
10/11/2010	14	14	3	3	13	1	6	261.43	294.26	290.20	302.27	281.17	310.60	290	2.00
14/11/2010	1	0	0	0	1	1	3	260.67	295.53	287.44	302.68	271.70	301.13	286.5	1.00
9/12/2010	12	0	2	2	15	13	5	355.10	NaN	405.09	422.84	384.03	448.60	403.1	3.00
10/12/2010	24	0	12	19	24	24	5	338.76	NaN	401.76	432.12	379.35	464.56	403.3	3.00
11/12/2010	10	0	4	5	10	8	5	356.93	NaN	410.57	423.63	388.67	460.85	408.1	3.00
12/12/2010	13	0	0	0	3	1	3	353.47	NaN	407.74	402.85	364.53	353.49	376.4	2.00

2011-12															
29/12/2011	11	0	4	5	0	9	4	373.39	NaN	427.34	413.84	NaN	432.22	411.7	3.00
30/12/2011	19	0	15	20	0	24	4	360.08	NaN	438.99	415.51	NaN	454.61	417.3	3.00
31/12/2011	13	0	0	3	0	14	3	368.96	NaN	428.81	409.23	NaN	450.97	414.5	3.00
11/01/2012	5	0	0	0	13	6	3	316.10	NaN	357.82	354.43	337.98	386.50	350.6	3.00
13/01/2012	2	0	0	0	9	3	3	336.32	NaN	368.75	372.54	360.06	397.69	367.1	2.00
22/02/2012	1	1	0	1	0	2	4	192.71	191.12	193.65	184.97	91.49	200.08	175.7	1.00
23/02/2012	1	1	0	0	0	1	3	181.25	180.83	182.32	172.83	83.11	190.44	165.1	1.00
2013-14															
15/11/2013	2	0	1	1	0	0	3	303.33	302.06	301.64	292.40	277.72	190.88	278	1.00
25/11/2013	3	2	4	5	10	0	5	337.38	271.41	311.08	287.13	318.32	140.90	277.7	4.00
26/11/2013	11	1	0	1	2	0	4	352.69	353.95	379.19	365.77	344.46	124.82	320.1	2.00
28/11/2013	2	0	1	0	9	0	3	248.75	264.64	288.79	288.98	232.52	73.57	232.9	1.00
3/12/2013	0	0	1	3	6	0	3	328.49	356.65	356.48	324.59	341.44	81.71	298.2	1.00
13/12/2013	7	3	0	0	16	0	3	386.71	392.23	416.06	405.42	387.16	78.21	344.3	3.00
27/12/2013	4	0	2	0	4	0	3	277.72	269.80	306.67	262.20	266.73	50.70	239	1.00
28/12/2013	4	2	0	0	5	0	3	392.57	385.96	428.66	384.95	391.61	76.15	343.3	2.00
31/12/2013	22	16	0	8	24	0	4	390.76	385.72	427.16	406.02	386.24	77.40	345.5	3.00
1/01/2014	20	22	16	14	24	24	6	388.53	384.98	429.30	405.24	384.67	77.40	345	3.00
2/01/2014	11	16	11	16	24	24	6	386.40	374.73	425.67	402.14	382.62	91.87	343.9	3.00
3/01/2014	4	0	0	0	8	9	3	380.96	371.26	420.59	393.70	377.84	413.91	393	3.00
18/01/2014	0	2	0	7	12	8	4	350.40	318.09	NaN	332.64	340.46	370.85	342.5	3.00
19/01/2014	0	3	0	2	5	5	4	270.74	253.05	NaN	288.78	246.83	287.79	269.4	1.00
8/02/2014	0	0	10	2	15	3	4	81.63	81.63	43.96	47.35	90.96	97.87	73.9	4.00
9/02/2014	0	0	2	0	3	1	3	200.72	169.18	184.38	171.25	195.45	195.69	186.1	1.00
11/02/2014	0	1	0	2	1	1	4	234.17	229.69	242.75	237.44	220.93	254.41	236.6	1.00
2014-15															
21/01/2015	0	1	1	1	1	0	4	294.74	293.46	336.71	308.62	281.24	325.11	306.6	2.00
6/02/2015	0	1	3	0	5	0	3	134.69	123.15	122.08	115.33	129.06	143.91	128	1.00

7/02/2015	0	2	0	1	8	0	3	101.51	77.39	62.25	63.36	93.52	102.26	83.38	1.00
8/02/2015	0	0	4	0	15	2	3	230.80	196.14	207.42	191.01	197.75	210.10	205.5	1.00
9/02/2015	1	0	0	1	4	0	3	191.45	177.36	141.89	145.14	195.96	218.14	178.3	1.00
16/02/2015	2	1	2	0	0	0	3	211.46	189.01	141.19	143.94	175.17	203.98	177.5	1.00
2015-16															
12/11/2015	1	1	0	0	0	1	3	217.28	259.04	260.62	255.53	NaN	230.68	244.6	1.00
29/11/2015	3	0	2	1	0	0	3	367.10	407.70	376.38	368.89	NaN	377.25	379.5	2.00
7/12/2015	0	1	2	0	6	1	4	375.49	369.17	364.99	312.97	355.09	322.74	350.1	2.00
8/12/2015	1	2	7	1	3	0	5	204.85	167.64	179.82	179.13	190.84	168.65	181.8	1.00
13/12/2015	7	2	0	0	9	8	4	382.85	375.78	346.72	390.85	396.52	401.90	382.4	3.00
14/12/2015	24	24	12	18	24	24	6	387.05	422.15	410.07	392.84	403.34	415.59	405.2	3.00
15/12/2015	21	0	0	1	21	0	3	354.26	385.42	359.44	343.25	336.31	349.12	354.6	2.00
16/12/2015	9	0	0	0	18	12	3	397.73	421.37	380.16	380.52	400.79	404.58	397.5	3.00
29/12/2015	1	1	0	0	2	4	4	386.15	424.92	423.22	408.01	399.15	408.32	408.3	2.00
30/12/2015	3	0	2	1	4	4	5	386.64	420.05	414.78	400.85	398.50	409.89	405.1	3.00
10/01/2016	1	2	0	0	2	3	4	330.28	303.10	271.64	272.56	305.82	328.84	302	2.00
11/01/2016	0	7	14	1	13	14	5	304.93	285.71	215.83	248.27	304.52	305.15	277.4	4.00
12/01/2016	10	0	0	0	1	6	3	298.98	316.00	288.97	267.33	260.64	297.28	288.2	1.00
14/01/2016	6	4	0	0	10	0	3	345.83	373.57	377.56	368.94	349.22	353.26	361.4	3.00
23/01/2016	20	4	1	3	0	10	5	324.38	341.52	340.88	333.18	NaN	342.81	336.6	3.00
24/01/2016	10	8	6	7	0	6	5	331.80	336.53	335.20	336.96	NaN	323.95	332.9	3.00
3/02/2016	3	3	0	1	0	3	4	251.89	264.08	258.40	246.06	NaN	264.81	257	1.00
4/02/2016	1	7	4	2	0	20	5	249.36	271.00	270.18	245.40	NaN	253.71	257.9	4.00
14/02/2016	3	0	2	1	1	0	4	226.47	240.07	223.94	219.63	198.22	228.63	222.8	1.00
2016-17															
7/11/2016	0	12	0	1	8	3	4	NaN	290.12	286.63	272.73	266.44	278.50	278.9	4.00
8/11/2016	0	7	0	2	19	1	4	NaN	271.91	290.86	276.02	253.64	252.82	269.1	4.00
10/11/2016	0	13	0	3	9	11	4	NaN	304.66	285.98	277.51	282.56	294.66	289.1	4.00
11/11/2016	0	1	0	0	2	1	3	NaN	312.84	307.63	292.04	286.64	293.95	298.6	2.00

21/11/2016	1	0	0	1	10	0	3	124.06	169.24	143.78	111.52	175.22	196.06	153.3	1.00
30/11/2016	1	0	0	0	13	11	3	330.00	380.93	348.94	331.86	367.73	372.22	355.3	3.00
1/12/2016	5	2	0	0	10	7	4	335.57	369.55	301.24	374.23	368.12	378.42	354.5	3.00
16/12/2016	13	8	0	5	21	13	5	333.52	363.58	384.75	372.82	338.02	355.06	358	3.00
3/01/2017	13	6	4	11	2	4	6	302.83	369.70	351.57	337.13	350.85	355.59	344.6	3.00
13/01/2017	0	0	2	1	2	1	4	151.83	200.18	177.19	159.86	180.36	187.48	176.2	1.00
26/01/2017	4	1	0	0	12	9	4	286.55	308.77	296.53	296.08	307.95	299.16	299.2	3.00
4/02/2017	3	1	2	0	0	0	3	158.99	212.74	177.66	170.47	169.60	191.95	180.2	1.00
8/02/2017	2	4	0	1	5	0	4	133.79	160.28	146.38	131.46	129.03	140.65	140.3	1.00
9/02/2017	3	1	0	0	3	0	3	223.68	244.76	232.32	229.65	224.77	240.25	232.6	1.00
2017-18															
25/11/2017	5	2	2	4	8	6	6	314.16	377.42	395.36	336.81	336.41	365.46	354.3	3.00
3/12/2017	2	0	2	1	0	0	3	336.78	369.65	412.89	381.46	365.27	385.51	375.3	2.00
13/12/2017	1	0	0	0	13	2	3	211.76	259.98	223.51	216.12	232.34	302.01	241	1.00
13/02/2018	2	1	1	1	1	2	6	202.82	222.75	232.59	223.05	215.89	236.15	222.2	1.00

Bibliography

Andersen, D. T., McKay, C. P., Wharton, R. A., & Rummel, J. D. (1992). Testing a Mars science outpost in the Antarctic dry valleys. *Advances in Space Research*, *12*(5), 205–209. https://doi.org/10.1016/0273-1177(92)90025-S

Andrew G. Fountain, et al. (1999). Physical Controls on the Taylor valley ecosystem of Antarctica

Archuleta, C.-A. M., Constance, E. W., Arundel, S. T., Lowe, A. J., Mantey, K. S., & Phillips, L. A. (2017). The National Map seamless digital elevation model specifications. *Techniques and Methods*. https://doi.org/10.3133/tm11B9

Baral, P., Haq, M. A., & Yaragal, S. (2020). Assessment of rock glaciers and permafrost distribution in Uttarakhand, India. *Permafrost and Periglacial Processes*, *31*(1), 31–56. https://doi.org/10.1002/ppp.2008

Bechtel, B., Langkamp, T., Böhner, J., Daneke, C., Oßenbrügge, J., & Schempp, S. (2012). Classification and modelling of urban micro-climates using multisensoral and multitemporal remote sensing data. *International Archives of the Photogrammetry, Remote Sensing and Spatial Information Sciences - ISPRS Archives*, *39*(September), 463–468. https://doi.org/10.5194/isprsarchives-XXXIX-B8-463-2012

Benali, A., Carvalho, A. C., Nunes, J. P., Carvalhais, N., & Santos, A. (2012). Estimating air surface temperature in Portugal using MODIS LST data. *Remote Sensing of Environment*, *124*, 108–121. https://doi.org/10.1016/j.rse.2012.04.024

Bintanja, R. (2000). Surface heat budget of Antarctic snow and blue ice: Interpretation of spatial and temporal variability. *Journal of Geophysical Research: Atmospheres*, *105*(D19), 24387–24407. https://doi.org/10.1029/2000JD900356

Bliss, A. K., Cuffey, K. M., & Kavanaugh, J. L. (2011). Sublimation and surface energy budget of Taylor Glacier, Antarctica. *Journal of Glaciology*, *57*(204), 684–696. https://doi.org/10.3189/002214311797409767

Bokhorst, S., Huiskes, A., Convey, P., Sinclair, B. J., Lebouvier, M., Van de Vijver, B., & Wall, D. H. (2011). Microclimate impacts of passive warming methods in Antarctica: Implications for climate change studies. *Polar Biology*, *34*(10), 1421–1435. https://doi.org/10.1007/s00300-011-0997-y

Bourke, M. C., Ewing, R. C., Finnegan, D., & McGowan, H. A. (2009). Sand dune movement in the Victoria Valley, Antarctica. *Geomorphology*, *109*(3–4), 148–160. https://doi.org/10.1016/j.geomorph.2009.02.028

Carlson, T. N., & Traci Arthur, S. (2000). The impact of land use - Land surface changes due to urbanization on surface microclimate and hydrology: A satellite perspective. *Global and Planetary Change*, *25*(1–2), 49–65. https://doi.org/10.1016/S0921-8181(00)00021-7

Carrasco, J. F., Bromwich, D. H., & Monaghan, A. J. (2003). Distribution and Characteristics of Mesoscale Cyclones in the Antarctic: Ross Sea Eastward to the Weddell Sea*. *Monthly Weather Review*, *131*, 289–301. https://doi.org/10.1175/1520-0493(2003)131<0289:DACOMC>2.0.CO;2

Chinn, T. J. (1980). Glacier balance in the Dry Valleys area, Victoria Land, Antarctica. *Proceedings of the Riederalp Workshop*, *126*, 237–248.

Ciappa, A., Pietranera, L., & Budillon, G. (2012). Observations of the Terra Nova Bay (Antarctica) polynya by MODIS ice surface temperature imagery from 2005 to 2010. *Remote Sensing of Environment*, *119*, 158–172. https://doi.org/10.1016/j.rse.2011.12.017

Colacino, M., & Stocchino, C. (1981). Climatological data and superficial thermal balance in the wright dry valley (South Victoria Land-Antarctica). *Il Nuovo Cimento C*, *4*(5), 583–602. https://doi.org/10.1007/BF02506961

Colombi, A., Michele, C. De, Pepe, M., & Rampini, A. (2007). Estimation of Daily Mean Air Temperature. *EAReL EProceedings 6*, *3*, 38–46.

Conovitz, P. A., Mcknight, D. M., Macdonaldl, L. H., Fountain, A. G., & House, H. R. (1998). Hydrologic processes influencing streamflow varioation in Fryxell basin, Antarctica. *Ecosystem Processes in a Polar Desert: The McMurdo Dry Valleys, Antarctica*, 93–108.

Conovitzl, P. A., Mcknight, D. M., Macdonaldl, L. H., Fountain, A. G., & House, H. R. (1998). *PROCESSES INFLUENCING FRYXELL BASIN , ANTARCTICA VARITaION IN between the glaciers and the lakes in the valley bottoms . This paper analyzes the*. 93–108.

Convey, P. (2010). Terrestrial biodiversity in Antarctica - Recent advances and future challenges. *Polar Science*, *4*(2), 135–147. https://doi.org/10.1016/j.polar.2010.03.003

Cozzetto, K., McKnight, D., Nylen, T., & Fountain, A. (2006). Experimental investigations into processes controlling stream and hyporheic temperatures, Fryxell Basin, Antarctica. *Advances in*

Water Resources, *29*(2), 130–153. https://doi.org/10.1016/j.advwatres.2005.04.012

Doran, P. T., McKay, C. P., Clow, G. D., Dana, G. L., Fountain, A. G., Nylen, T., & Lyons, W. B. (2002). Valley floor climate observations from the McMurdo dry valleys, Antarctica, 1986-2000. *Journal of Geophysical Research Atmospheres*, *107*(24), 1–12. https://doi.org/10.1029/2001JD002045

Doran, P. T., McKay, C. P., Fountain, A. G., Nylen, T., McKnight, D. M., Jaros, C., & Barrett, J. E. (2008). Hydrologic response to extreme warm and cold summers in the McMurdo Dry Valleys, East Antarctica. *Antarctic Science*, *20*(05), 499–509. https://doi.org/10.1017/S0954102008001272

Doran, P. T., Priscu, J. C., Lyons, W. B., Walsh, J. E., Fountain, A. G., Mcknight, D. M., & Moorhead, D. L. (2006). *Antarctic climate cooling and terrestrial ecosystem response*. *1999*.

Doran, P. T., Priscu, J. C., Lyons, W. B., Walsh, J. E., Fountain, A. G., McKnight, D. M., Moorhead, D. L., Virginia, R. a, Wall, D. H., Clow, G. D., Fritsen, C. H., McKay, C. P., & Parsons, A. N. (2002). Antarctic climate cooling and terrestrial ecosystem response. *Nature*, *415*(6871), 517–520. https://doi.org/10.1038/nature710

Dowling, C. B., Poreda, R. J., & Lyons, W. B. (2014). The effects of high meltwater on the limnology of Lake Fryxell and Lake Hoare, Taylor Valley, Antarctica, as shown by dissolved gas, tritium and chlorofluorocarbons. *Antarctic Science*, *26*(04), 331–340. https://doi.org/10.1017/S095410201300062X

Ebnet, A., Fountain, A. G., & Nylen, T. H. (2005). An index model of stream flow at below freezing-temperatures in Taylor Valley, Antarctica. *Annals of Glaciology*, *40*, 76–82. https://doi.org/10.3189/172756405781813519

Energy Balance - an overview | ScienceDirect Topics. (n.d.). Retrieved January 5, 2021, from https://www.sciencedirect.com/topics/earth-and-planetary-sciences/energy-balance

foehn - an overview | ScienceDirect Topics. (n.d.). Retrieved December 4, 2020, from https://www.sciencedirect.com/topics/earth-and-planetary-sciences/foehn

Fountain, A G, Nylen, T. H., MacClune, K. J., & Dana, G. L. (2006). Glacier mass balances (1993-2001) Taylor Valley, McMurdo Dry Valleys, Antarctica. *Journal of Glaciology*, *52*(178), 451–462.

Fountain, Andrew G., Nylen, T. H., Monaghan, A., Basagic, H. J., & Bromwich, D. H. (2009). Snow

in the McMurdo Dry Valleys, Antarctica. *International Journal of Climatology*, *642*(5), 633–642. https://doi.org/10.1002/joc.1933

Fountain, Andrew G, Lyons, W. B., Burkins, M. B., Dana, G. L., Peter, T., Lewis, K. J., Mcknight, D. M., Moorhead, D. L., Parsons, A. N., John, C., Wall, D. H., Jr, R. a W., & Virginia, R. a. (1999). Physical Controls on. *BioScience*, *49*(12), 961–971. https://doi.org/10.1525/bisi.1999.49.12.961

Garratt, J. R. (1990). Boundary layer climates. In *Earth-Science Reviews* (Vol. 27, Issue 3). https://doi.org/10.1016/0012-8252(90)90005-G

Gusain, H. S., Mishra, V. D., & Arora, M. K. (2014). A four-year record of the meteorological parameters, radiative and turbulent energy fluxes at the edge of the East Antarctic Ice Sheet, close to Schirmacher Oasis. *Antarctic Science*, *26*(01), 93–103. https://doi.org/10.1017/S095410201300028X

Hereher, M. E. (2019). Estimation of monthly surface air temperatures from MODIS LST time series data: application to the deserts in the Sultanate of Oman. *Environmental Monitoring and Assessment*, *191*(9), 1–11. https://doi.org/10.1007/s10661-019-7771-y

Hoffman, M. J., Fountain, A. G., & Liston, G. E. (2008). Surface energy balance and melt thresholds over 11 years at Taylor Glacier, Antarctica. *Journal of Geophysical Research: Earth Surface*, *113*(4), 1–12. https://doi.org/10.1029/2008JF001029

Hoffman, M. J., Fountain, A. G., & Liston, G. E. (2016). Distributed modeling of ablation (1996-2011) and climate sensitivity on the glaciers of Taylor Valley, Antarctica. *Journal of Glaciology*, *62*(232), 215–229. https://doi.org/10.1017/jog.2015.2

Hunt, H. W., Fountain, A. G., Doran, P. T., & Basagic, H. (2010). A dynamic physical model for soil temperature and water in Taylor Valley, Antarctica. *Antarctic Science*, *22*(04), 419–434. https://doi.org/10.1017/S0954102010000234

Impacts of climate change - Discovering Antarctica. (n.d.). Retrieved January 14, 2021, from https://discoveringantarctica.org.uk/challenges/sustainability/impacts-of-climate-change/

IPCC, 2001: Climate change. (2001). Contribution of Working Group I to the Third Assessment Report of the Intergovernmental Panel on Climate Change [Houghton, J.T. Ding, Y. Griggs, D.J. Noguer, M. Linden, P.J. van der Dai, X. Maskell, K. Johnson, C.A.]. *Cambridge University Press*, 94.

Jia, W., & Zhao, S. (2020). Trends and drivers of land surface temperature along the urban-rural

gradients in the largest urban agglomeration of China. *Science of the Total Environment*, *711*, 134579. https://doi.org/10.1016/j.scitotenv.2019.134579

Kang, J., Tan, J., Jin, R., Li, X., & Zhang, Y. (2018). Reconstruction of MODIS Land Surface Temperature Products Based on Multi-Temporal Information. *Remote Sensing*, *10*(7), 1112. https://doi.org/10.3390/rs10071112

Katurji, M., Zawar-Reza, P., & Zhong, S. (2013). Surface layer response to topographic solar shading in Antarctica's dry valleys. *Journal of Geophysical Research Atmospheres*, *118*(22), 12332–12344. https://doi.org/10.1002/2013JD020530

Knox, M. A., Andriuzzi, W. S., Buelow, H. N., Takacs-Vesbach, C., Adams, B. J., & Wall, D. H. (2017). Decoupled responses of soil bacteria and their invertebrate consumer to warming, but not freeze–thaw cycles, in the Antarctic Dry Valleys. *Ecology Letters*, *20*(10), 1242–1249. https://doi.org/10.1111/ele.12819

Knuth, S. L., Tripoli, G. J., Thom, J. E., & Weidner, G. A. (2010). The influence of blowing snow and precipitation on snow depth change across the Ross Ice Shelf and Ross Sea regions of Antarctica. *Journal of Applied Meteorology and Climatology*, *49*(6), 1306–1321. https://doi.org/10.1175/2010JAMC2245.1

Lacelle, D., Lapalme, C., Davila, A. F., Pollard, W., Marinova, M., Heldmann, J., & McKay, C. P. (2016). Solar Radiation and Air and Ground Temperature Relations in the Cold and Hyper-Arid Quartermain Mountains, McMurdo Dry Valleys of Antarctica. *Permafrost and Periglacial Processes*, *27*(2), 163–176. https://doi.org/10.1002/ppp.1859

Land Surface Temperature - Applications - Sentinel-3 SLSTR - Sentinel Online. (n.d.). Retrieved January 17, 2020, from https://sentinel.esa.int/web/sentinel/user-guides/sentinel-3-slstr/overview/geophysical-measurements/land-surface-temperature

Land, V., Nylen, T. H., Fountain, A. G., & Doran, P. T. (2004). *Climatology of katabatic winds in the McMurdo dry valleys ,*. *109*, 1–9. https://doi.org/10.1029/2003JD003937

Landsat Image Mosaic Of Antarctica (LIMA): Index Page. (n.d.). Retrieved January 20, 2021, from https://lima.usgs.gov/

Lewthwaite, W. D., Mckendry, G., & Meteorological, N. Z. (1990). *Local winds in the*. 321–342.

Lindsey, R. (2009). *Climate and Earth's Energy Budget : Feature Articles*. https://earthobservatory.nasa.gov/Features/EnergyBalance/page5.php

Lubin, D., Ayres, G., & Hart, S. (2009). Remote sensing of polar regions. *Bulletin of the American Meteorological Society*, *90*(6), 825–835. https://doi.org/10.1175/2008BAMS2596.1

Marchant, D. R., & Head., and J. W. (2005). Lunar and Planetary Science XXXVI (2005). *Image (Rochester, N.Y.)*, *02215*, 5–6. https://doi.org/10.1029/2002JE001982.

Marchant, D. R., & Head, J. W. (2007). Antarctic dry valleys: Microclimate zonation, variable geomorphic processes, and implications for assessing climate change on Mars. *Icarus*, *192*(1), 187–222. https://doi.org/10.1016/j.icarus.2007.06.018

McKendry, I. G., & Lewthwaite, E. W. D. (1992). Summertime along-valley wind variations in the wright valley Antarctica. *International Journal of Climatology*, *12*(6), 587–596. https://doi.org/10.1002/joc.3370120605

MCM LTER Data File Format Protocols for Database Submission | McMurdo Dry Valleys LTER. (n.d.). Retrieved January 24, 2021, from https://mcm.lternet.edu/data/mcm-lter-data-file-format-protocols-database-submission

McMurdo Dry Valleys LTER. (n.d.). Retrieved November 27, 2017, from https://www.mcmlter.org/

Meyer, H., Katurji, M., Appelhans, T., Müller, M. U., Nauss, T., Roudier, P., & Zawar-Reza, P. (2016). Mapping daily air temperature for Antarctica Based on MODIS LST. *Remote Sensing*, *8*(9), 732. https://doi.org/10.3390/rs8090732

Miliaresis, G. C. (2014). Spatiotemporal patterns of land surface temperature of Antarctica from MODIS monthly LST (MYD11C3) data. *Journal of Spatial Science*, *59*(1), 157–166. https://doi.org/10.1080/14498596.2013.857382

Miotke, F.-D. (1988). *3.1 Microclimate, Weathering Processes and Sah within Ice-free Continental Antarctica*. *58*(213), 201–209.

MODIS Land Team Home Page. (n.d.). Retrieved December 30, 2020, from https://modis-land.gsfc.nasa.gov/temp.html

MSFC, J. W. : (2015). *What Is Antarctica?* http://www.nasa.gov/audience/forstudents/5-8/features/nasa-knows/what-is-antarctica-58.html

Nylen, T. H., Fountain, A. G., & Doran, P. T. (2004). Climatology of katabatic winds in the McMurdo dry valleys, southern Victoria Land, Antarctica. *Journal of Geophysical Research: Atmospheres*, *109*(D3), n/a-n/a. https://doi.org/10.1029/2003JD003937

Oliphant, A. J., Hindmarsh, R. C. A., Cullen, N. J., & Lawson, W. (2015). Microclimate and mass fluxes of debris-laden ice surfaces in Taylor Valley, Antarctica. *Antarctic Science*, *27*(01), 85–100. https://doi.org/10.1017/S0954102014000534

Passive vs. Active Sensing | Natural Resources Canada. (n.d.). Retrieved January 17, 2020, from https://www.nrcan.gc.ca/maps-tools-publications/satellite-imagery-air-photos/remote-sensing-tutorials/introduction/passive-vs-active-sensing/14639

Physical-Chemical Characteristics of Soils and the Subsurface - ScienceDirect. (n.d.). Retrieved March 13, 2020, from https://www.sciencedirect.com/science/article/pii/B9780128147191000021

Ragotzkie, R. A., & Likens, G. E. (1964). the Heat Balance of Two Antarctic Lakes1. *Limnology and Oceanography*, *9*(3), 412–425. https://doi.org/10.4319/lo.1964.9.3.0412

Riordan, J. (1982). *simultaion valleys and of the of the testing of a climtaonomic of the in america Although nearly all the antarctic continent is covered by a permanent ice sheet, snowless oases lie scattered through the Transantarctic mountains and at several loca*. *24*, 295–329.

Sharples, J. J. (2018). foehn Winds. In *Encyclopedia of Wildfires and Wildland-Urban Interface (WUI) Fires* (pp. 1–7). Springer International Publishing. https://doi.org/10.1007/978-3-319-51727-8_71-1

Speirs, J. C., Mcgowan, H. A., & Neil, D. T. (2008). *Meteorological controls on sand transport and dune morphology in a polar desert: Victoria Valley, Antarctica*. *1891*, 1875–1891. https://doi.org/10.1002/esp

Speirs, J. C., Mcgowan, H. A., Steinhoff, D. F., & Bromwich, D. H. (2013a). Regional climate variability driven by foehn winds in the McMurdo Dry Valleys, Antarctica. *International Journal of Climatology*, *33*(4), 945–958. https://doi.org/10.1002/joc.3481

Speirs, J. C., Mcgowan, H. A., Steinhoff, F., & Bromwich, D. H. (2013b). *Regional climate variability driven by foehn winds in the McMurdo Dry Valleys , Antarctica*. *958*(April 2012), 945–958. https://doi.org/10.1002/joc.3481

Speirs, J. C., Steinhoff, D. F., McGowan, H. A., Bromwich, D. H., & Monaghan, A. J. (2010). foehn winds in the McMurdo Dry Valleys, Antarctica: The origin of extreme warming events. *Journal of Climate*, *23*(13), 3577–3598. https://doi.org/10.1175/2010JCLI3382.1

Steinhoff, D. F., Bromwich, D. H., & Monaghan, A. (2013). Dynamics of the foehn mechanism in the

mcmurdo dry valleys of Antarctica from polar WRF. *Quarterly Journal of the Royal Meteorological Society*, *139*(675), 1615–1631. https://doi.org/10.1002/qj.2038

Steinhoff, D. F., Bromwich, D. H., Speirs, J. C., Mcgowan, H. A., & Monaghan, A. J. (2014). Austral summer foehn winds over the McMurdo dry valleys of Antarctica from Polar WRF. *Quarterly Journal of the Royal Meteorological Society*, *140*(683), 1825–1837. https://doi.org/10.1002/qj.2278

Steinhoff, D. F., & David, H. (2006). *foehn Mechanism in the McMurdo Dry Valleys from Polar WRF McMurdo Dry Valleys (MDVs):*

Takacs-Vesbach, C., Zeglin, L. H., Gooseff, M. N., Barrett, J. E., & Priscu, J. C. (2010). Factors promoting microbial diversity in the McMurdo Dry Valleys. *Life in Antarctic Deserts and Other Cold Dry Environments: Astrobiological Analogues*, *5*, 221–257. https://doi.org/10.1017/CBO9780511712258.008

The Earth's Radiation Budget | Science Mission Directorate. (n.d.). Retrieved January 14, 2020, from https://science.nasa.gov/ems/13_radiationbudget

Turner, J. (2004). The El Niño-Southern Oscillation and Antarctica. *International Journal of Climatology*, *24*(1), 1–31. https://doi.org/10.1002/joc.965

van den Broeke, M., van de Berg, W. J., van Meijgaard, E., & Reijmer, C. (2006). Identification of Antarctic ablation areas using a regional atmospheric climate model. *Journal of Geophysical Research*, *111*(D18), D18110. https://doi.org/10.1029/2006JD007127

Vancutsem, C., Ceccato, P., Dinku, T., & Connor, S. J. (2010). Evaluation of MODIS land surface temperature data to estimate air temperature in different ecosystems over Africa. *Remote Sensing of Environment*, *114*(2), 449–465. https://doi.org/10.1016/j.rse.2009.10.002

Wan, Z. (2014). New refinements and validation of the collection-6 MODIS land-surface temperature/emissivity product. *Remote Sensing of Environment*, *140*, 36–45. https://doi.org/10.1016/j.rse.2013.08.027

Wang, Y., Wang, M., & Zhao, J. (2013). A Comparison of MODIS LST Retrievals with <i>in Situ</i> Observations from AWS over the Lambert Glacier Basin, East Antarctica. *International Journal of Geosciences*, *04*(03), 611–617. https://doi.org/10.4236/ijg.2013.43056

Waters, R., Allen, R., Tasumi, M., Trezza, R., & Bastiaanssen, W. (2002). *Manual for Surface Energy Balance Algorithms for Land*. 1–98.

Willmott 1981 file:///C:/Users/rajas/AppData/Local/Temp/hessd-10-C3817-2013-supplement.pdf

Westermann, S., Langer, M., & Boike, J. (2012). Systematic bias of average winter-time land surface temperatures inferred from MODIS at a site on Svalbard, Norway. *Remote Sensing of Environment*, *118*, 162–167. https://doi.org/10.1016/j.rse.2011.10.025

Zeglin, L. H., Sinsabaugh, R. L., Barrett, J. E., Gooseff, M. N., & Takacs-Vesbach, C. D. (2009). Landscape distribution of microbial activity in the McMurdo dry valleys: Linked biotic processes, hydrology, and geochemistry in a cold desert ecosystem. *Ecosystems*, *12*(4), 562–573. https://doi.org/10.1007/s10021-009-9242-8

Zhou, C., & Wang, K. (2016). Land surface temperature over global deserts: Means, variability, and trends. *Journal of Geophysical Research: Atmospheres*, *121*(24), 14,344-14,357. https://doi.org/10.1002/2016JD025410

Zhu, W., Lu, A., & Jia, S. (2013). Estimation of daily maximum and minimum air temperature using MODIS land surface temperature products. *Remote Sensing of Environment*, *130*, 62–73. https://doi.org/10.1016/j.rse.2012.10.034